JAERI-M
86-196

COBRA/TRAC ANALYSIS OF TWO-DIMENSIONAL THERMAL-HYDRAULIC BEHAVIOR IN SCTF REFLOOD TESTS

January 1987

Takamichi IWAMURA, Akira OHNUKI
Makoto SOBAJIMA and Hiromichi ADACHI

日本原子力研究所
Japan Atomic Energy Research Institute

JAERI-Mレポートは，日本原子力研究所が不定期に公刊している研究報告書です。
入手の問合わせは，日本原子力研究所技術情報部情報資料課（〒319-11茨城県那珂郡東海村）あて，お申しこしください。なお，このほかに財団法人原子力弘済会資料センター（〒319-11 茨城県那珂郡東海村日本原子力研究所内）で複写による実費頒布をおこなっております。

JAERI-M reports are issued irregularly.
Inquiries about availability of the reports should be addressed to Information Division Department of Technical Information, Japan Atomic Energy Research Institute, Tokai-mura, Naka-gun, Ibaraki-ken 319-11, Japan.

編集兼発行　日本原子力研究所
印　　刷　㈱高野高速印刷

COBRA/TRAC Analysis of Two-Dimensional Thermal-Hydraulic Behavior in SCTF Reflood Tests

Takamichi IWAMURA, Akira OHNUKI
Makoto SOBAJIMA and Hiromichi ADACHI

Department of Reactor Safety Research,
Tokai Research Establishment
Japan Atomic Energy Research Institute
Tokai-mura, Naka-gun, Ibaraki-ken
(Received December 25, 1986)

The effects of radial power distribution and non-uniform upper plenum water accumulation on thermal-hydraulic behavior in the core were observed in the reflood tests with Slab Core Test Facility (SCTF). In order to examine the predictability of these two effects by a multi-dimensional analysis code, the COBRA/TRAC calculations were made. The calculated results indicated that the heat transfer enhancement in high power bundles above quench front was caused by high vapor flow rate in those bundles due to the radial power distribution. On the other hand, the heat transfer degradation in the peripheral bundles under the condition of non-uniform upper plenum water accumulation was caused by the lower flow rates of vapor and entrained liquid above the quench front in those bundles by the reason that vapor concentrated in the center bundles due to the cross flow induced by the horizontal pressure gradient in the core. The above-mentioned two-dimensional heat transfer behaviors calculated with the COBRA/TRAC code is similar to those observed in SCTF tests and therefore those calculations are useful to investigate the mechanism of the two-dimensional effects in SCTF reflood tests.

Keywords: LOCA, ECCS, PWR, Computer Code, COBRA/TRAC, Reflood, Two-Phase Flow, Heat Transfer, Quench, Two-dimensional Flow, Thermal-Hydraulic Behavior, SCTF

The work was performed under contract with the Atomic Energy Bureau of Science and Technology Agency of Japan.

ＳＣＴＦ再冠水試験における２次元熱水力挙動のＣＯＢＲＡ／ＴＲＡＣ解析

日本原子力研究所東海研究所原子炉安全工学部
岩村　公道・大貫　晃・傍島　眞・安達　公道

（１９８６年１２月２５日受理）

平板炉心試験装置（ＳＣＴＦ）の再冠水試験において，半径方向出力分布効果と不均一上部プレナム蓄水効果に基づく炉心内２次元熱水力挙動が観察された。この２種類の効果が多次元解析コードＣＯＢＲＡ／ＴＲＡＣでいかに表現されるかを調べるための計算を行った。その結果，半径方向出力分布が存在すると，高出力バンドルでの蒸気流量が増大するため，クエンチフロント上方における高出力バンドルでの熱伝達が促進されることが示された。また，不均一上部プレナム蓄水が存在すると，炉心内の水平方向圧力勾配により蒸気が中心バンドルに集中し，クエンチフロント上方での蒸気及び液滴の流量が周辺バンドル内で低下するため，同バンドル内での熱伝達が低下することが示された。以上の２次元熱伝達挙動の計算結果は，ＳＣＴＦで観察された炉心熱伝達挙動と類似した傾向を示しており，ＳＣＴＦ再冠水試験における２次元効果のメカニズムを考察する上で有用である。

東海研究所：〒319-11　茨城県那珂郡東海村白方字白根２－４

本報告書は，電源開発促進対策特別会計法に基づき，科学技術庁からの受託によって行なった研究の成果である。

CONTENTS

目　　次

List of Tables

List of Figures

1. INTRODUCTION

The Slab Core Test Facility (SCTF) test program is a part of the large scale reflood test program under contract with Atomic Energy Bureau of Science and Technology Agency of Japan together with the Cylindrical Core Test Facility (CCTF) test program. One of the major objectives of the SCTF program is to investigate the two-dimensional thermal-hydraulic behavior in the core during the reflood phase of a loss-of-coolant accident (LOCA) of a pressurized water reactor (PWR). In order to meet this objective, SCTF simulates a full radius slab section of a PWR with 8 bundles arranged in a row and the heating power can be independently controlled for each bundle. Therefore, the effects of radial core power profile can be investigated with SCTF. On the other hand, the major objective of the CCTF test program is to investigate system characteristics during the reflood phase of a PWR-LOCA.

In the SCTF Core-I and Core-II tests(1),(2), it was found that the heat transfer was enhanced in the higher power bundles and degraded in the lower power bundles in the steep radial power distribution test especially at the upper elevation. Another type of two-dimensional flow in the core was also induced by the non-uniform water accumulation in the upper plenum and the quench was delayed resultantly in the bundles corresponding to the peripheral bundles of a PWR. However, the mechanism of the two-dimensional heat transfer characteristics caused by the radial power profile in the core and the non-uniform water accumulation in the upper plenum have not been clarified yet.

COBRA/TRAC code(3), which was introduced from Pacific Northwest Laboratory (PNL)to Japan Atomic Energy Reseach Institute (JAERI) in 1981, was used to examine the mechanism of heat transfer enhancement or degradation due to the two-dimensional effects. The used version of COBRA/TRAC code in this study was derived from the merging of COBRA-TF code in the vessel component and TRAC-P1A code in the primary system. The COBRA/TRAC code solves the three-dimensional, two-fluid, and three-field equations for two-phase flow. The three fields are vapor, continuous liquid and entrained liquid. Therefore, the vertical and horizontal flow components for each of these three fields in the SCTF core can be calculated with the COBRA/TRAC code. In addition, since the COBRA/TRAC code has flexible noding capability with Cartesian

coordinates, it is considered to be suitable for the noding of the slab geometry of the SCTF core.

In the present report, the effects of the radial core power distribution and the non-uniform upper plenum water accumulation on the two-dimensional behavior in the core are separately evaluated based on the COBRA/TRAC calculation results. The input modeling, initial conditions, and boundary conditions for the calculations are also described in this report.

2. SCTF TEST DESCRIPTION

2.1 Test Facility

A schematic diagram of Slab Core Test Facility (SCTF) is shown in Fig. 2.1. The primary coolant loops consist of a hot leg equivalent to four actual hot legs, a steam/water separator corresponding to four actual steam generators, an intact cold leg equivalent to three intact cold legs, a broken cold leg on the pressure vessel side, and a broken cold leg on the steam/water separator side. These broken cold legs are connected to two containment tanks one by one and the two containment tanks are connected to each other by a pressure equalizing pipe.

The nominal flow area scaling ratio is 1/21 of a 1,100 MWe PWR, whereas the heights of each component are preserved.

The emergency core cooling system (ECCS) consists of an accumulator system (Acc) and a low pressure coolant injection system (LPCI). The injection ports for the Acc and LPCI are the lower plenum and the intact cold leg, respectively, in the cold leg injection test series.

Figure 2.2 shows a vertical cross section of the pressure vessel. The pressure vessel includes a simulated core, an upper plenum with internals, a lower plenum, a core baffle and a downcomer. The SCTF pressure vessel simulates a full radius and one bundle width slab section of a 1,100 MWe PWR.

The simulated core consists of 8 bundles arranged in a row. Each bundle consists of 234 heater rods and 22 non-heated rods arranged in 16 x 16 array. The outer diameter and the heated length of the heater rod are 10.7 mm and 3660 mm, respectively. The dimensions and arrangement pitch of the rods are the same as those for a 15 x 15 fuel rod bundle of a Westinghouse type PWR.

The core and the upper plenum are enveloped by honeycomb thermal insulators to minimize the wall thermal effects.

More detailed information on SCTF is available in references (4) and (5).

2.2 Test Conditions and Procedure for Radial Power Profile Tests

Test S2-SH2 (flat radial power distribution) and Test S2-06 (steep radial power distribution) were performed to investigate the effects of radial core power distribution on the two-dimensional thermal-hydraulic behavior in the core. These two test results are compared with the

COBRA/TRAC results in Chapter 4. Major test conditions for these two tests are listed in Table 2.1.

These two tests were performed under almost the same conditions with each other except the radial core power distribution. The normalized bundle power for Test S2-06 was 1.0 (Bundles 1 & 2), 1.2 (Bundles 3 & 4), 1.0 (Bundles 5 & 6) and 0.8 (Bundles 7 & 8) while that for Test S2-SH2 was 1.0 for all bundles. The total core heating power and the initial stored energy in the core were set to be the same for these two tests.

The test conditions commom to these two tests have been selected to reasonably represent the situation of the typical reflood phase of a PWR-LOCA. However, the accumulator injection rate was reduced from the scaled injection rate and the injection period was extended from the typical case for preventing from the significant U-tube oscillation occurred during the accumulator injection period at the scaled injection rate(6). The accumulator injection water temperature was determined so as to give the same core inlet water temperature as in a typical CCTF test. The LPCI flow rate was also reduced from the scaled value of a 1,100 MWe Westinghouse type PWR for compensating the weak steam binding effect in SCTF. The accumulator and LPCI flow rates were 19.3 and 5.41 kg/s, respectively, which correspond to about 5.71 and 1.59 cm/s of nominal flooding velocities. The intended system pressure in the containment tanks was 0.2 MPa.

The test procedure for these two tests is as follows. After setting the initial pressure and temperature conditions, core heating was initiated. In order to make the initial stored energy the same, when four cladding temperatures exceeded 1013 K and 1137 K for Tests S2-SH2 and S2-06, respectively, the accumulator injection into the lower plenum was initiated. The initial saturation water level in the lower plenum was 0.14 m below the bottom of heated part. After keeping the core power constant for 40 s from accumulator injection initiation, the core power decay simulation started simulating the reactor power transient from 40 s after shutdown. The decay curve was based on the 1.02 x (ANS standard+Actinides). The injection location was switched from the lower plenum to the intact cold leg at 55 s after the accumulator injection initiation. At this time, accumulator injection was terminated and LPCI injection was initiated. At 900 s after the initiation of LPCI injection, the test was terminated.

The chronologies of major events for these two tests are summarized in Table 2.2.

2.3 Two-Dimensional Thermal-Hydraulic Behavior Observed in the Tests

Two kinds of two-dimensional effects on the core thermal behavior were observed in these two tests.

Figures 2.3 and 2.4 show the transients of cladding temperatures and heat transfer coefficients in Bundles 2, 4 and 8 at 2.33 m from the bottom of heated part in Tests S2-SH2 and S2-06. As shown in these figures, the heat transfer in the core was enhanced for the higher power bundle (Bundle 4) and degraded for the peripheral lower power bundle (Bundle 8) and resultantly the turnaround temperature was reduced for the former bundle and increased for the latter bundle in the steep radial power distribution test(Test S2-06), as compared with the test with a flat radial power distribution test (Test S2-SH2) under the same total heating power and initial core stored energy. These heat transfer behaviors are considered to be caused by the two-dimensional flow induced by the radial power profile.

Figure 2.5 shows the collapsed liquid level in the upper plenum in these two tests. As shown in this figure, the collapsed liquid level in the upper plenum was higher in the hot leg side (Bundle 8 side) than in the opposite side and the difference increased with time due to the water carryover to and de-entrainment in the hot leg side and, in addition, the flow reversal in the hot leg in the later portion of the transient. The variation of radial power distribution has little effect on the non-uniform water accumulation behavior in the upper plenum. The quench in the upper half of the core was delayed in the Bundle 8 side for these two tests as shown in Fig. 2.6. This is considered to be caused by the flow reduction trend in those bundles because the pressure in the Bundle 8 side became higher than the pressure in the Bundle 1 side due to the non-uniform water accumulation in the upper plenum.

The above-mentioned two effects were overlapped with each other in SCTF tests. However, the turnaround temperature was not much affected by the non-uniform water accumulation in the upper plenum because the effect dominated after the turnaround of the cladding temperature in the present tests.

Table 2.1 Test conditions for Tests S2-SH2 and S2-06

	Test S2-SH2 (flat power)	Test S2-06 (steep power)
Test type	modified cold leg injection	
Initial system pressure	0.2 MPa	0.2 MPa
Initial total power	7.12 MW	7.12 MW
Maximum rod temperature at BOCREC		
Bundles 1 & 2	1012 K	1060 K
" 3 & 4	1022 K	1163 K
" 5 & 6	1040 K	1072 K
" 7 & 8	1035 K	955 K
Acc injection condition		
Flow rate	19.3 kg/s	19.1 kg/s
Temperature	364 K	362 K
Time	55 s	55 s
LPCI injection condition		
Flow rate	5.41 kg/s	5.41 kg/s
Temperature	350 K	350 K
Radial power ratio		
Bundles 1 & 2	1.0	1.0
" 3 & 4	1.0	1.2
" 5 & 6	1.0	1.0
" 7 & 8	1.0	0.8
Decay curve	1.02 × (ANS + Actinides)	

Table 2.2 Chronologies of major events for Tests S2-SH2 and S2-06

(1) Test S2-SH2

	Time after BOCREC (s)
Core power "ON"	- 139
Acc injection initiation	- 2.5
BOCREC	0
Maximum containment tank-II pressure (0.217 MPa)	32.5
Core power decay initiation	37.5
Maximum core pressure (0.266 MPa)	53.5
Switching of ECC from lower plenum to cold leg and From Acc to LPCI	55
Maximum core temperature (1142 K)	145
Whole core quenched	473.5

(2) Test S2-06

	Time after BOCREC (s)
Core power "ON"	- 150
Acc injection initiation	- 3.5
BOCREC	0
Maximum containment tank-II pressure (0.217 MPa)	29
Core power decay initiation	36.5
Maximum core temperature (1244 K)	42
Switching of ECC from lower plenum to cold leg and from Acc to LPCI	54
Maximum core pressrue (0.274 MPa)	59
Whole core quenched	475.5

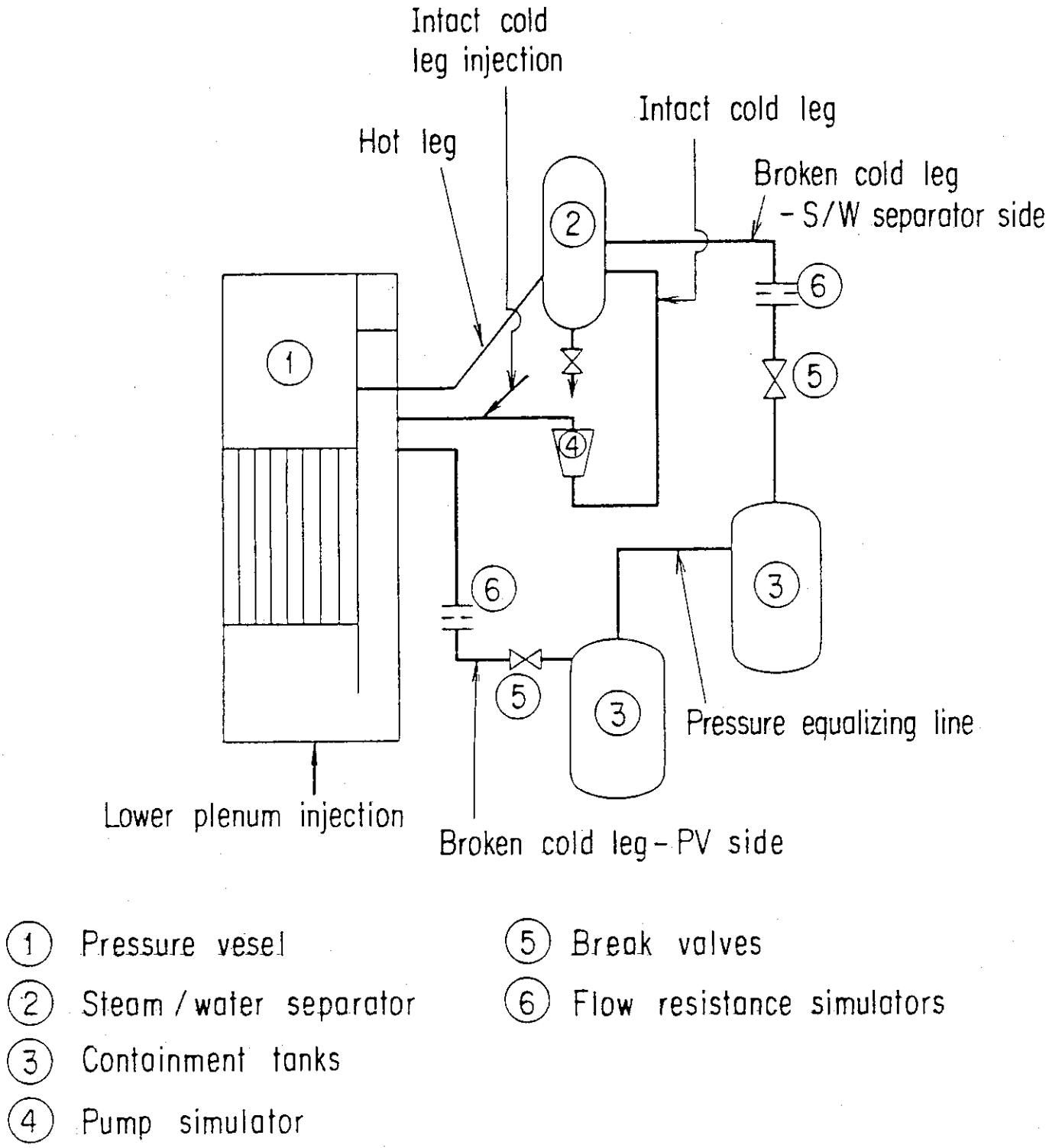

Fig. 2.1 Schematic diagram of Slab Core Test Facility

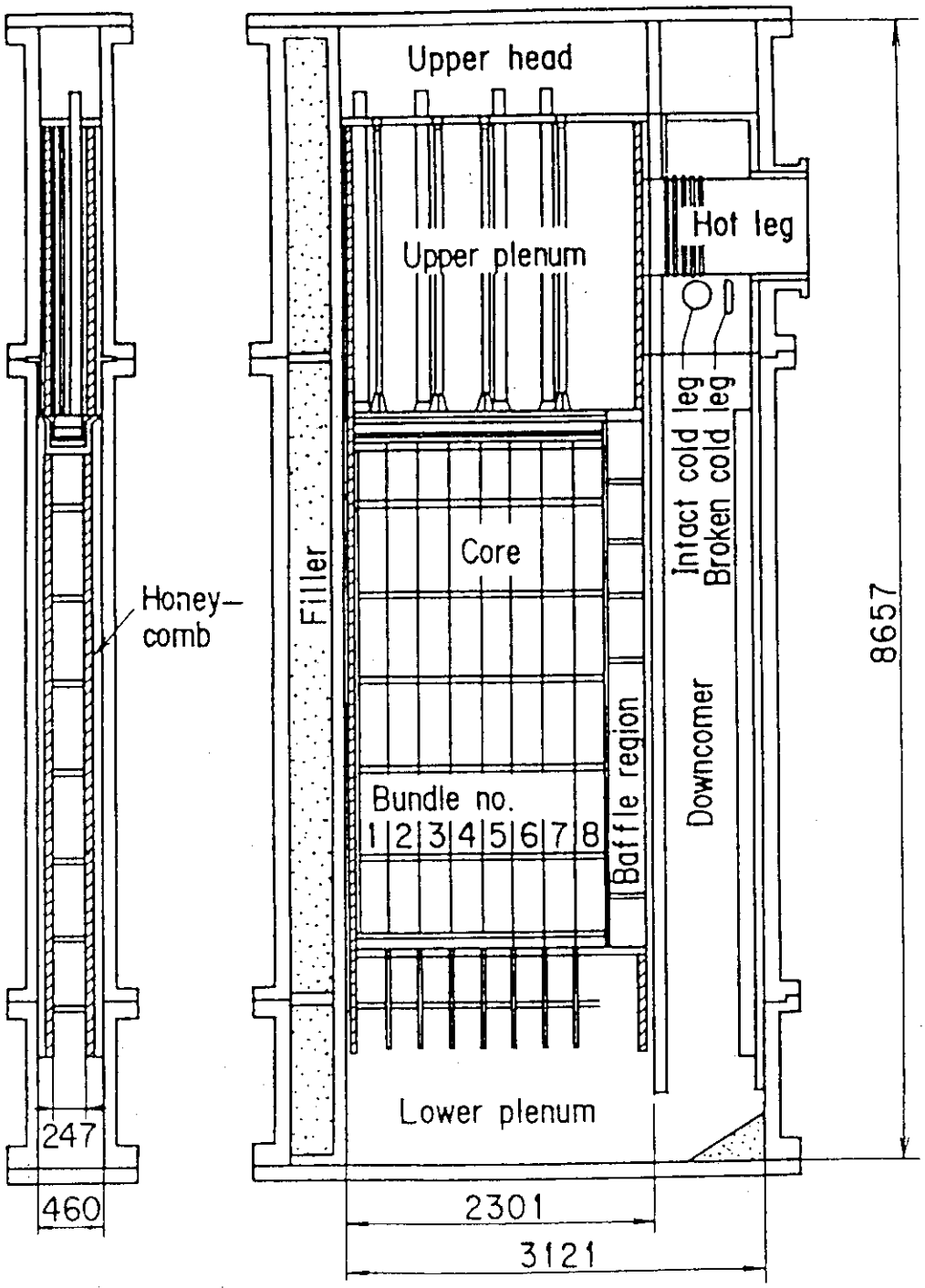

Fig. 2.2 Vertical cross section of pressure vessel

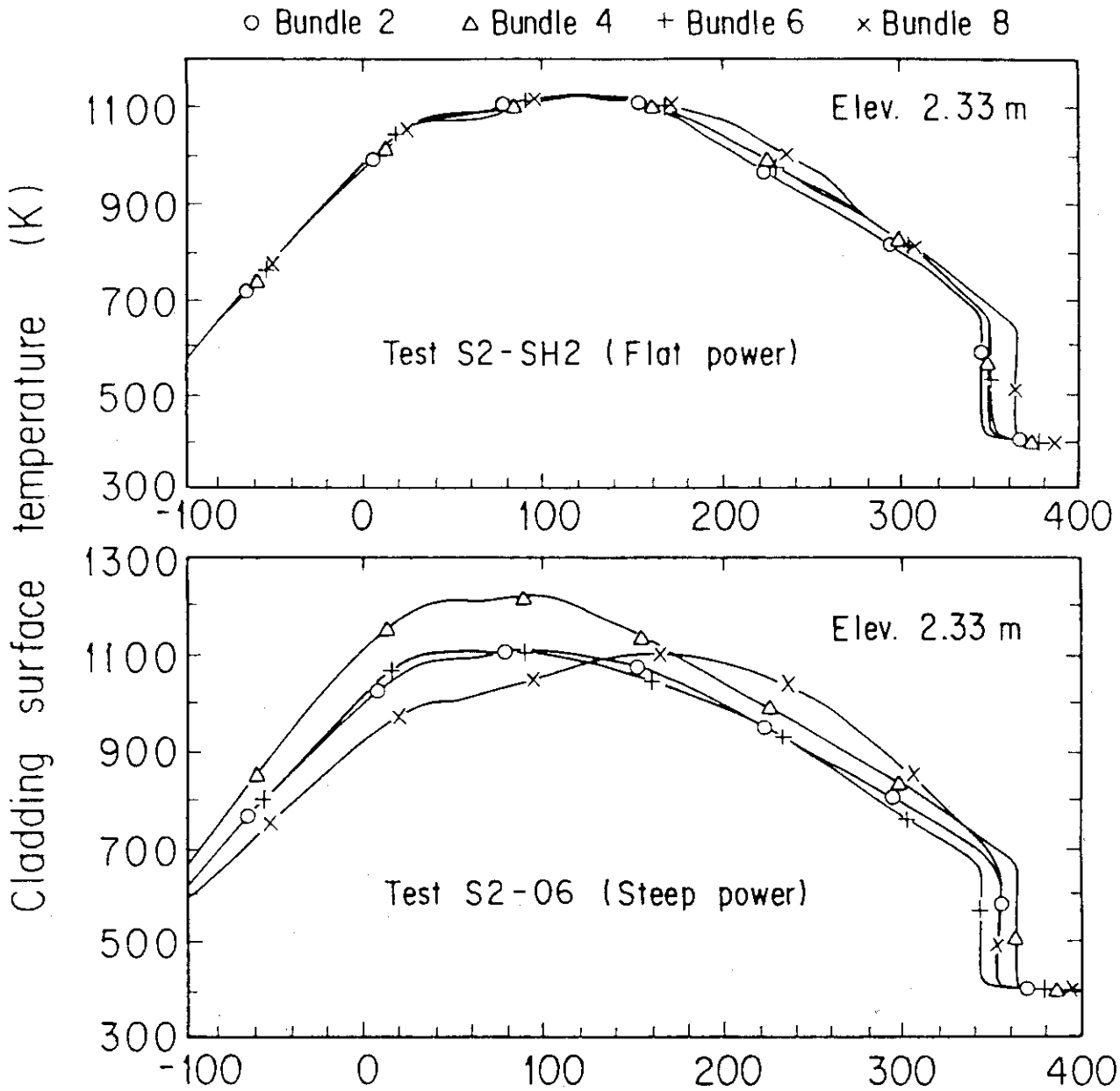

Fig. 2.3 Comparison of cladding temperatures in Bundles 2, 4, 6 and 8 in Tests S2-SH2 and S2-06

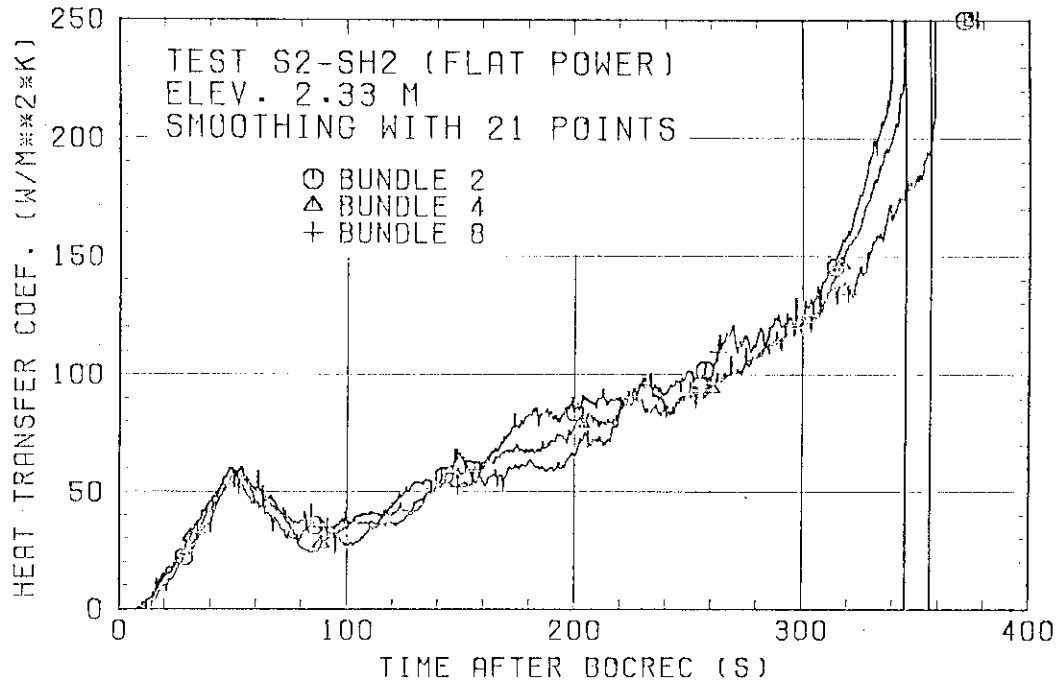

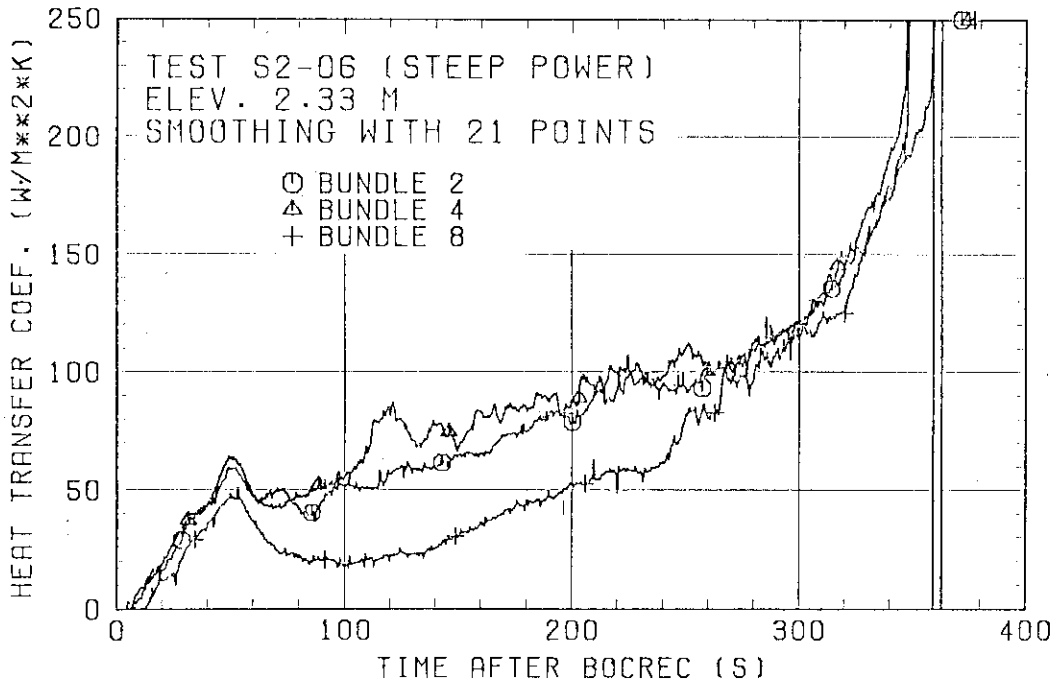

Fig. 2.4 Comparison of heat transfer coefficient in Bundles 2, 4, 6 and 8 in Tests S2-SH2 and S2-06

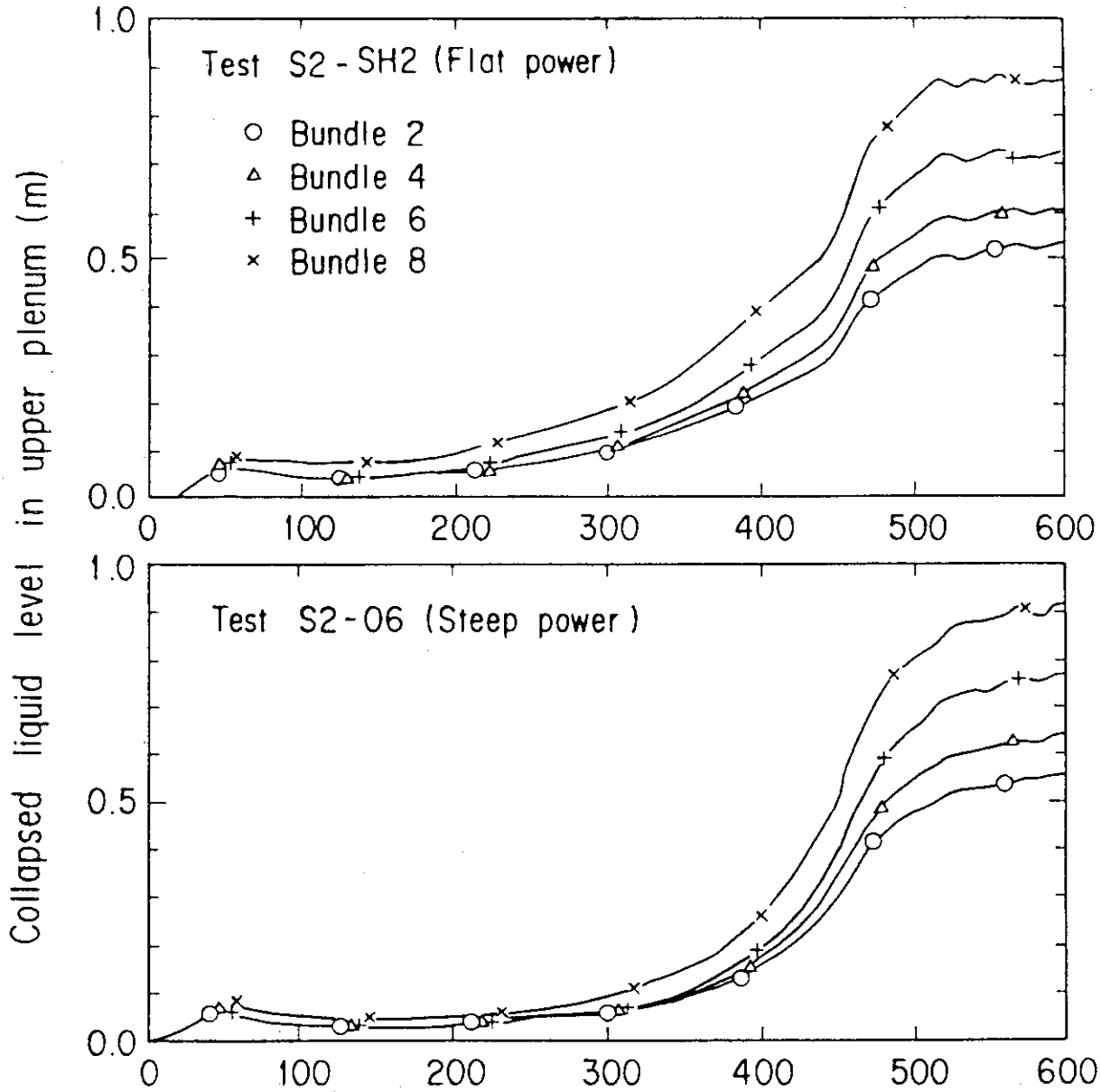

Fig. 2.5 Comparison of collapsed liquid level in upper plenum

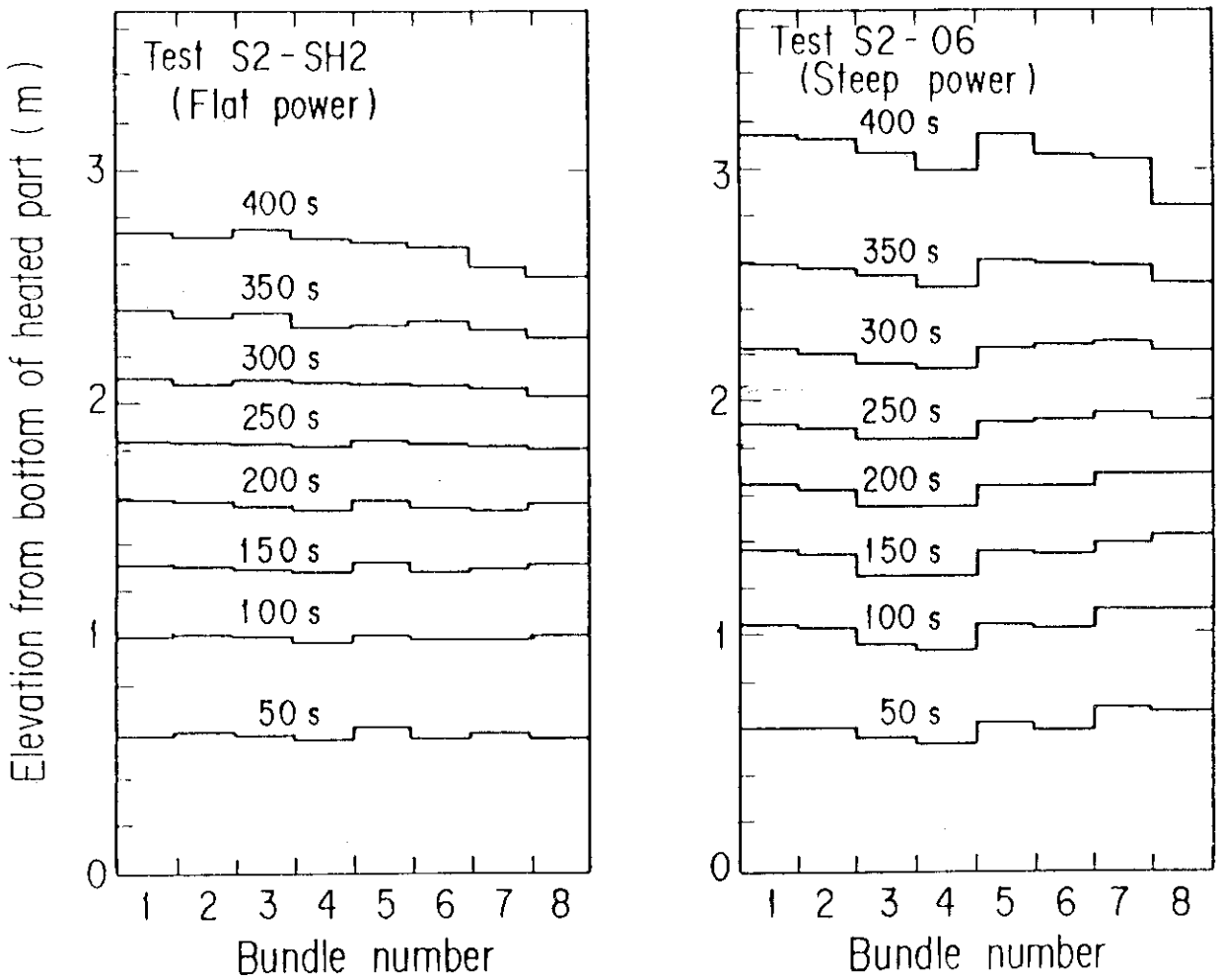

Fig. 2.6 Bottom quench front distribution in Tests S2-SH2 and S2-06

3. COBRA/TRAC INPUT MODEL DESCRIPTION

3.1 Noding Model

Figure 3.1 shows the COBRA/TRAC noding model of the SCTF core in the present study. Since the purpose of the present calculations is to investigate the two-dimensional behavior in the core, only the core part of SCTF is modeled and the core inlet flow condition and the pressure at the outlet are given as the boundary conditions. As shown in Fig. 3.1, the core is divided into six vertical and four horizontal cells. Each cell is 0.61 m high and equal to two bundles of SCTF. The horizontal and vertical flow areas and number of heated and nonheated rods for each cell are exactly corresponding to the SCTF core. The lower ends of the bottom cells are commonly connected to one lower plenum cell. The flow area of the lower plenum simulates the SCTF lower plenum but the height is 0.5 m instead of 1.717 m in SCTF. Flow rate and enthalpy boundary conditions are applied at the bottom of the lower plenum cell simulating the transients of flow rate and enthalpy at the core inlet. Each of four top cells is connected to a pipe and a break components. The upper plenum is not simulated in the present model. The flow area of each pipe component is the same as the flow area of the cells below the pipe component. Two kinds of pressure boundary conditions are used at the break components as described in Section 3.2.

In the present noding model, emergency core cooling (ECC) water is directly injected into the lower plenum and the effluent two-phase mixture flows out of the core. Therefore, the water fall back from the upper plenum into the core cannot be simulated in the present calculation.

The noding models of the heater rod and the non-heated rod are shown in Fig. 3.2. The physical properties of the heater rod are based on the heater rod for the SCTF Core-I though BN is used for the outer insulator material instead of MgO at the elevation between 1.275 and 2.385 m in the SCTF Core-IL

3.2 Initial and Boundary Conditions

In order to investigate the effects of the radial core power distribution and the non-uniform water level distribution in the upper plenum, three calculations were performed with the COBRA/TRAC code. Major calculational conditions for these three calculations are listed

in Table 3.1.

Figures 3.3 and 3.4 show the radial core power distribution and the pressure distributions at the four break components for these three cases. The radial core power distribution is flat for Cases 02 and 03 and steep for Case 01. The flat and steep power distributions are corresponding to those in Test S2-SH2 and Test S2-06, respectively. The pressure distribution at the top of the core is flat for Cases 01 and 02 and inclined for Case 03. Although the flat upper plenum water distribution was not observed in the SCTF tests, the flat pressure boundary condition at the top of the core was adopted in Cases 01 and 02 in order to separately evaluate the effect of radial core power distribution under the condition of flat water distribution in the upper plenum. The inclined pressure distribution at the top of the core in Case 03 does not quantitatively simulate the transients of accumulated water level in the upper plenum in the SCTF test results shown in Fig. 2.5, because the major purpose of the present calculation is not to quantitatively simulate the SCTF tests but to investigate the two-dimensional thermal-hydraulic characteristics under a simplified water distribution in the upper plenum. The pressure distribution at the top of the core in Case 03 was varied stepwise. That is, the pressure above Bundles 7 & 8 was the highest and the pressure above Bundles 1 & 2 was the lowest. The maximum pressure difference between Bundles 7 & 8 and 1 & 2 is 2 KPa which is almost comparable to the maximum difference of upper plenum water level between Bundles 8 and 1 in Test S2-06 as shown in Fig. 3.4.

Other input data except the radial power profile and the pressure distribution at the core outlet are the same for these three calculations. These input data were basically based on the test conditions and results of Test S2-06 which is the steep radial power distribution test in the SCTF Core-II cold leg injection test series.

Figure 3.5 shows the axial power profile in the SCTF heater rod and the corresponding COBRA/TRAC input data. The initial surface temperatures of heater rods and non-heated rods in Case 01 were based on the corresponding temperatures in Test S2-06 at 7 s before the beginning of reflood as shown in Figs. 3.6 and 3.7, respectively. The initial radial temperature distribution in Cases 02 and 03 was flat as well as the radial power distribution and the initial axial temperature distribution in Bundles 1 & 2 in Case 01 was commonly used for all

bundles in Cases 02 and 03.

The core power transient curve used in the calculation was based on the power decay curve in Test S2-06 as shown in Fig. 3.8. The power decay curve was based on the 1.02 x (ANS standard + Actinides).

Figure 3.9 shows a comparison between the input data for the core inlet flow rate and the estimated core inlet mass flow rate obtained by a mass balance method(2) in Test S2-06. The water level in the lower plenum was set to reach the bottom of the core at 7 s to fill the lower plenum volume. During the period from 7 s to about 100 s, the transient of core inlet flow rate in Test S2-06 was not exactly simulated in the calculation because an abnormal hydraulic behavior was induced by using the estimated core inlet flow transient. During the LPCI period, the COBRA/TRAC input data agreed well with the test data.

The COBRA/TRAC input data for the transient of core inlet water enthalpy was in good agreement with the test data in Test S2-06 as shown in Fig. 3.10.

A cross flow loss coefficient is required for the calculation of cross flow rate. Since the cross flow loss coefficient should be specified as a constant value in the COBRA/TRAC code, the cross flow loss coefficient across a rod row was chosen to be 0.5 based on the COBRA/TRAC recommendation(3).

The COBRA/TRAC input data for those three Cases are listed in the Appendix.

Table 3.1 Calculational conditions

Case	Radial power distribution	Pressure distribution at top of core	CPU time*1 (s)	Calculation time (s)	Plotting interval (s)
01	steep*2	flat	6353	390	1.0
02	flat	flat	5846	390	1.0
03	flat	inclined*3	7447	390	1.0

Notes *1 FACOM M-380

*2 see Fig. 3.3

*3 see Fig. 3.4

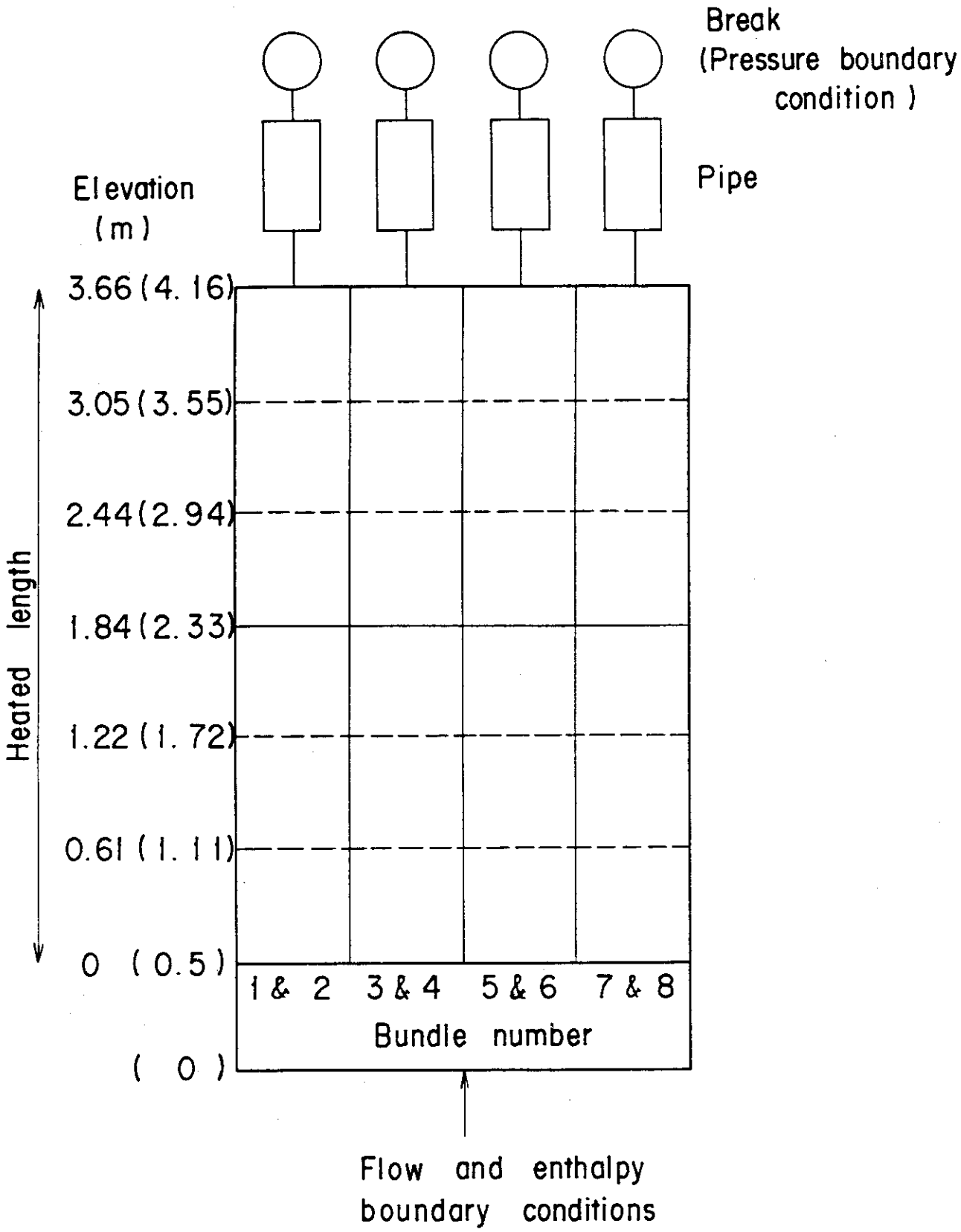

Fig. 3.1 Noding model of SCTF core

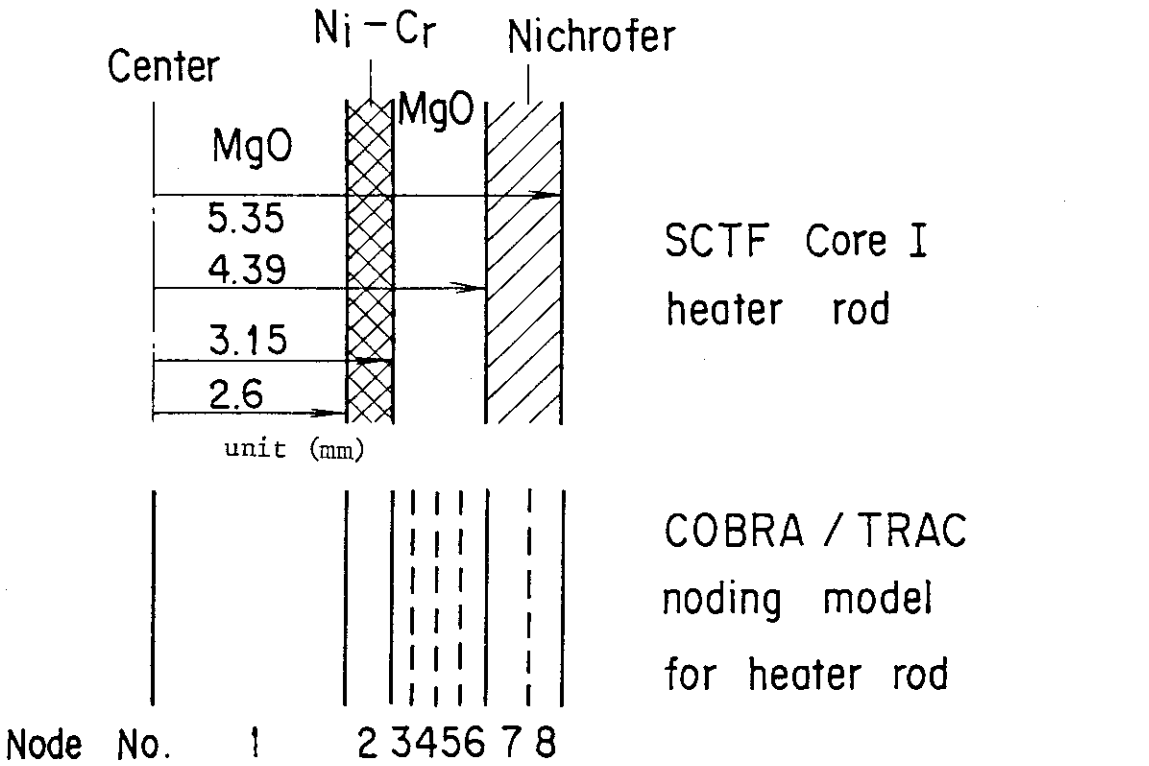

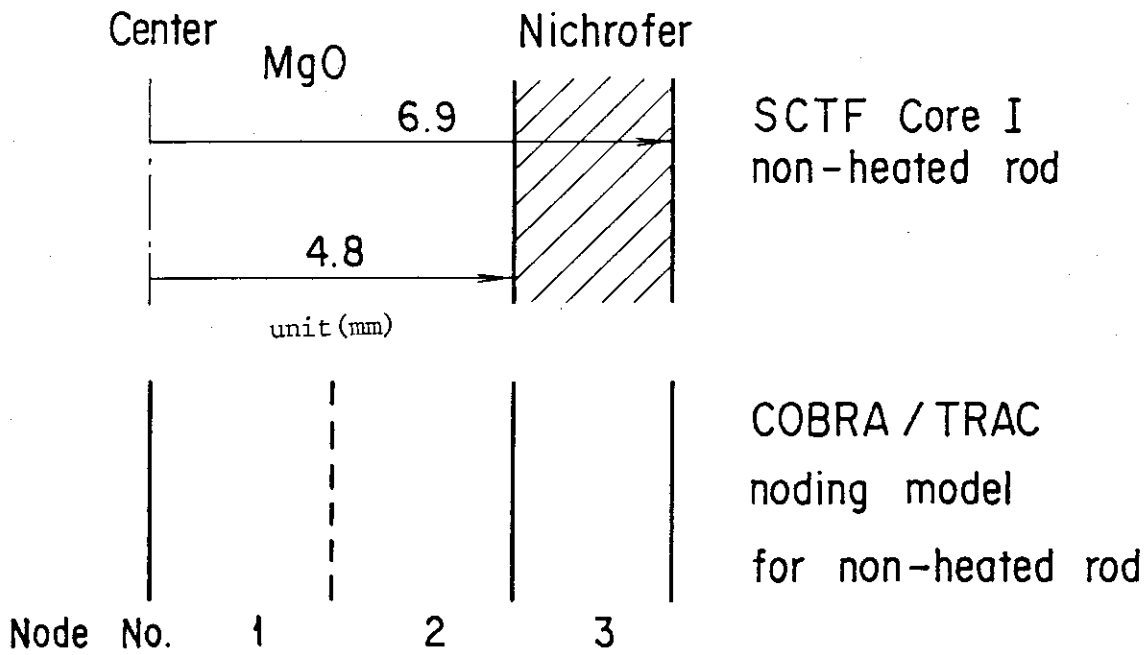

Fig. 3.2 Noding model of heater rod and non-heated rod

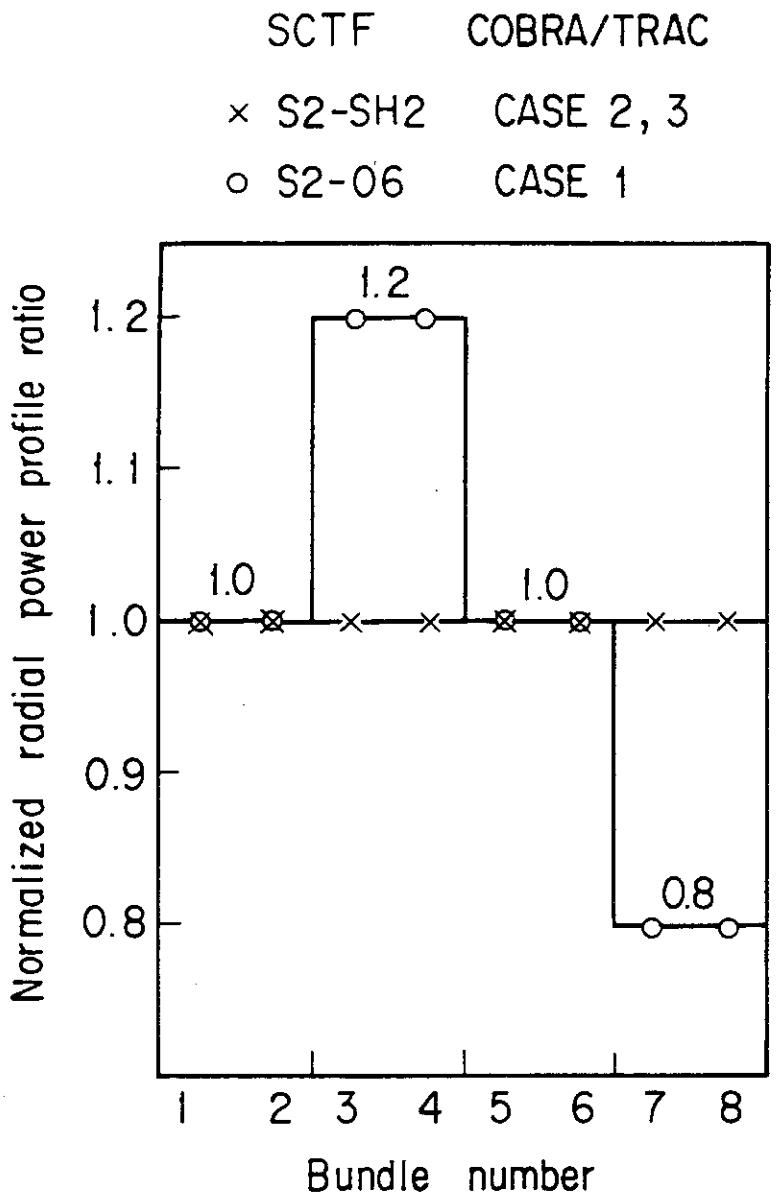

Fig. 3.3 Radial power distributions

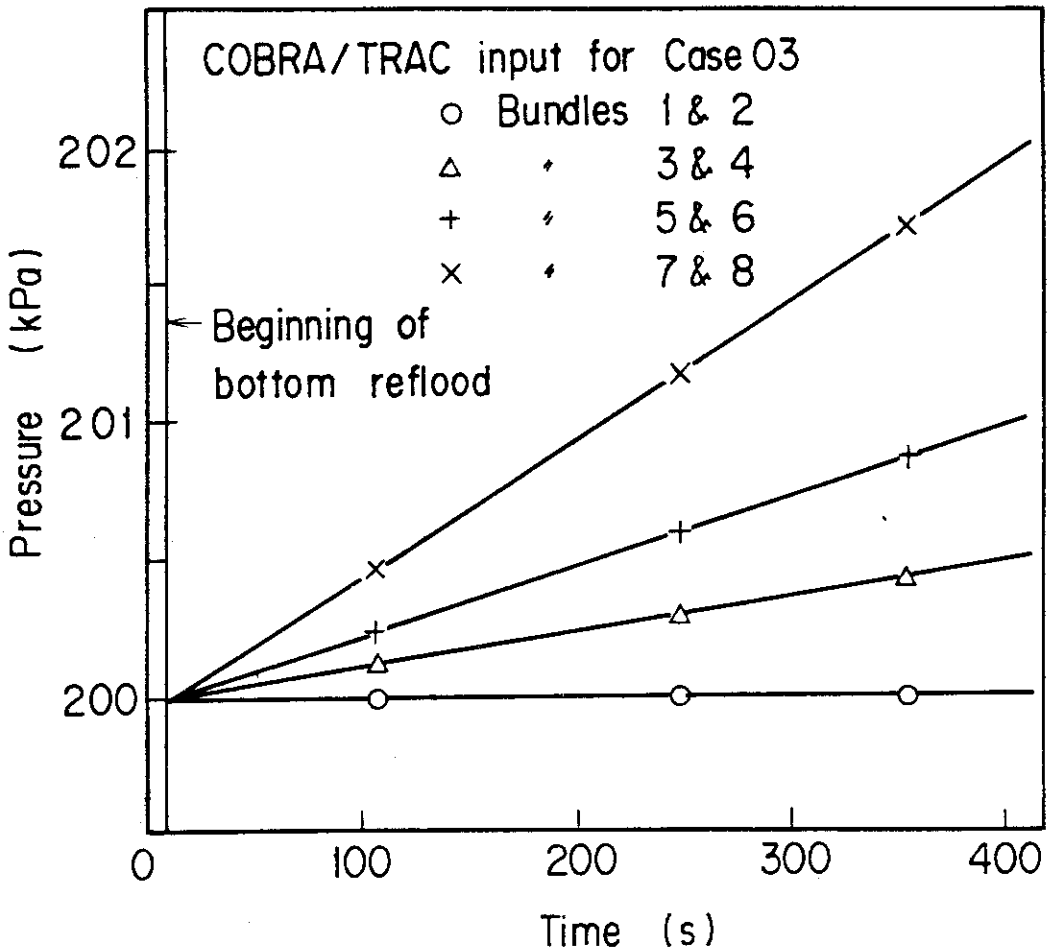

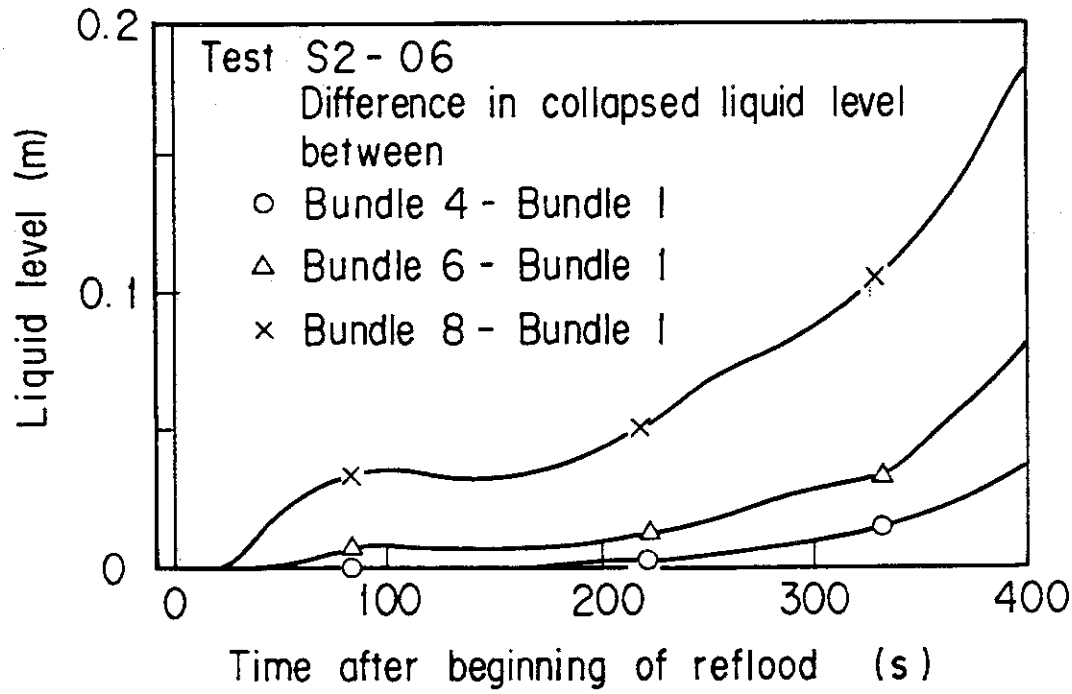

Fig. 3.4 Pressure distributions at core outlet and difference of liquid level in upper plenum for Test S2-06

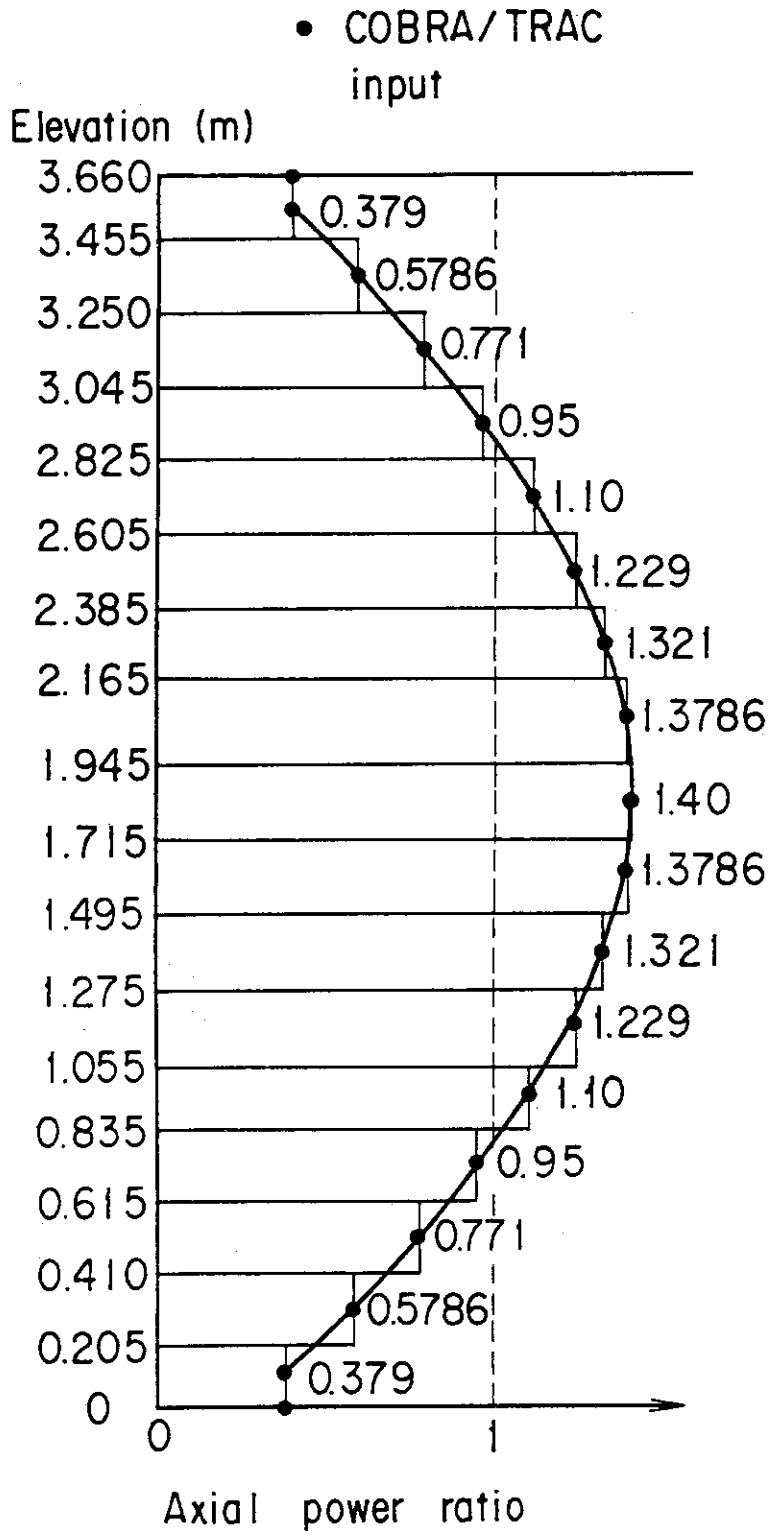

Fig. 3.5 Comparison of axial power profile between SCTF and COBRA/TRAC input data

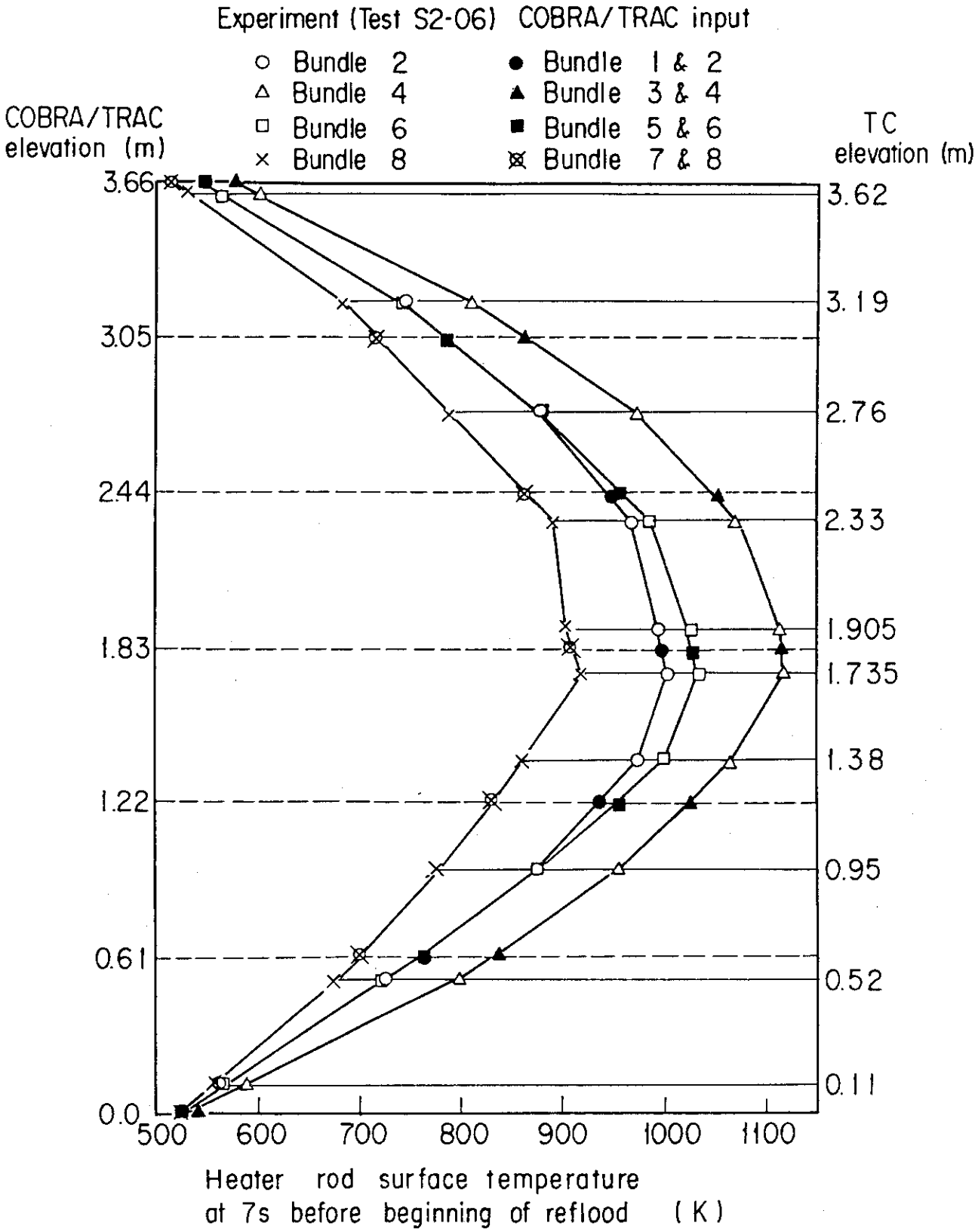

Fig. 3.6 Comparison of initial heater rod surface temperatures between SCTF data and COBRA/TRAC input data

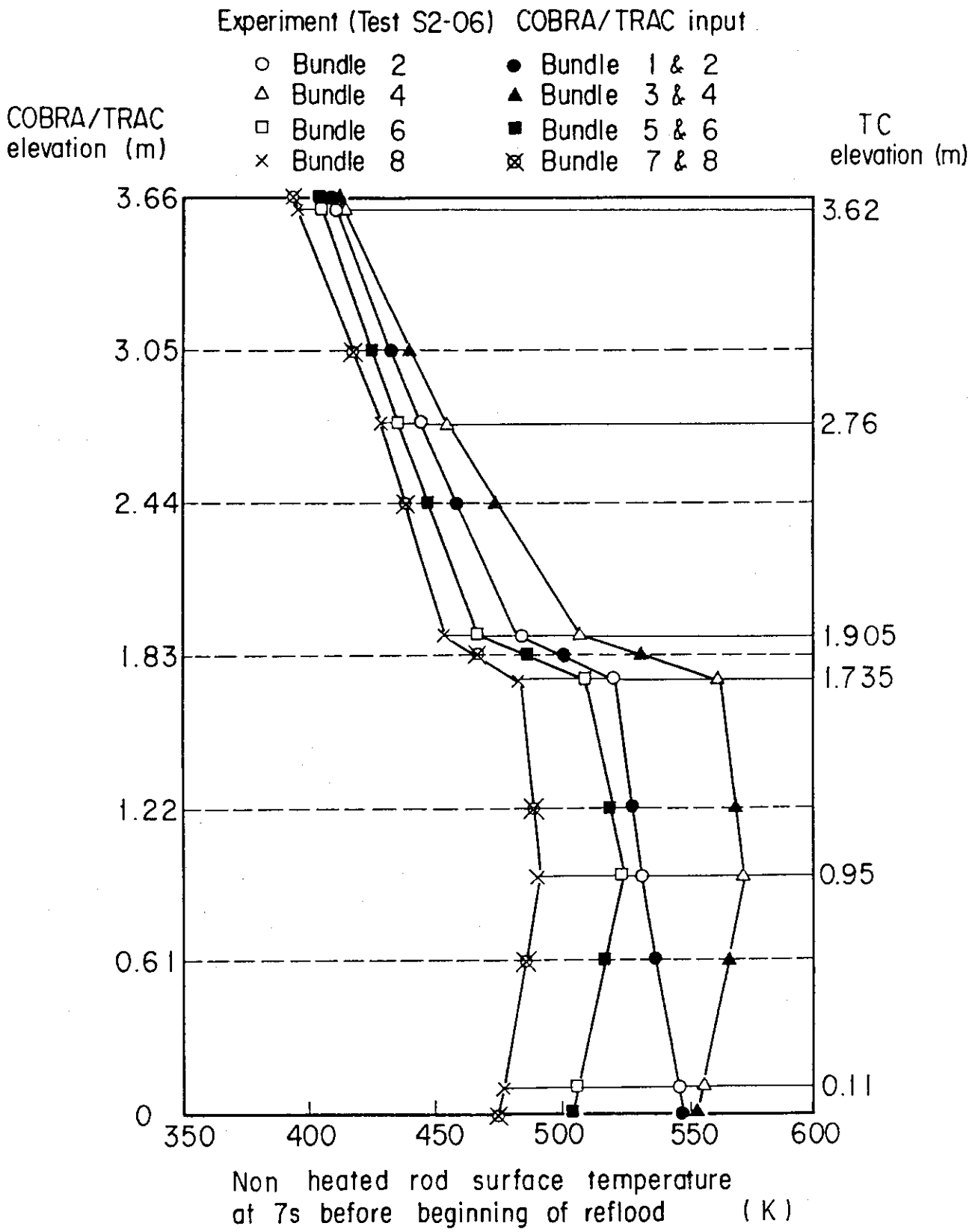

Fig. 3.7 Comparison of initial non-heated rod surface temperatures between SCTF data and COBRA/TRAC input data

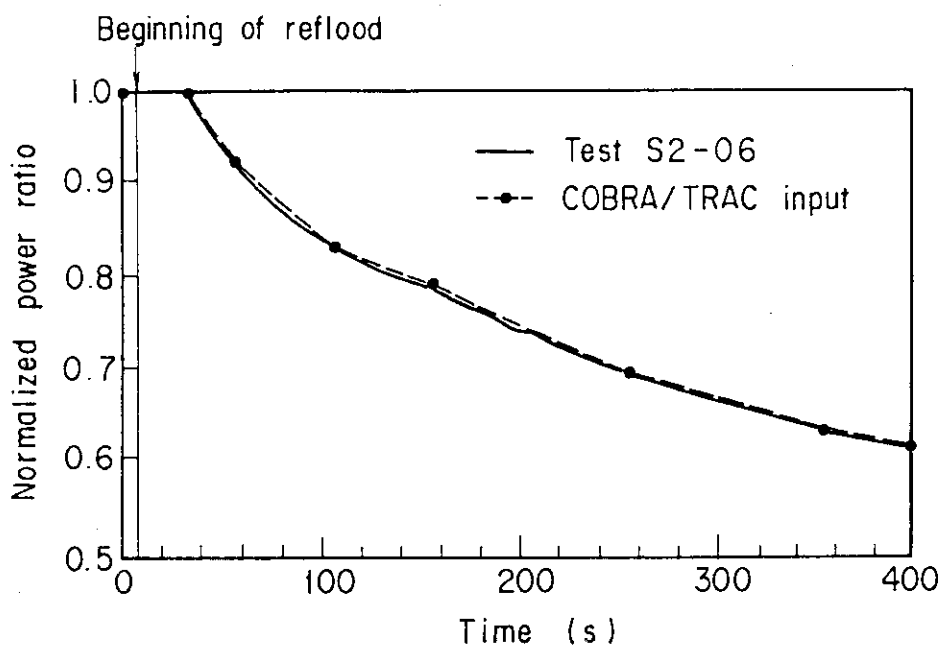

COBRA/TRAC input

Time	Power ratio
0s	1.0
34s	1.0
57s	0.922
107s	0.837
157s	0.795
257s	0.702
357s	0.646
400s	0.626

Fig. 3.8 Comparison of power transient curve between SCTF data and COBRA/TRAC input data

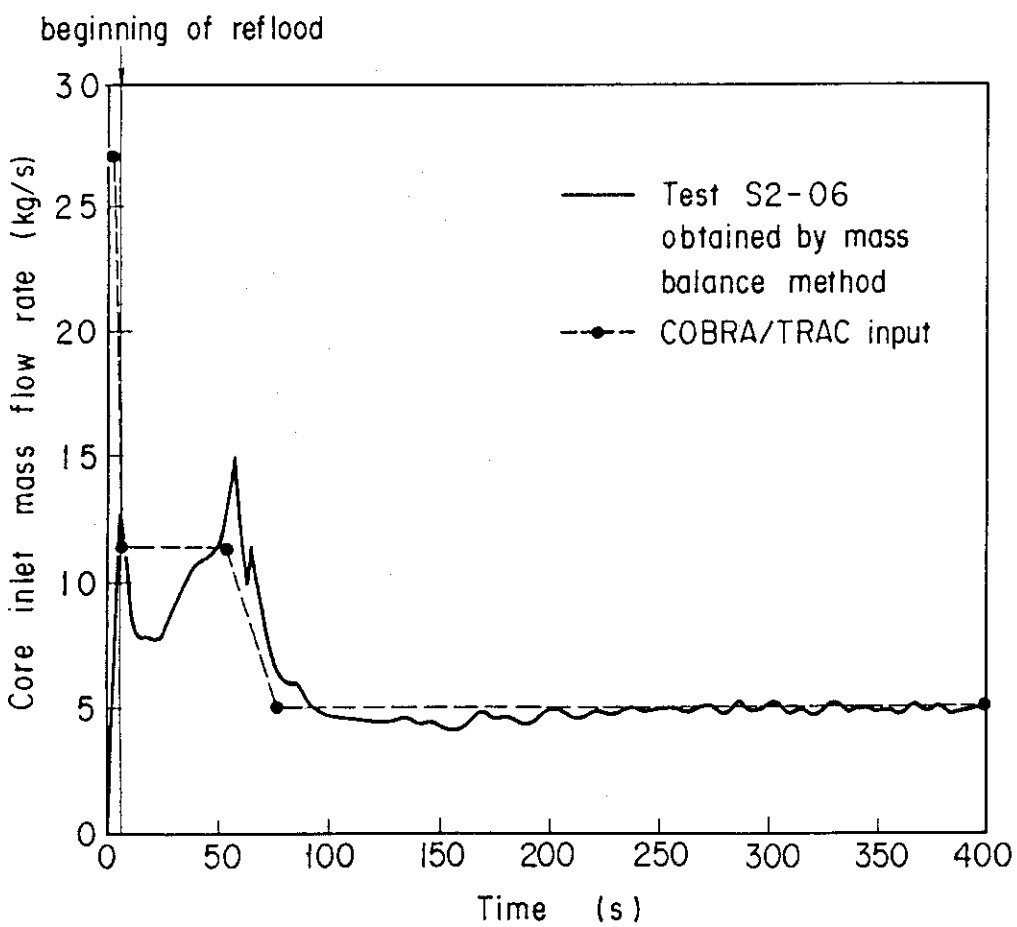

COBRA/TRAC input

Initial mass flow rate = 27 kg/s

Time	Flow rate ratio
0s	1.0
4s	1.0
7s	0.426
52s	0.426
76.5s	0.185
400s	0.185

Fig. 3.9 Comparison of core inlet mass flow rate between SCTF data and COBRA/TRAC input data

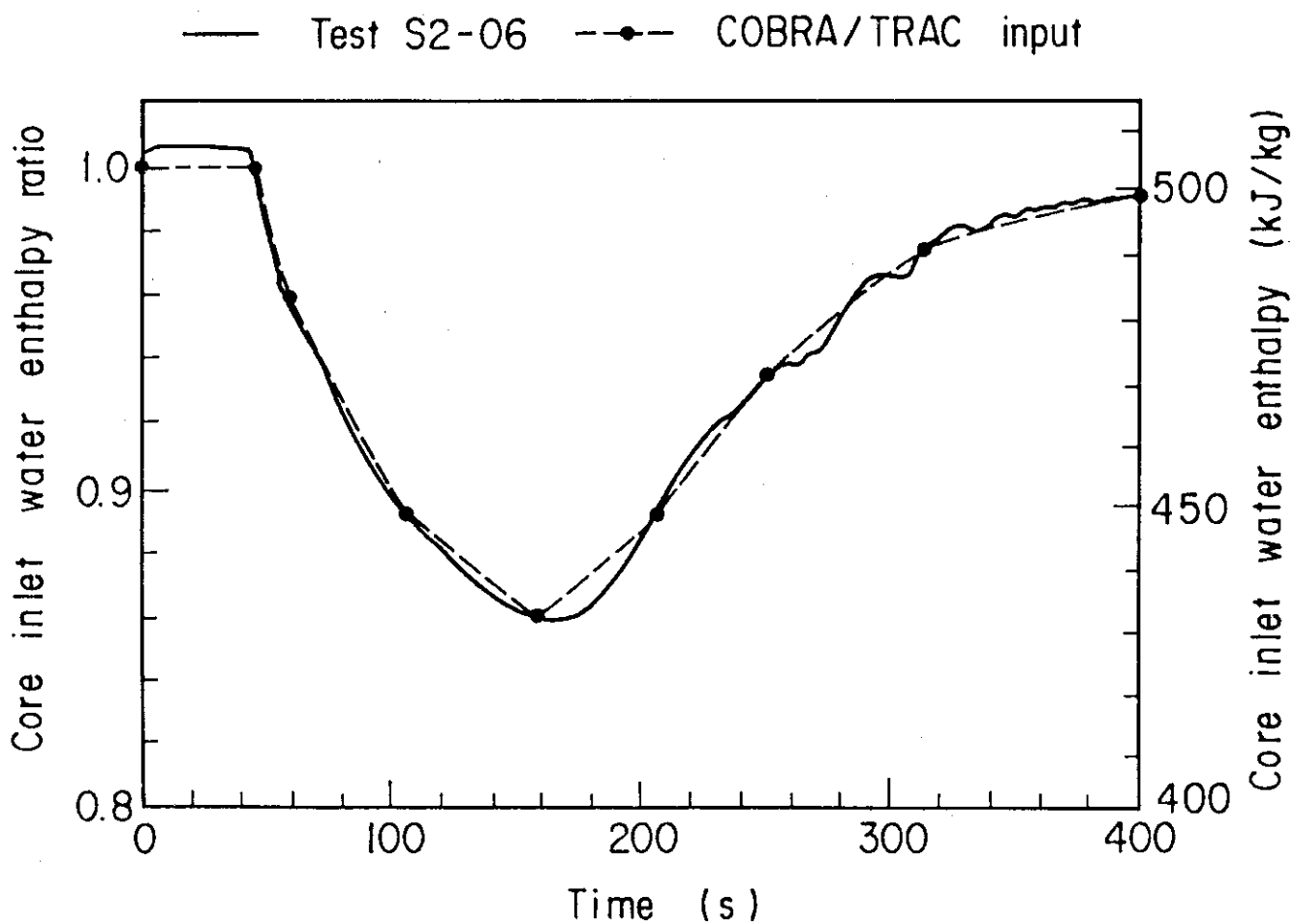

COBRA/TRAC input

Initial enthalpy = 503.7 kJ/kg

Time	Enthalpy ratio
0s	1.0
46s	1.0
57s	0.958
105s	0.890
157s	0.857
208s	0.890
250s	0.933
315s	0.975
400s	0.992

Fig. 3.10 Comparison of inlet water enthalpy between SCTF data and COBRA/TRAC input data

4. CALCULATED RESULTS AND DISCUSSIONS

4.1 Characteristics of COBRA/TRAC Results and Comparison with SCTF Results

Since the major purpose of the present study is not to correctly simulate the SCTF tests but to clarify the mechanism of the two-dimensional thermal-hydraulic characteristics induced by the radial power profile and the non-uniform upper plenum water accumulation by using the COBRA/TRAC code, the simplified transients of core inlet mass flow rate and pressure at the core outlet based on the test results of Test S2-06 were used in the calculations as shown in Figs. 3.9 and 3.4. These transients in Test S2-06 were approximately equal to those in Test S2-SH2. The other initial and boundary conditions such as the initial temperatures, the axial and radial power profiles, the power decay curve, and the enthalpy transient at the core inlet were based on the SCTF test conditions and results as correctly as possible.

Although some of the boundary conditions are not exactly corresponding to the SCTF tests, the general trends of the calculated results may be compared with the SCTF results to evaluate the predictability of the COBRA/TRAC code for the thermal-hydraulic behavior during the reflood phase.

4.1.1 Hydraulic Behavior

Figure 4.1 compares the calculated water head in the core with the measured differential pressure across the core full height. The calculated water head was obtained by the sum of water heads at all elevations. As shown in this figure, the calculated and measured transients of the accumulated water head are qualitatively similar with each other. However, the COBRA/TRAC result is higher than the SCTF result until 240 s and thereafter the COBRA/TRAC underpredicts the accumulated water head.

Figure 4.2 compares the calculated and measured void fractions at 4 elevations in the core. The measured void fractions were obtained from the vertical differential pressures by neglecting the effects of frictional and accelerational pressure drops. At the upper half of the core the calculated void fractions remain at approximately 1.0 until about 230 s at 3.05 m and 190 s at 2.44 m, respectively, after the bottom of core recovery (BOCREC) while the measured void fractions decrease to about 0.95 at about 50 s after the BOCREC. At 310 s at 3.05 m and 230 s at 2.44 m, the calculated void fractions rapidly

decrease. At the elevation of 2.44 m, the calculated void fraction increases stepwise at about 310 and 350 s. The above-mentioned rapid decrease and recovery of void fraction are seen at all elevations in the COBRA/TRAC calculations while the measured void fractions exhibit gradual and monotonous decrease. Therefore, the present version of the COBRA/TRAC code cannot predict well the void fraction transient during the reflood phase.

Figure 4.3 compares the calculated and measured horizontal differential pressures at the center elevation of the core. As shown in Fig. 4.3 (a), the average of the calculated horizontal differential pressure between the centers of Bundles 1 & 2 and Bundles 3 & 4 at elevation of 1.83 m is approximately zero. Similar is the measured horizontal differential pressure between Bundles 1 and 4 at elevation of 1.905 m, though the calculated horizontal differential pressure oscillates with much larger amplitude than the measured one due to a calculational instability. As shown in Fig. 4.3(b), on the other hand, the average of calculated horizontal differential pressure between the centers of Bundles 5 & 6 and Bundles 7 & 8 at elevation of 1.83 m is also approximately zero or even negative, while the measured between Bundles 4 and 8 is always positive (pressure is higher in Bundle 4 than in Bundle 8) during the initial 400 s. Therefore, it is indicated that the cross flow characteristics in the SCTF core cannot be predicted well by the COBRA/TRAC code.

4.1.2 Thermal Behavior

Figure 4.4 (a) through (c) show the comparisons between the calculated and measured cladding temperatures and heat transfer coefficients at three elevations. The heat transfer mode in the calculation is also shown in these figures. Since the heat transfer coefficients to vapor and liquid phases are separately calculated in the COBRA/TRAC code with two different temperatures, the calculated heat transfer coefficients in Fig. 4.4 are obtained by summing up of these two heat transfer coefficients by correcting the temperature difference as follows :

$$(HTC)_{total} = (HTC)_{liquid} + (HTC)_{vapor}(Tw-Tv)/(Tw-Ts)$$

where, $(HTC)_{total}$ = total heat transfer coefficient

$(HTC)_{liquid}$ = heat transfer coefficient to liquid phase

$(HTC)_{vapor}$ = heat transfer coefficient to vapor phase
Tw = heater rod surface temperature
Tv = vapor temperature
Ts = saturation temperature

As shown in Fig. 4.4, the heat transfer mode is initially the vapor single phase flow, and then successively changes to the dispersed flow, the ramp mode between the inverted annular flow and the dispersed flow, the transition boiling, and finally to the saturated or subcooled nucleate boiling. The inverted annular flow mode was seldom seen in the present calculations. The heat transfer regime selection logic in the present version of COBRA/TRAC code is shown in Fig. 4.5. The heat transfer correlations used in each mode are summarized in Table 4.1.

The calculated heat transfer coefficient for the period of the dispersed flow mode is larger than the measured. The calculated heat transfer coefficients in the ramp mode between the inverted annular flow and the dispersed flow, and the transition boiling mode approximately agree with the tests results.

The calculated cladding temperatures are lower than the measured temperatures especially in the dispersed flow mode in accordance with the above-mentioned heat transfer characteristics. However, the ovarall cladding temperature transients including the quench time are similar between the calculated and measured results.

4.2 Calculated Results of Flat Radial Power and Upper Plenum Water Distribution Case

In order to have the reference case for investigating the effects of radial power distribution and non-uniform upper plenum water distribution, Case 02 was calculated under the conditions of flat radial power distribution and flat upper plenum water distribution. In the present Section, the calculated results of Case 02 are described for comparing with the other cases in the following Sections.

Since some of the original calculated results such as heat transfer coefficients, void fractions and flow rates violently oscillate, those calculated results were smoothed using a moving average method in order to make clear the horizontal differences in the calculated results. For examples, the original and smoothed curves for vapor and liquid flow rates are compared in Fig. 4.6. As shown in these examples, the smoothed curve well represents the average characteristics of the calculated result but does not represent the

instantaneous value.

Figures 4.7 through 4.9 show the horizontal comparisons of cladding temperatures, heat transfer coefficients to vapor and heat transfer coefficients to liquid, respectively, at elevation of 2.14 m in Case 02. As shown in these figures, no significant horizontal difference is observed in the core thermal behavior.

Figures 4.10 through 4.13 show the horizontal comparisons of void fractions, vapor flow rates, continuous liquid flow rates, and entrained liquid flow rates, respectively, at the node boundaries of 2.44 and 1.83 m in Case 02. As shown in Fig. 4.10, the horizontal distribution of void fractions is approximately flat. The horizontal distributions of vapor, continuous liquid and entrained liquid flow rates shown in Figs. 4.11, 4.12 and 4.13 are also approximately flat especially above the quench front. After the quench at 240 s (1.83 m) or 330 s (2.44 m), slight horizontal differences in the vapor and continuous liquid flow rates are observed. These differences are considered to be caused by a calculational instability below the quench front. The negative entrained liquid flow rates observed after 240 s at 1.83 m in Fig. 4.13 are physically doubtful because the entrained liquid phase is not considered to exist below the quench front.

Figure 4.14 (a) through (c) show the flow direction and magnitude of continuous liquid, vapor and entrained liquid phases at vertical and horizontal cell boundaries at 100, 200 and 300 s in Case 02. The quench front elevation at each time is also shown in these figures. As shown in these figures, the cross flow components are relatively small in comparison to the vertical flow components for all of these three phases above the quench front. Therefore, it is suggested that the thermal-hydraulic behavior calculated under the conditions of flat radial power distribution and flat pressure distribution at the core outlet is approximately one-dimensional above the quench front. Below the quench front, however, the asymmetric cross flow of continuous liquid exists in spite of the flat radial power distribution. Therefore, the two-dimensional continuous liquid flow behavior below the quench front is not predicted well by the COBRA/TRAC code. In addition, the flow direction of entrained liquid does not agree with that of continuous liquid and vapor, suggesting that the entrained liquid behavior below the quench front is also not predicted well by this code.

4.3 Effects of Radial Power Distribution

The effects of radial power distribution on the thermal-hydraulic behavior in the core are investigated by comparing the calculated results of Case 01 (steep radial power distribution) with those of Case 02 (flat radial power distribution). These two calculations were performed with the flat pressure distribution at the outlet of the core to avoid the effect of non-uniform water accumulation in the upper plenum.

Figures 4.15 through 4.17 show the comparisons of cladding temperatures, heat transfer coefficients to vapor, and heat transfer coefficients to liquid in Bundles 1 & 2, 3 & 4, and 7 & 8 at 2.14 m in Case 01. The heat transfer modes in Bundles 3 & 4 and 7 & 8 at this elevation are shown in Fig. 4.18. The heat transfer coefficient to vapor phase is the highest in the highest power bundles 3 & 4 and the lowest in the lowest power bundles 7 & 8. This trend in the horizontal distribution of heat transfer coefficient is consistent with the test results in Test S2-06 shown in Fig. 2.4. It is noted by comparing Fig. 4.16 and Fig. 4.18 that the horizontal difference in the heat transfer coefficient to vapor phase is most clear in the dispersed flow mode. In this mode, the heat transfer to vapor phase is much larger than the heat transfer to liquid phase as shown in Fig. 4.16 and 4.17. Therefore, most of the horizontal difference in the heat transfer is attributed to the horizontal difference in the heat transfer to vapor phase.

Figure 4.19 compares the quench front distributions between Case 01 and Case 02. The quench front elevation in Case 01 is the lowest in the highest power Bundle 3 & 4 and the highest in the lowest power Bundle 7 & 8 in accordance with the radial power distribution. On the other hand, the quench front elevations in the average power Bundles 1 & 2 and 5 & 6 in Case 01 are in good agreement with the quench front elevation in Case 02, suggesting that the effect of radial power distribution is not significant in the average power bundles. On the other hand, the SCTF results indicated that the heat transfer was enhanced even in the average power bundles as well as in the higher power bundles[2].

Figures 4.20 through 4.23 show the comparisons of vapor, continuous liquid and entrained liquid flow rates, and void fractions, respectively, in Bundles 1 & 2, 3 & 4 and 7 & 8 at 2.44 and 1.83 m in

Case 01. As shown in Fig. 4.20, the vapor flow rate is higher in Bundles 3 & 4 and lower in Bundles 7 & 8. The horizontal distribution of the vapor flow rate results in the horizontal distribution of heat transfer coefficients to vapor phase as shown in Fig. 4.16. As shown in Fig. 4.21, the continuous liquid flow rate remains at low value during the dispersed flow region. Since the continuous liquid flow rate exhibits violent oscillations in the later period as shown in Fig. 4.6(b) probably due to the calculational instability below and just above the quench front, the calculated continuous liquid flow rates after about 160 s at 1.83 m and about 280 s at 2.44 m seem to be doubtful. The entrained liquid flow rate also tends to be higher in the higher power bundles and lower in the lower power bundles as shown in Fig. 4.22. It is seen in Fig. 4.23 that the rapid descrease of void fraction is earlier in the lower power bundles and later in the higher power bundles. This is due to the fact that the quench front proceeds faster in the lower power bundles than in the higher power bundles as indicated in Fig. 4.19.

Figure 4.24 (a) through (e) show the flow directions and magnitudes of continuous liquid, vapor and entrained liquid phases at vertical and horizontal cell boundaries at 50, 100, 150, 200 and 300 s in Case 01 together with the quench front distribution at each time. By 200 s when the quench front is in the lower half of the core, the vapor cross flow direction is from Bundles 3 & 4 to Bundles 7 & 8 above the quench front. The vertical vapor flow rate tends to be higher in the higher power bundles than in the lower power bundles due to the higher vapor generation rate in the former bundles. The difference of vertical vapor flow rate between Bundles 3 & 4 and 7 & 8 is most clear around the quench front because the vapor cross flow below the quench front is negliegibly small. Above the quench front, on the other hand, the vapor cross flow tends to flatten the distribution of vapor up-flow rates though the latter is still slightly higher in the higher power bundles than in the lower power bundles.

The entrained liquid flow rate also tends to become larger in the higher power bundles than in the lower power bundles because the entrainment generation rate is higher in the higher power bundles due to the higher vapor flow rate. However, the contribution of the liquid phase to the total heat transfer coefficient is relatively small

compared with the vapor phase during the dispersed flow region in this calculation as shown in Figs. 4.16 and 4.18.

Since the cross flow of continuous liquid phase below the quench front cannot be calculated well by the COBRA/TRAC code as discussed in Section 4.2, the two-dimensional flow behavior of continuous liquid phase below the quench front is not reliable in this calculation. However, it is noted that a natural convection trend is slightly observed below the quench front except the result at about 100 s. That is, the liquid vertical up-flow rate is higher in Bundles 3 & 4 and the vertical liquid flow rate is lower or even negative in Bundles 1 & 2 and 7 & 8 in comparison with Bundles 5 & 6.

4.4 Effects of Non-Uniform Water Accumulation in Upper Plenum

As shown in Fig. 2.5, the water accumulation level in the upper plenum became higher in the Bundle 8 side than in the Bundle 1 side in Tests S2-SH2 and S2-06. The non-uniform water accumulation in the upper plenum resulted in the higher cladding temperature and the later quench time in Bundle 8 after the quench front reaches the upper part of the core in Test S2-SH2[2]. The effects of the non-uniform water accumulation in the upper plenum on the thermal-hydraulic behavior in the core are investigated by comparing the calculated results of Case 03 (inclined pressure distribution at the core outlet as shown in Fig. 3.4) with those of Case 02 (flat pressure distribution). These two calculations were performed under the flat radial power distribution.

Figures 4.25 through 4.27 show the comparisons of cladding temperatures, heat transfer coefficients to vapor, and heat transfer coefficients to liquid in Bundles 1 & 2, 3 & 4 and 7 & 8 at 2.14 m in Case 03. The heat transfer modes in Bundles 3 & 4 and 7 & 8 at this elevation are shown in Fig. 4.28.

As shown in Fig. 4.25 the cladding temperature becomes higher in the Bundle 8 side though the radial distributions of initial temperature and core heating power are flat. The similar trend of cladding temperature is also observed in Test S2-SH2 as shown in Fig. 2.3 when the water level in the upper plenum becoms higher in the Bundle 8 side as shown in Fig. 2.5.

As shown in Figs. 4.26 and 4.27 the heat transfer to vapor phase is much larger than the heat transfer to liquid phase before about 220 s and thereafter the heat transfer to liquid phase is dominant. This

is approximately corresponding to the transition of heat transfer mode after about 220 s as shown in Fig. 4.28. It is also indicated in Figs. 4.26 and 4.27 that the heat transfer coefficient to vapor phase is lower in the Bundle 8 side before about 220 s and after that time the heat transfer coefficient to liquid is also lower in the Bundle 8 side. Therefore, the total heat transfer is always lower in the Bundle 8 side.

Figure 4.29 compares the quench front distributions between Case 03 and Case 02. The quench propagates uniformly in all bundles in Case 02 for all time and also in Case 03 before 100 s. On the other hand, the quench propagation velocity in Case 03 becomes higher in the Bundle 1 side and the horizontal difference of the quench front elevation increases with time after 150 s. The similar trend is also observed in Test S2-SH2 as shown in Fig. 2.6 though the difference of the quench front elevation between bundles is much less in TestS2-SH2 than in Case 03.

Figure 4.30 (a) through (f) show the directions and magnitudes of continuous liquid, vapor and entrained liquid flow rates at vertical and horizontal cell boundaries at 50 , 100, 150, 200, 250 and 300 s in Case 03 together with the quench front distribution at each time. As shown in these figures, the vapor cross flow direction above the quench front is from the Bundle 8 side to the Bundle 1 side and the flow rate increases with time as the pressure difference between bundles increases because the pressure in the Bundle 8 side becomes higher than the pressure in the Bundle 1 side as shown in Fig. 4.31. Resultantly, the vapor up-flow rate becoms higher in the Bundle 1 side though the vapor generation rate below the quench front is the same in all bundles due to the flat radial power distribution. Therefore, the heat transfer coefficient to vapor is enhanced in the Bundle 1 side and degraded in the Bundle 8 side as shown in Fig. 4.26. The horizontal distribution of vapor up-flow rate results in the horizontal distribution of the entrainment generation rate and the entrained liquid up-flow rate. Also the entrained liquid cross flow from the Bundle 8 side to the Bundle 1 side is induced by the vapor cross flow from the Bundle 8 side to the Bundle 1 side. Consequently, the void fraction at 2.44 m is larger in the Bundle 8 side than in the Bundle 1 side from about 220s to about 310 s as shown in Fig. 4.32. Since the heat transfer area to liquid phase decreases as increasing the void

fraction, the heat transfer to liquid phase becomes much lower in the Bundle 8 side than in the Bundle 1 side as shown in Fig. 4.27. The continuous liquid up-flow rate above the quench front is also slightly higher in the Bundle 1 side and considered to contribute to the higher heat transfer to liquid phase in the Bundle 1 side as well as the entrained liquid phase. However, the calculation of continuous liquid cross flow below the quench front is not reliable as discussed in Section 4.2.

Table 4.1 Heat transfer correlations used in COBRA/TRAC code for reflood phase

Heat transfer mode	mode No.	Correlation
Single phase vapor	2	Maximum of "Dittus-Boelter" turbulent convection equation and "McAdams" steam natural convection equation
Nucleate boiling	5	"Chen" nucleate boiling correlation
Subcooled nucleate boiling	4	"Chen" nucleate boiling correlation using subcooled liquid properties
Transition boiling	6	Interpolation between critical heat flux and minimum film boiling points
Dispersed flow flim boiling	9	$q'' = q''_{FC} + q''_R + q''_{W-D}$ where $q''_{FC} = H_{SPV}(T_W - T_V)$ H_{SPV} - "Dittus-Boelter" T_W - wall temp. T_V - superheated vapor temp. q''_R = wall-drop radiation heat flux given by "Sun" correlation q''_{W-D}= drop impingement heat flux given by "Forslund-Rohsenow"
Inverted annular film boiling	7	Maximum of modified "Bromley" and dispersed flow film boiling

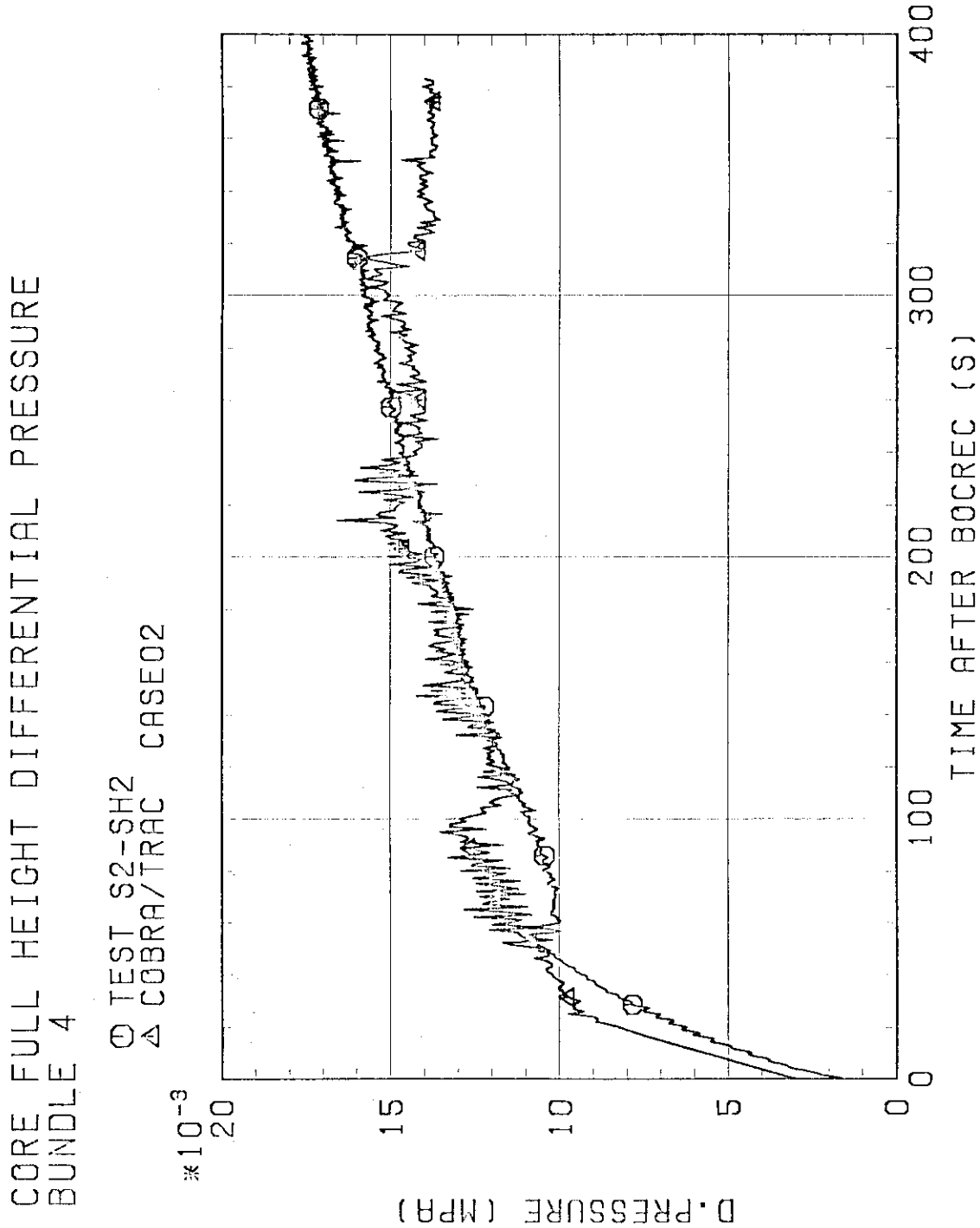

Fig. 4.1 Comparison of calculated and measured water accumulation levels

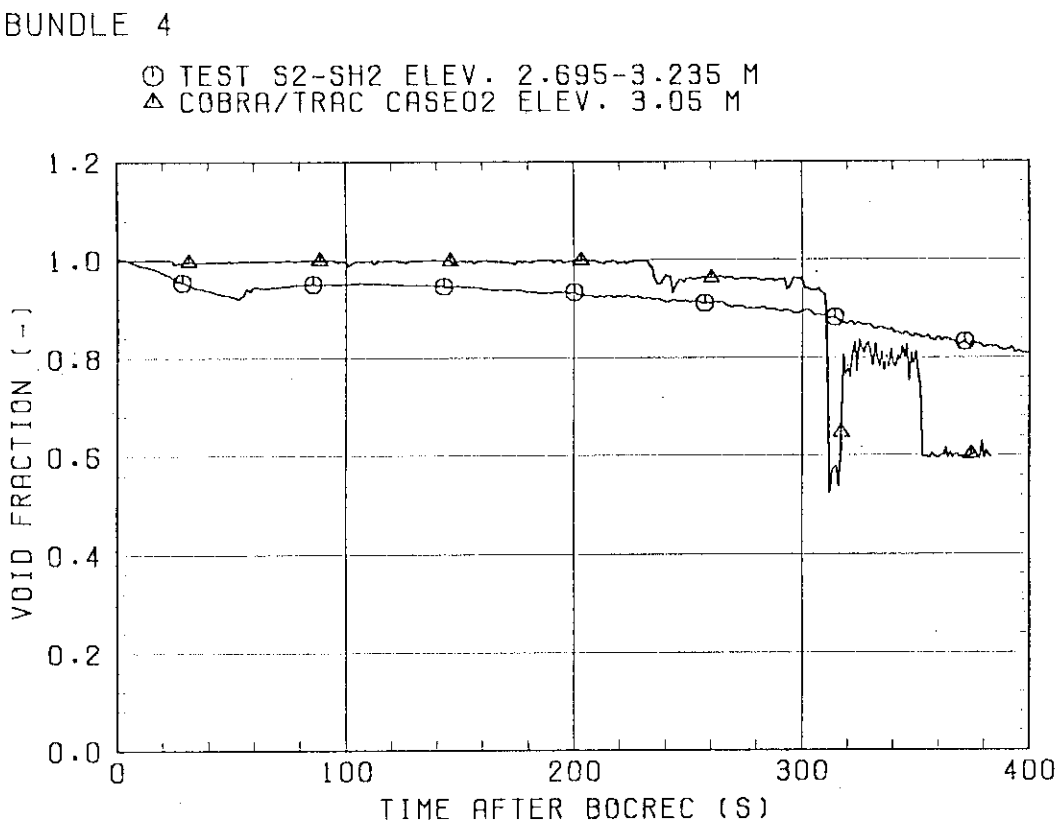

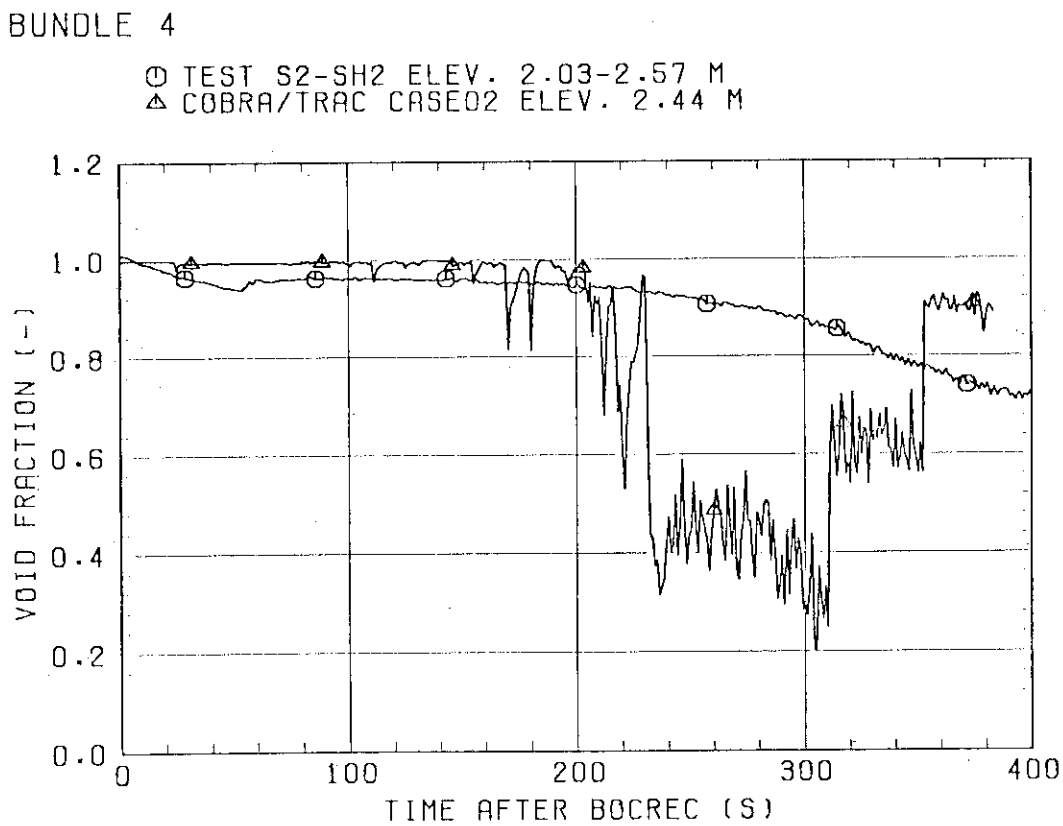

Fig. 4.2 Comparison of calculated and measured void fractions

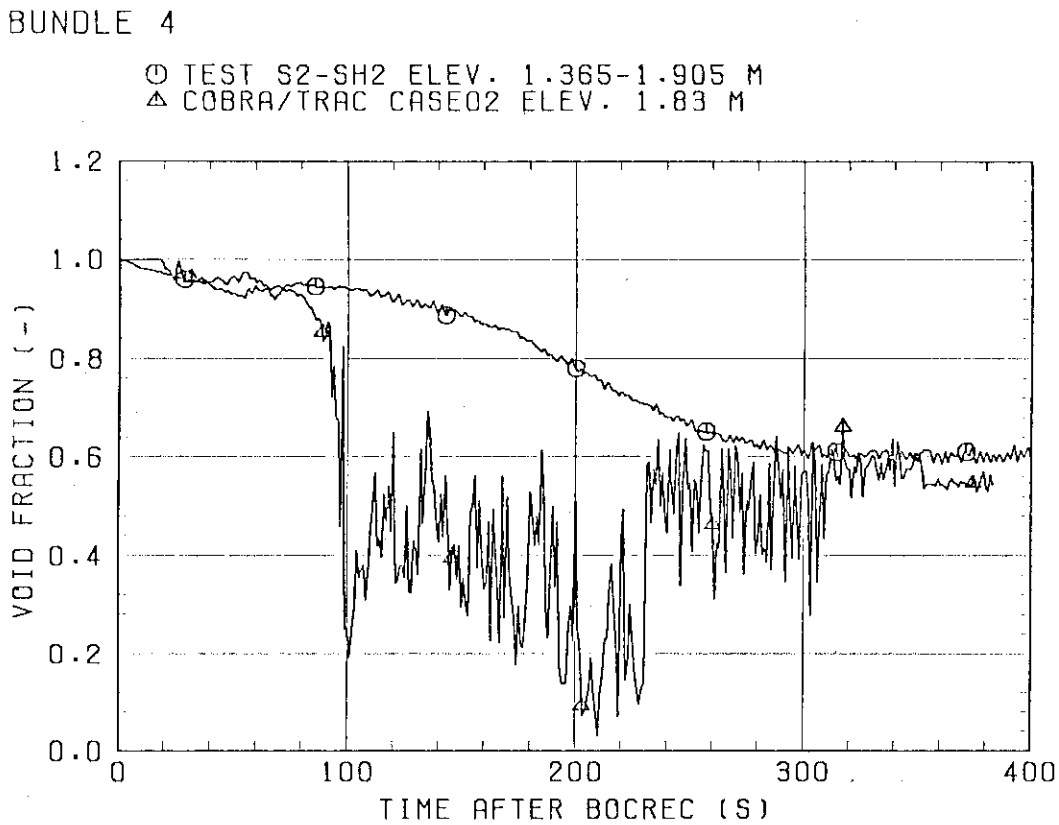

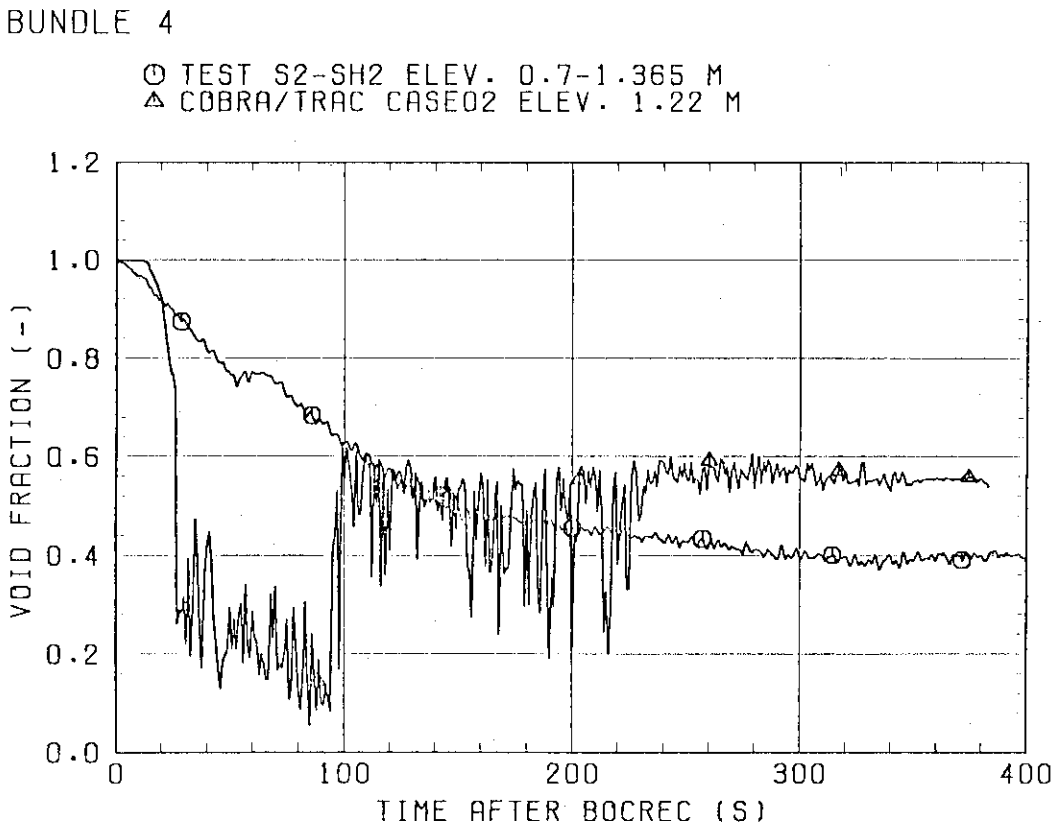

Fig. 4.2 (continue)

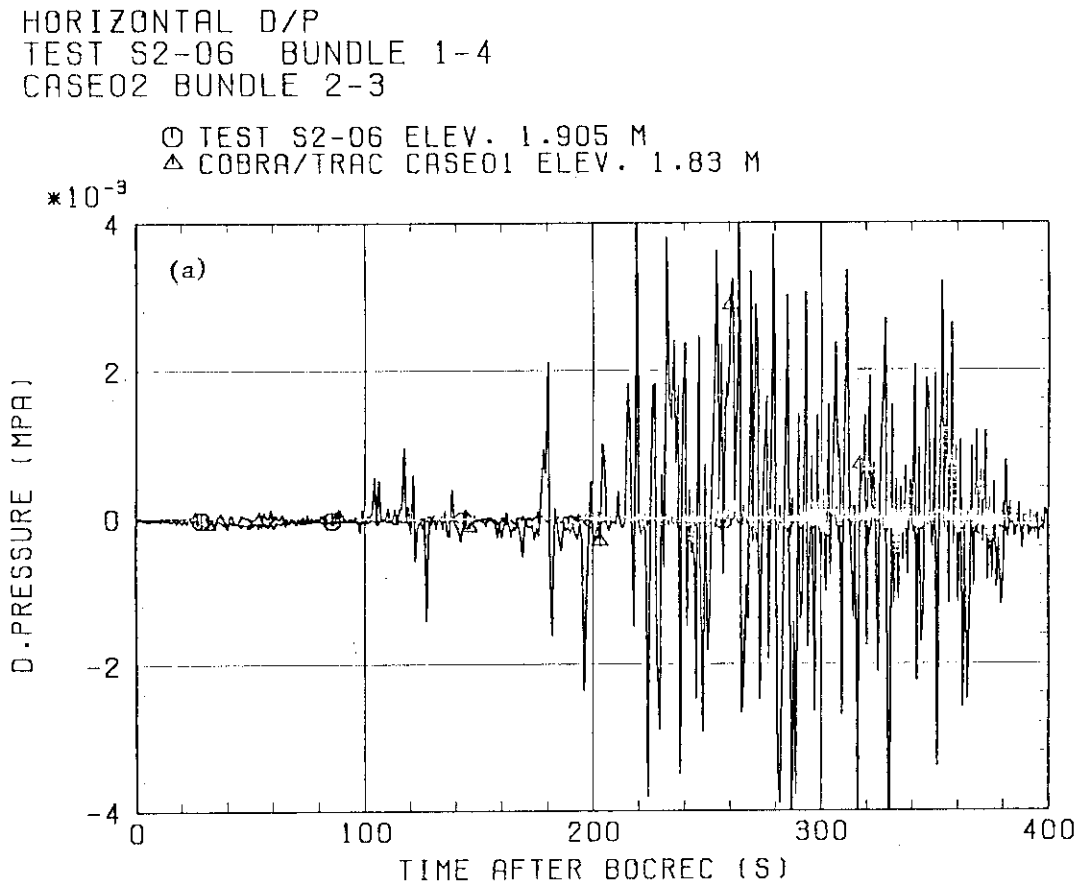

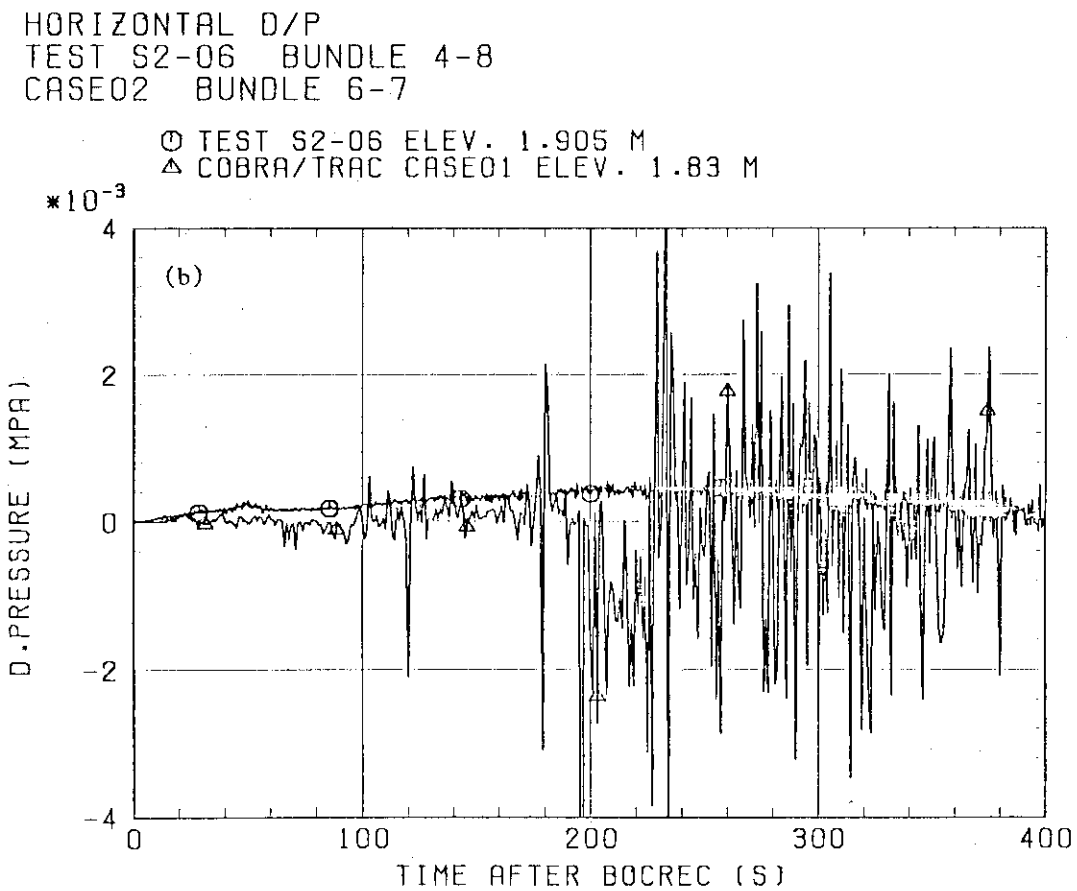

Fig. 4.3 Comparison of calculated and measured horizontal differential pressures

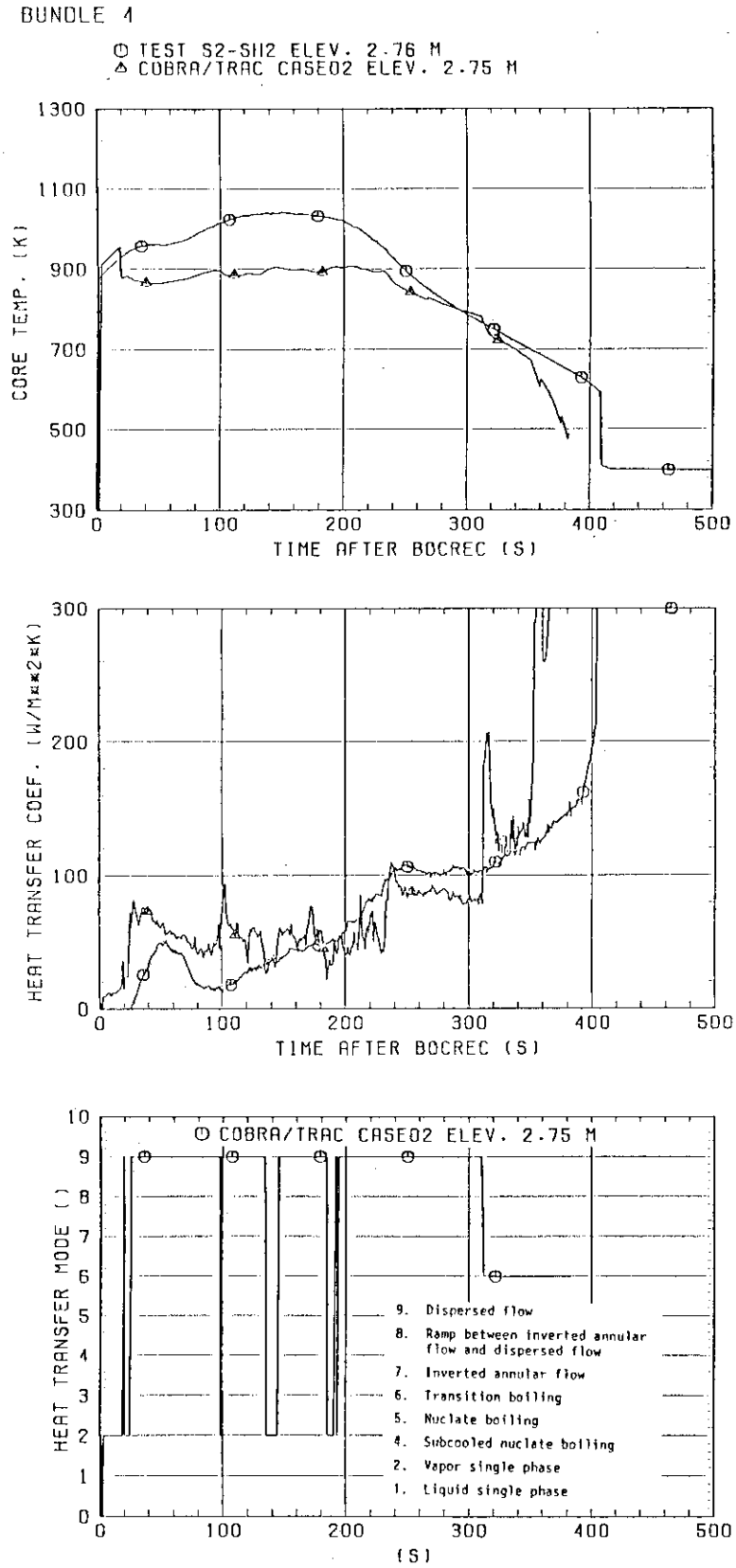

Fig. 4.4(a) Comparison of calculated and measured cladding temperatures and heat transfer coefficients and heat transfer mode (Elevation 2.75 m)

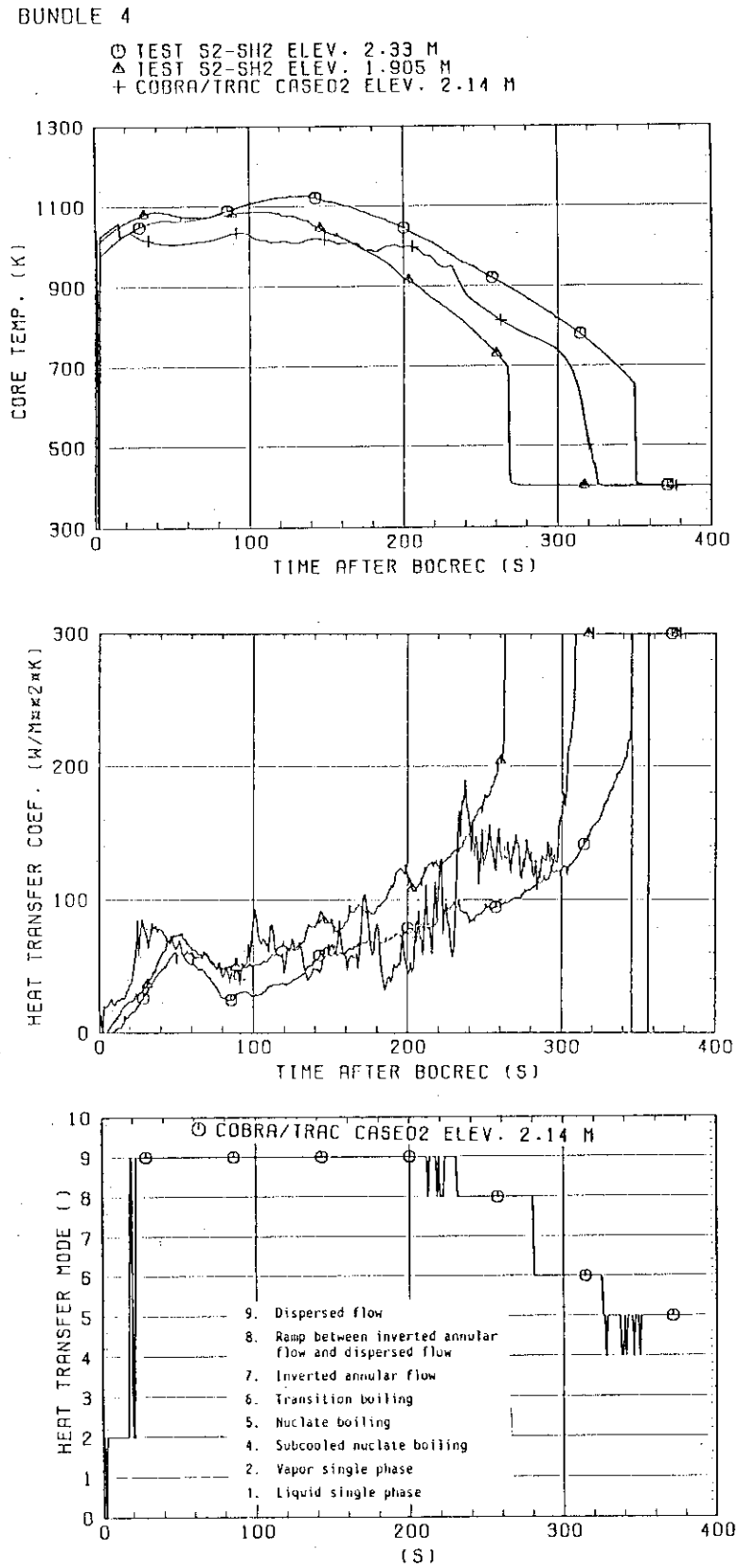

Fig. 4.4(b) Comparison of calculated and measured cladding temperatures and heat transfer coefficients and heat transfer mode (Elevation 2.14 m)

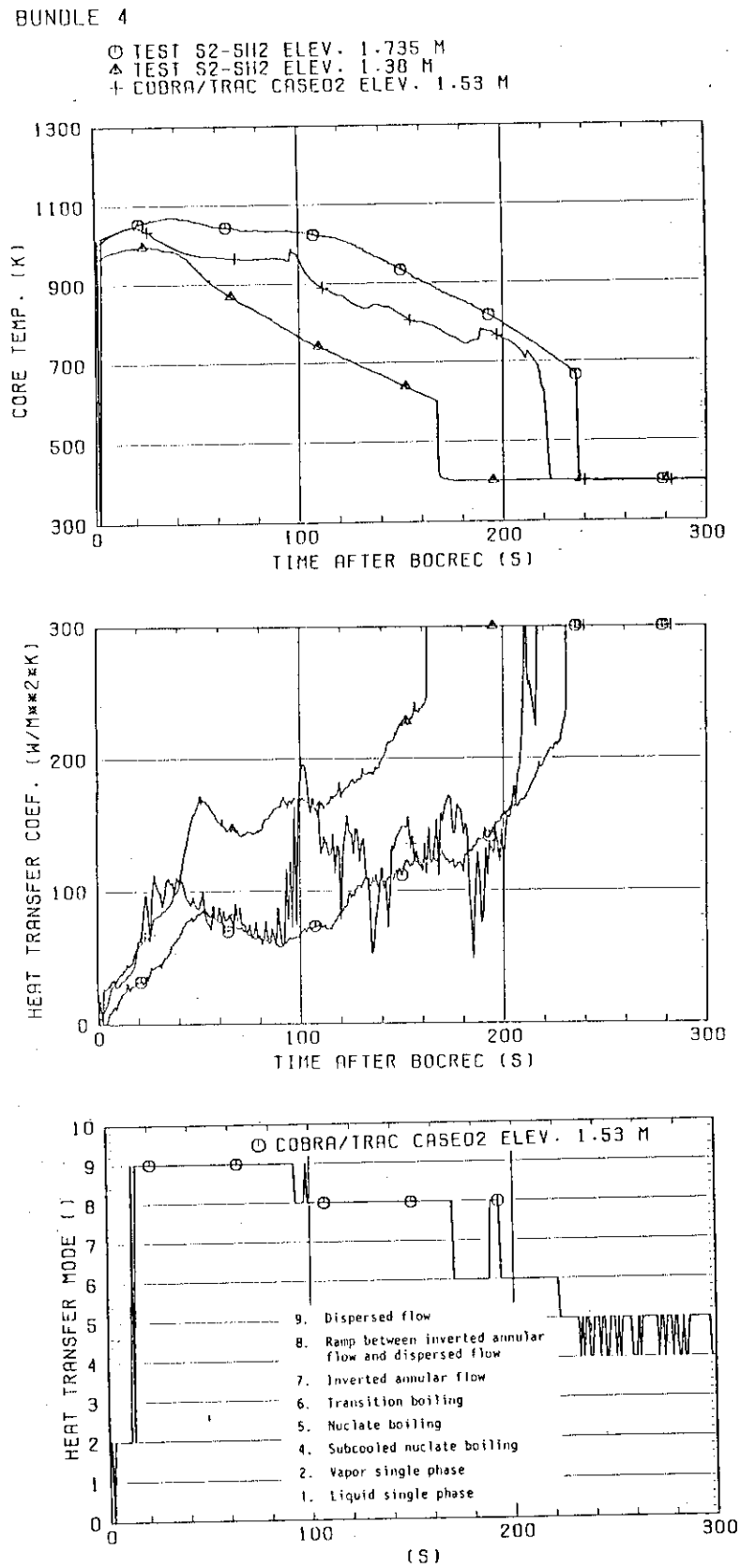

Fig. 4.4(c) Comparison of calculated and measured cladding temperatures and heat transfer coefficients and heat transfer mode (Elevation 1.53 m)

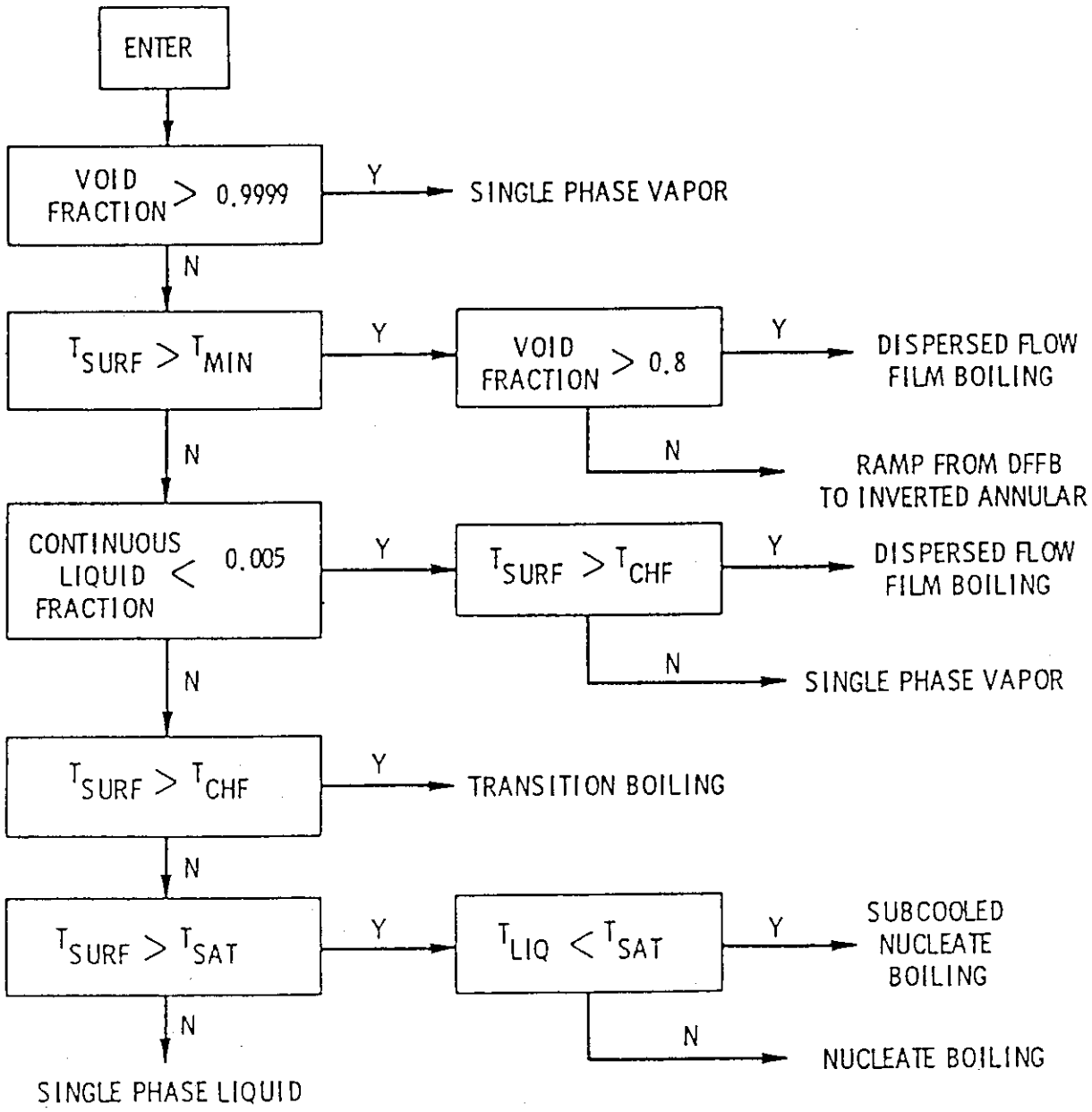

Fig. 4.5 Heat transfer regime selection logic

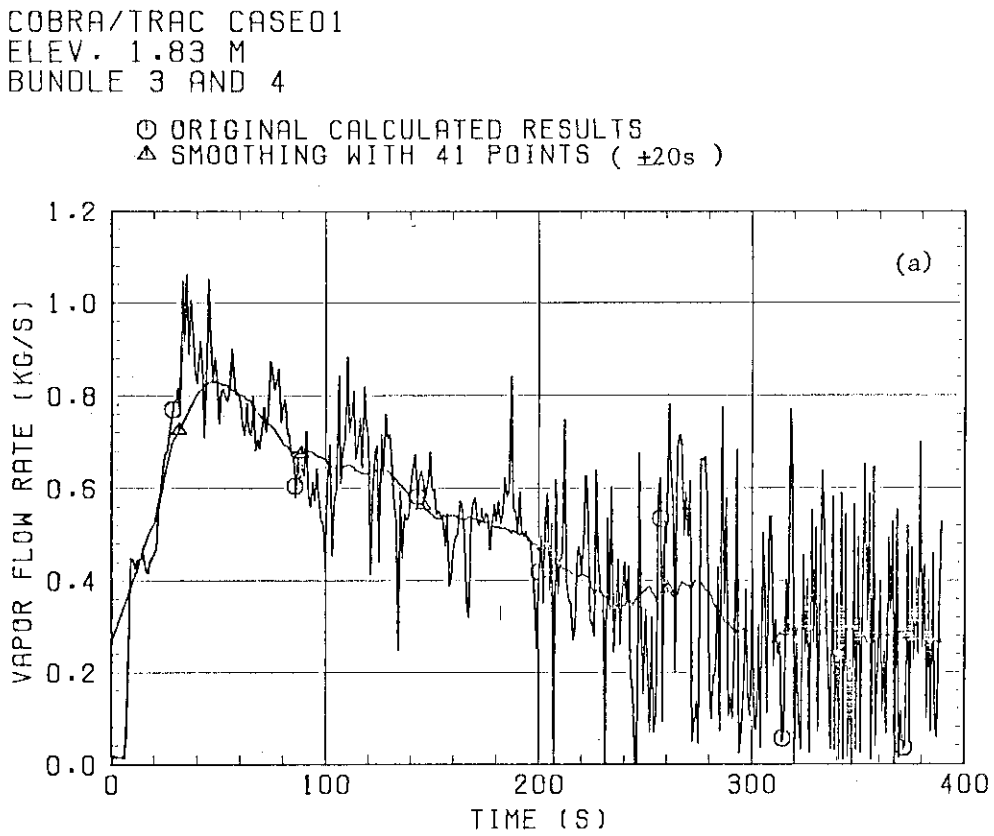

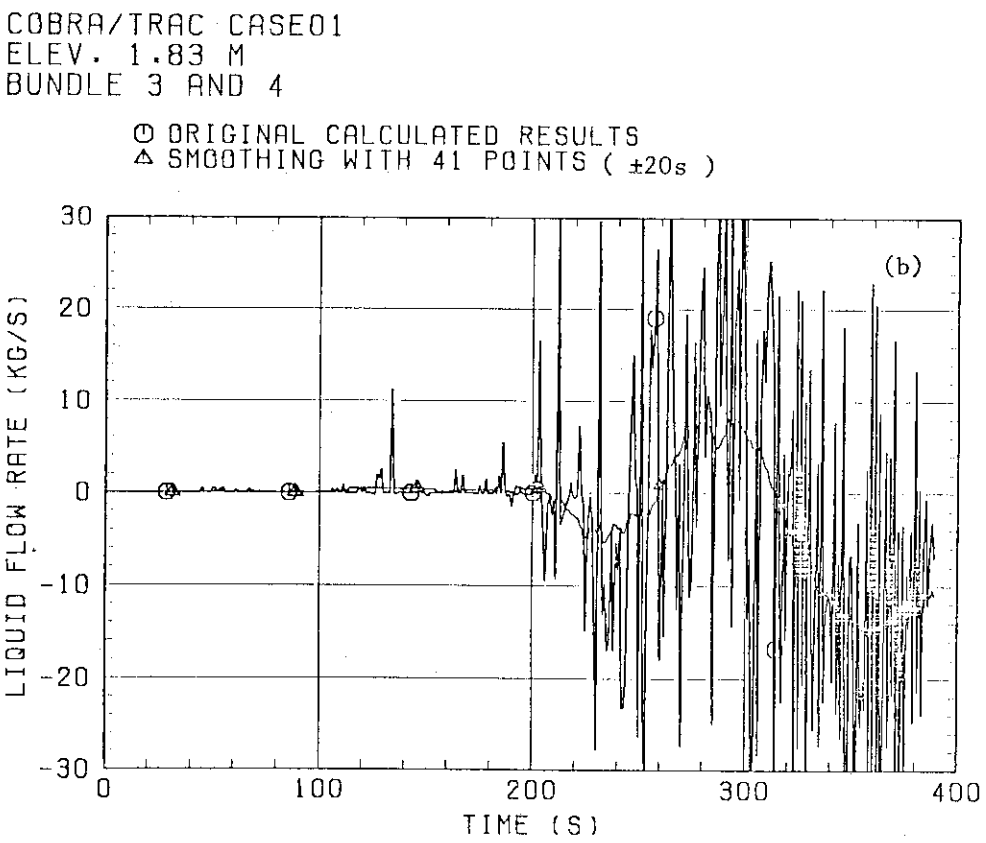

Fig. 4.6 Comparison of original and smoothed curves for vapor and liquid flow rates

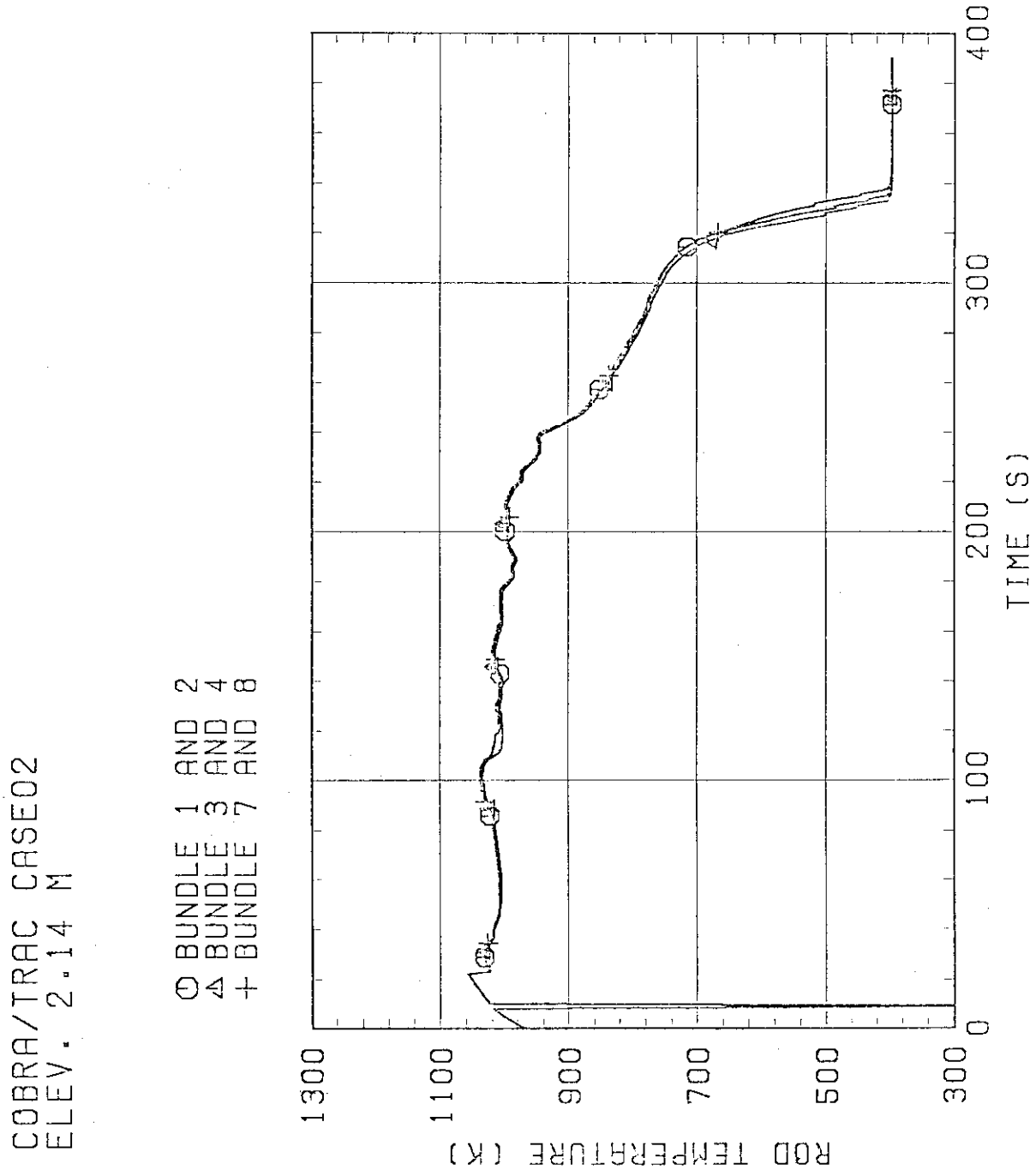

Fig. 4.7 Cladding temperatures in Case 02
(Bundles 1 & 2, 3 & 4, and 7 & 8, Elevation 2.14 m)

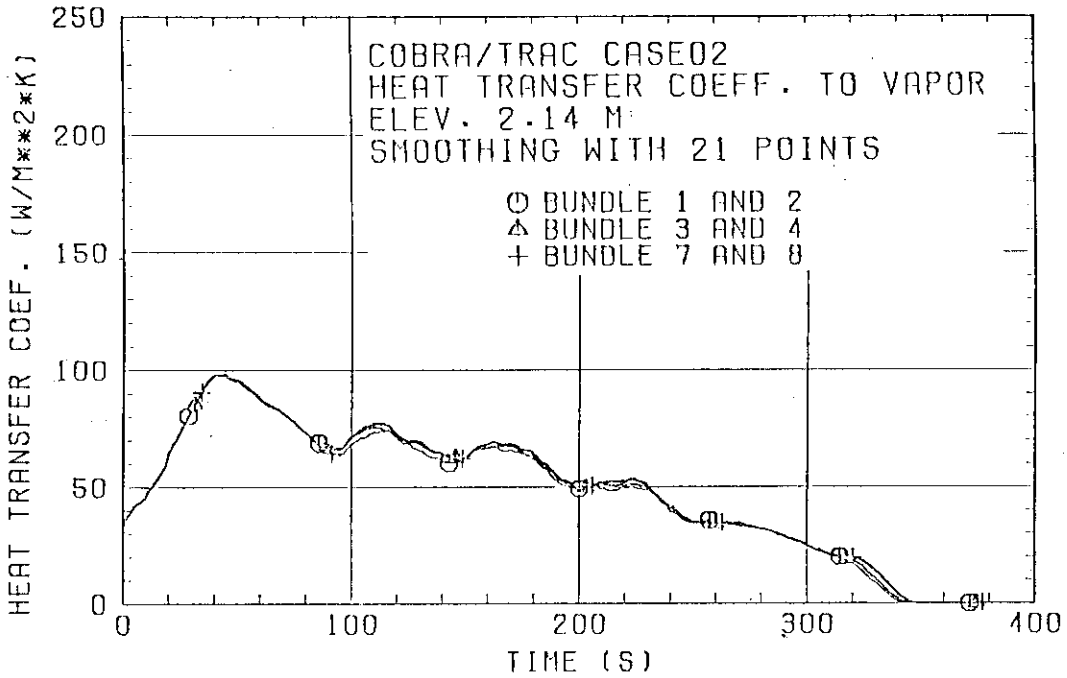

Fig. 4.8 Heat transfer coefficients to vapor in Case 02 (Bundles 1 & 2, 3 & 4, and 7 & 8, Elevation 2.14 m)

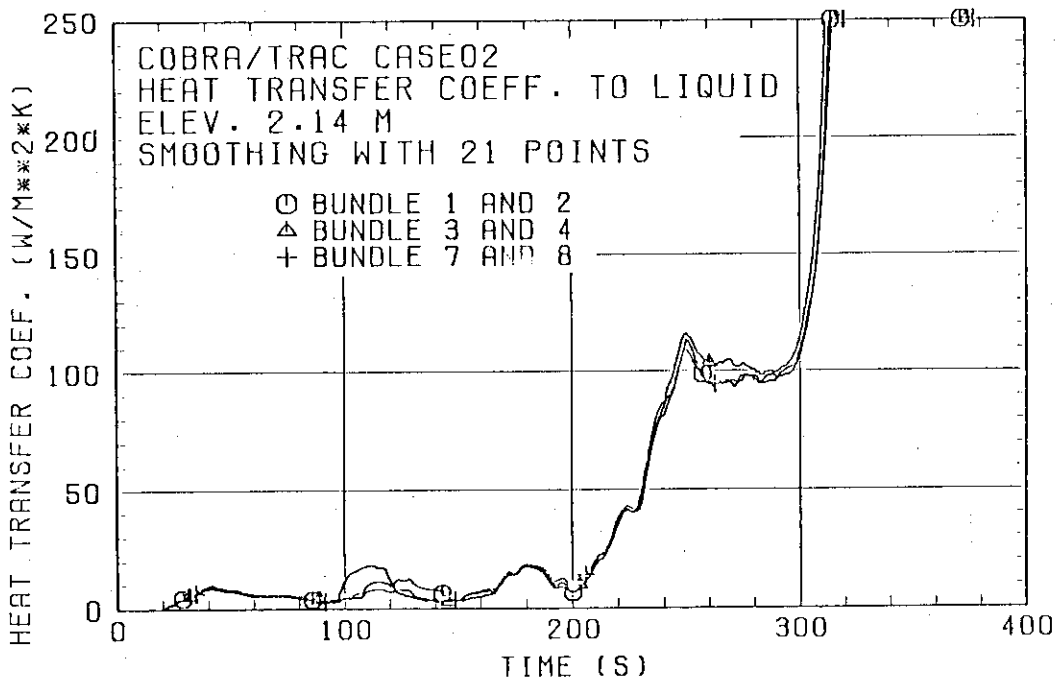

Fig. 4.9 Heat transfer coefficients to liquid in Case 02 (Bundles 1 & 2, 3 & 4, and 7 & 8, Elevation 2.14 m)

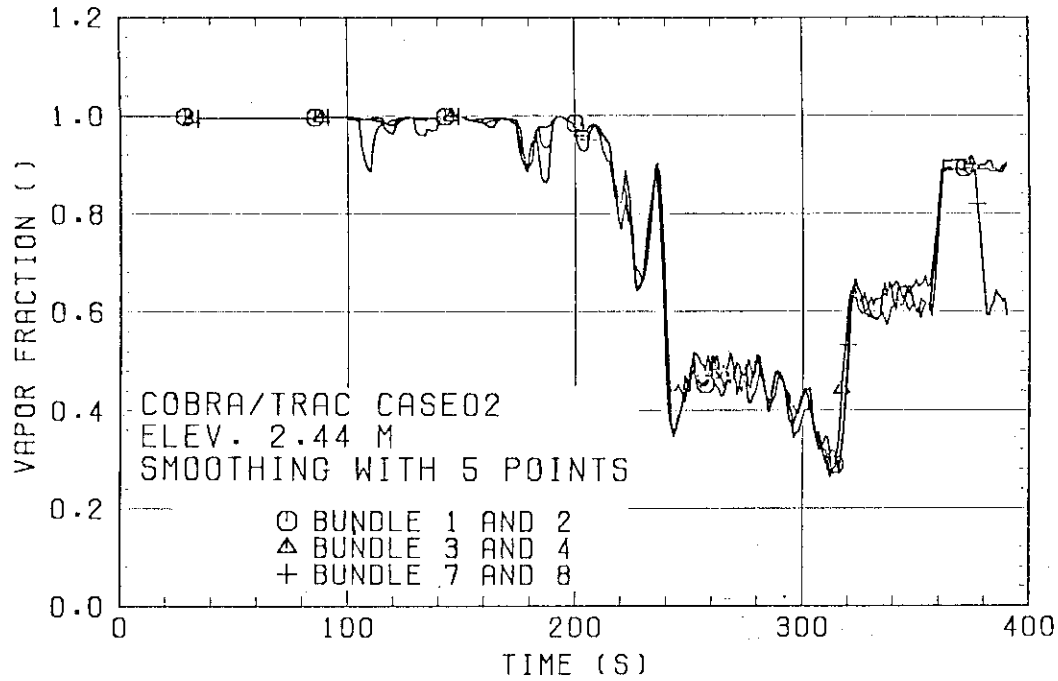

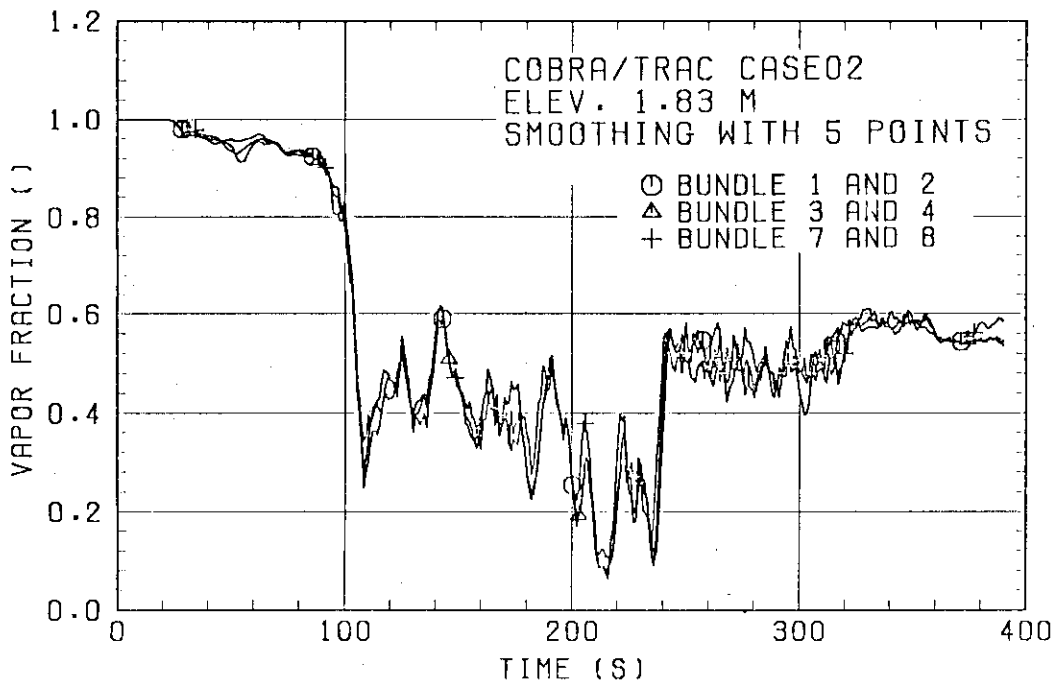

Fig. 4.10 Void fraction in Case 02
(Bundles 1 & 2, 3 & 4, and 7 & 8, Elevations 2.44 and 1.83 m)

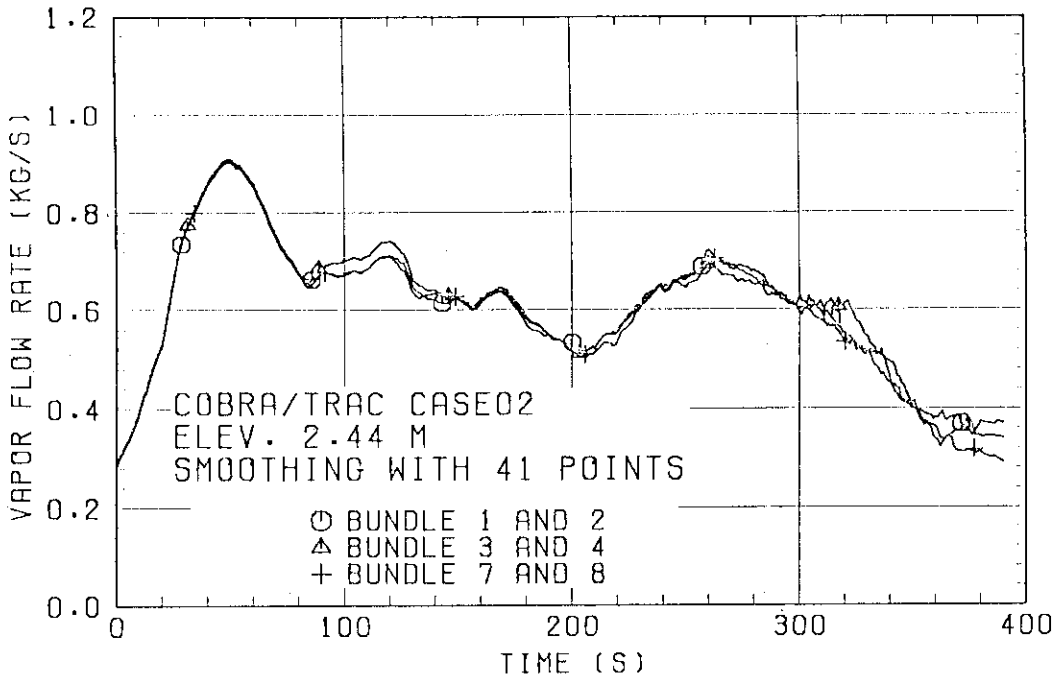

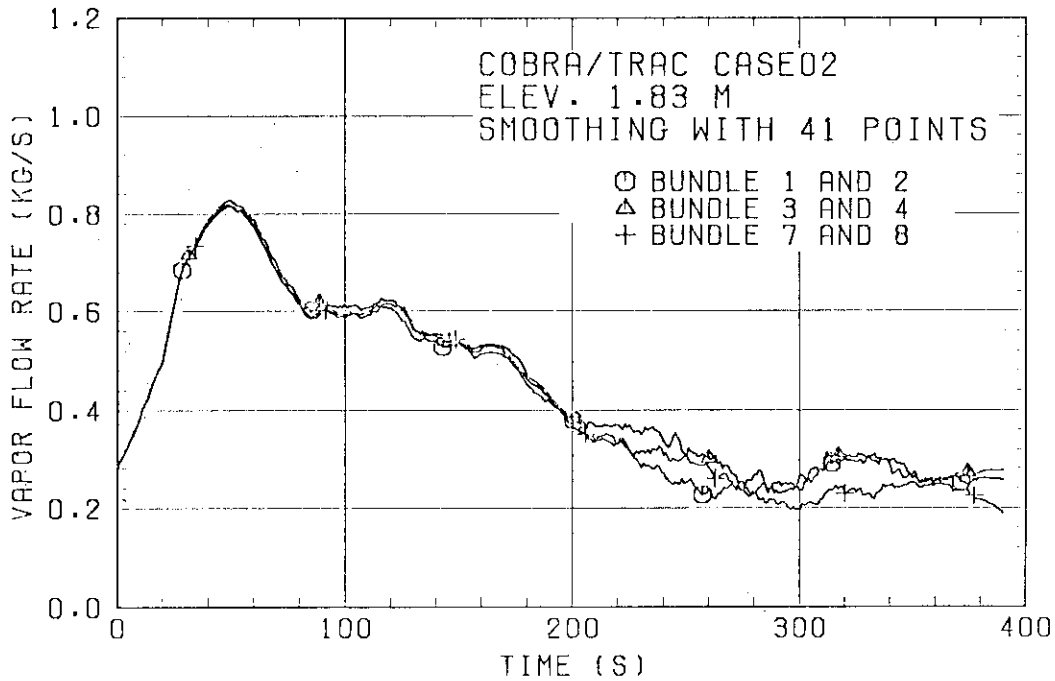

Fig. 4.11 Vapor up-flow rates in Case 02 (Bundles 1 & 2, 3 & 4, and 7 & 8, Elevations 2.44 and 1.83 m)

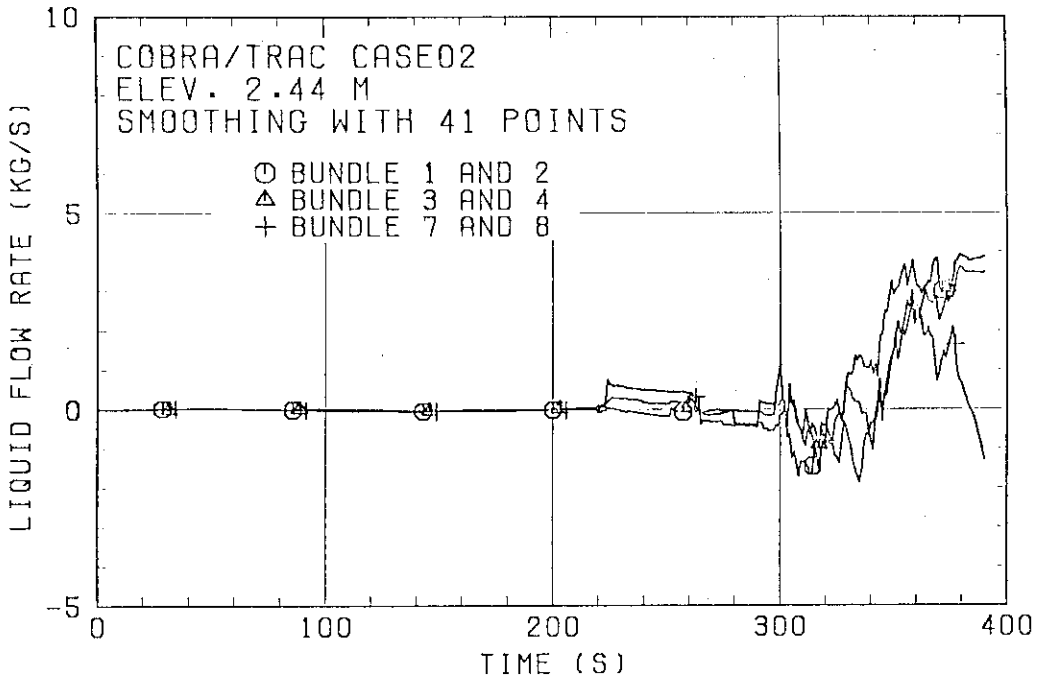

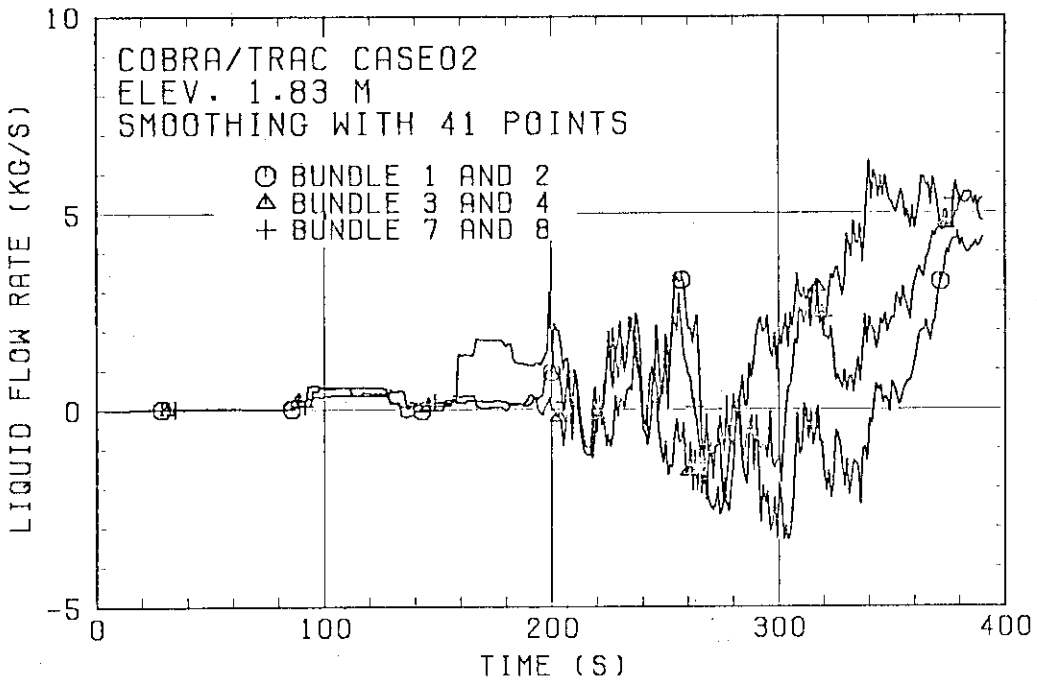

Fig. 4.12 Continuous liquid up-flow rates in Case 02 (Bundles 1 & 2, 3 & 4, and 7 & 8, Elevations 2.44 and 1.83 m)

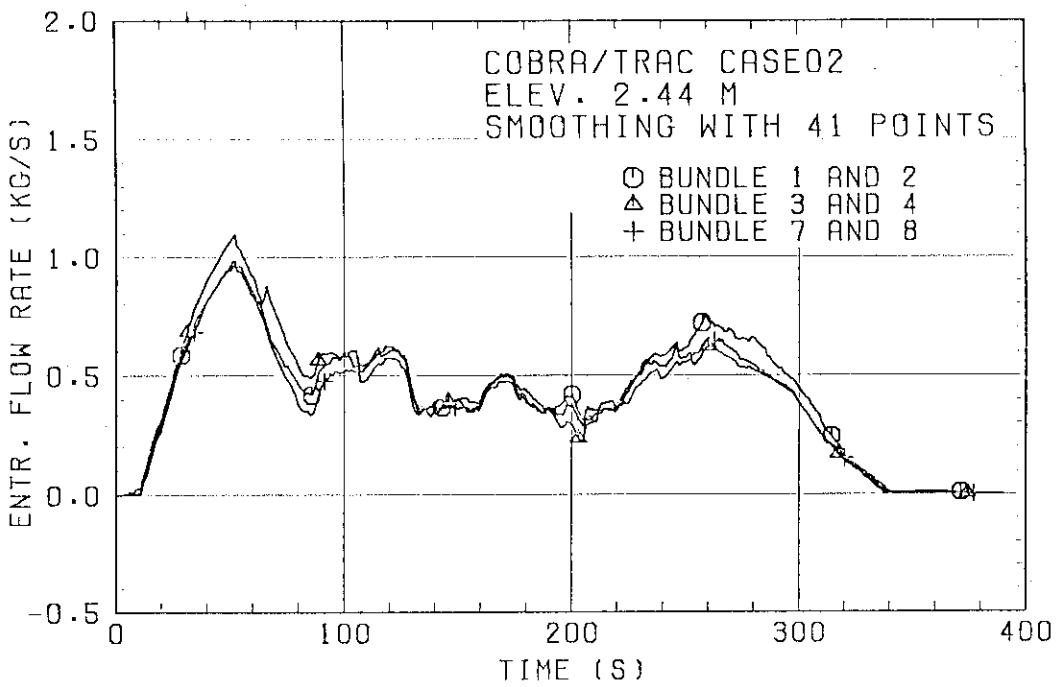

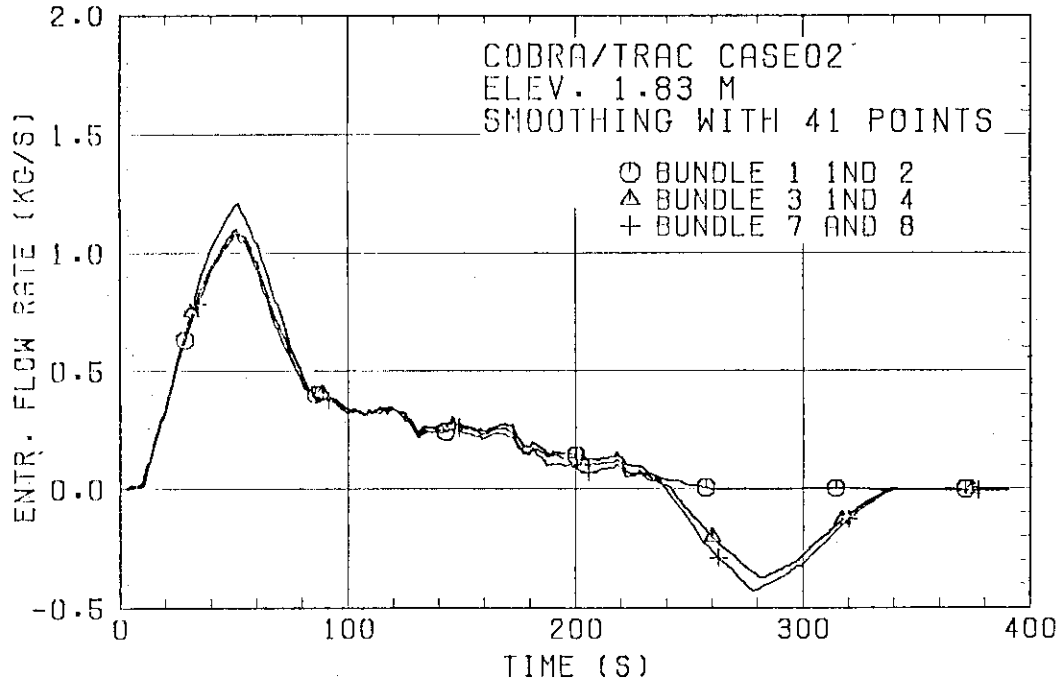

Fig. 4.13 Entrained liquid up-flow rates in Case 02 (Bundles 1 & 2, 3 & 4, and 7 & 8, Elevations 2.44 and 1.83 m)

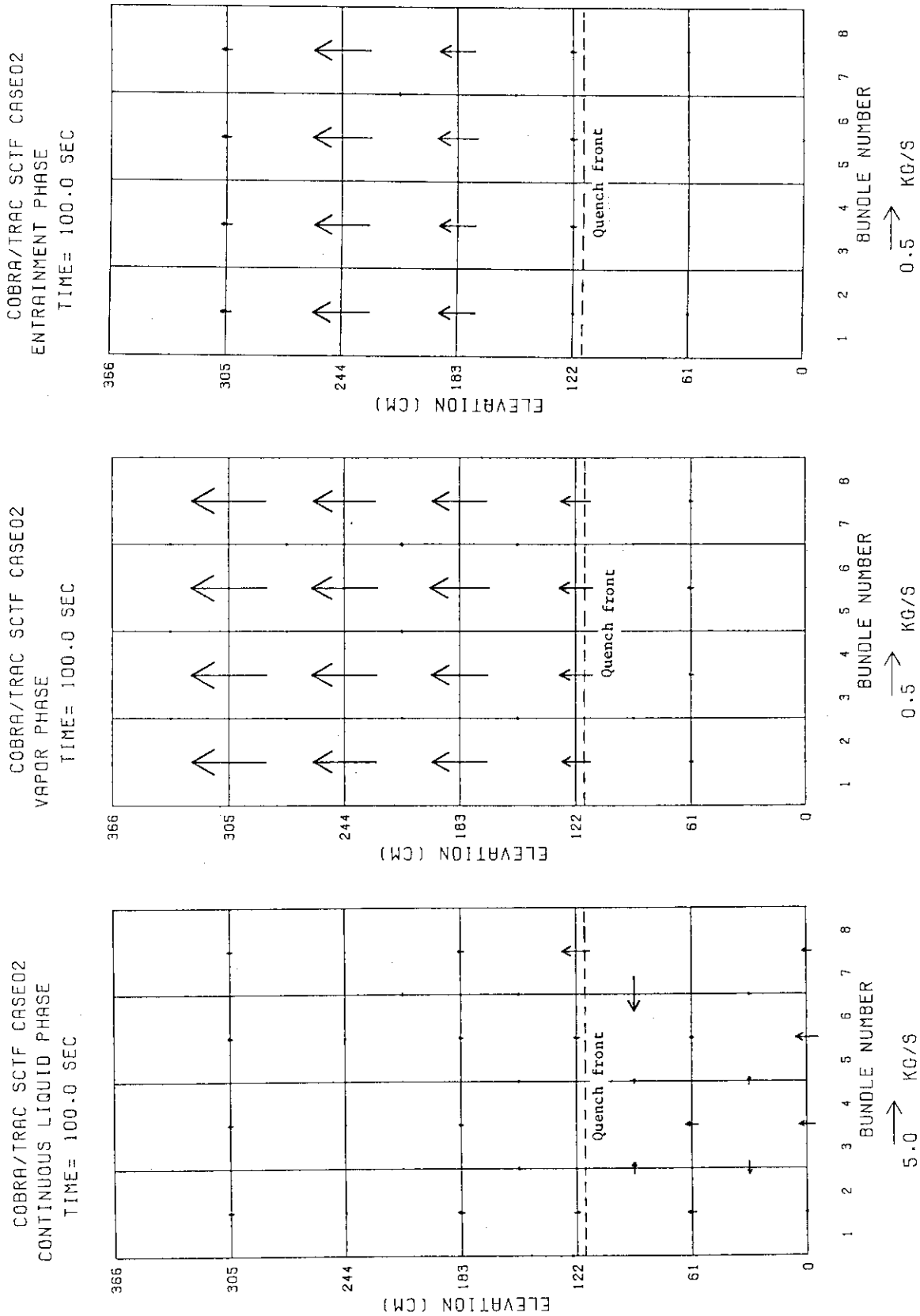

Fig. 4.14(a) Flow direction and magnitude of continuous liquid, vapor and entrained liquid phases in Case 02 (Time = 100 s)

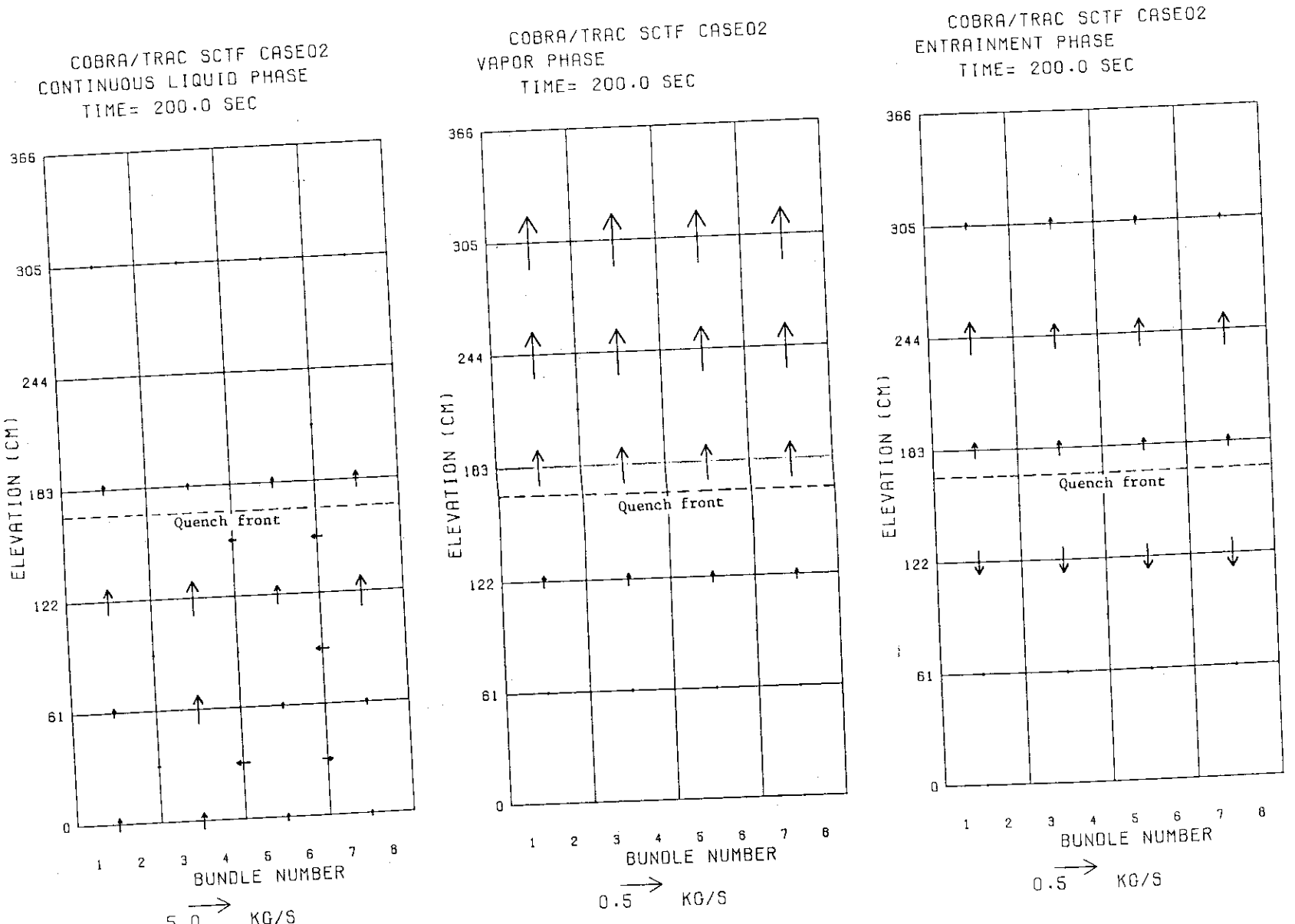

Fig. 4.14(b) Flow direction and magnitude of continuous liquid, vapor and entrained liquid phases in Case 02 (Time = 200 s)

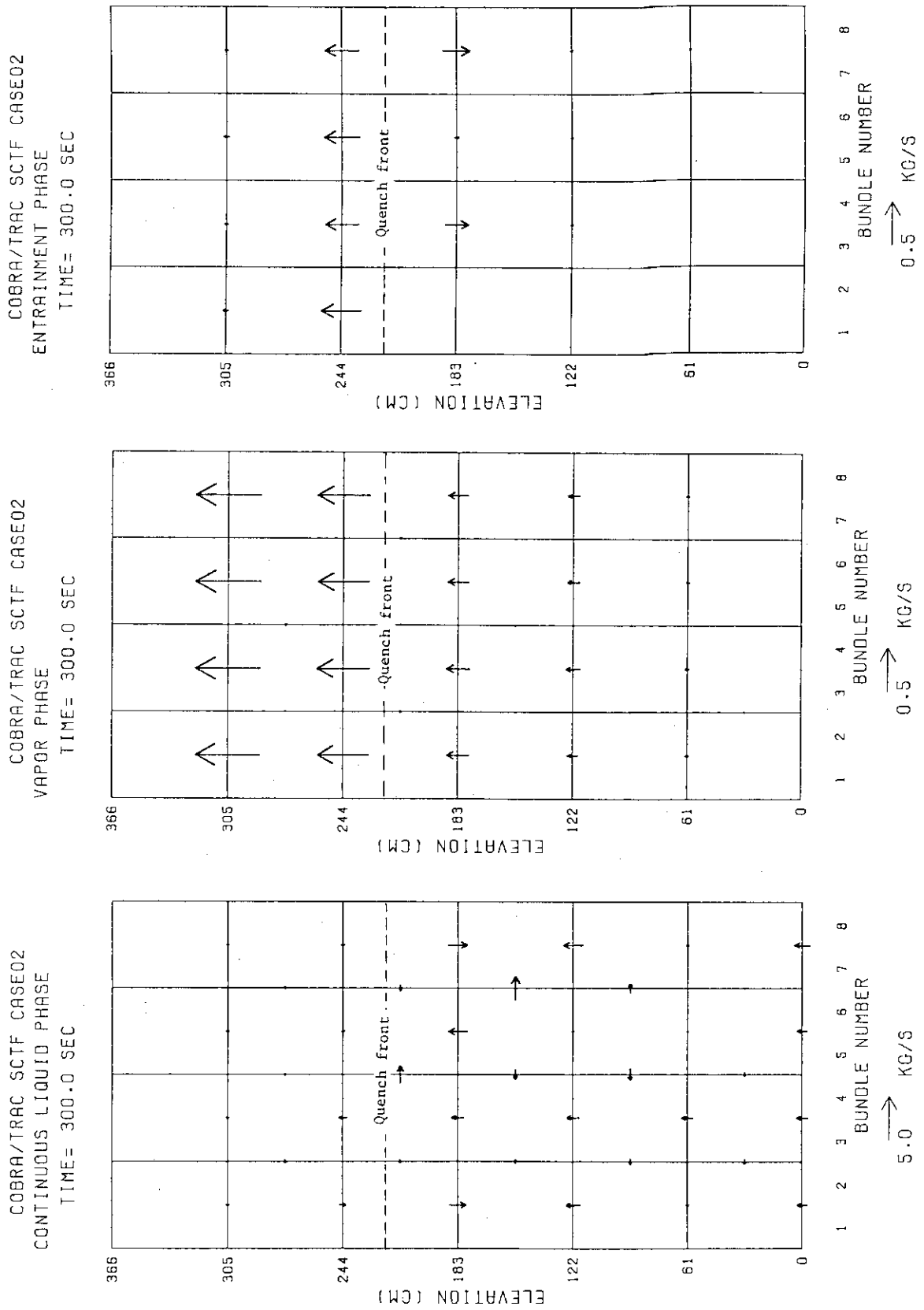

Fig. 4.14(c) Flow direction and magnitude of continuous liquid, vapor and entrained liquid phases in Case 02 (Time = 300 s)

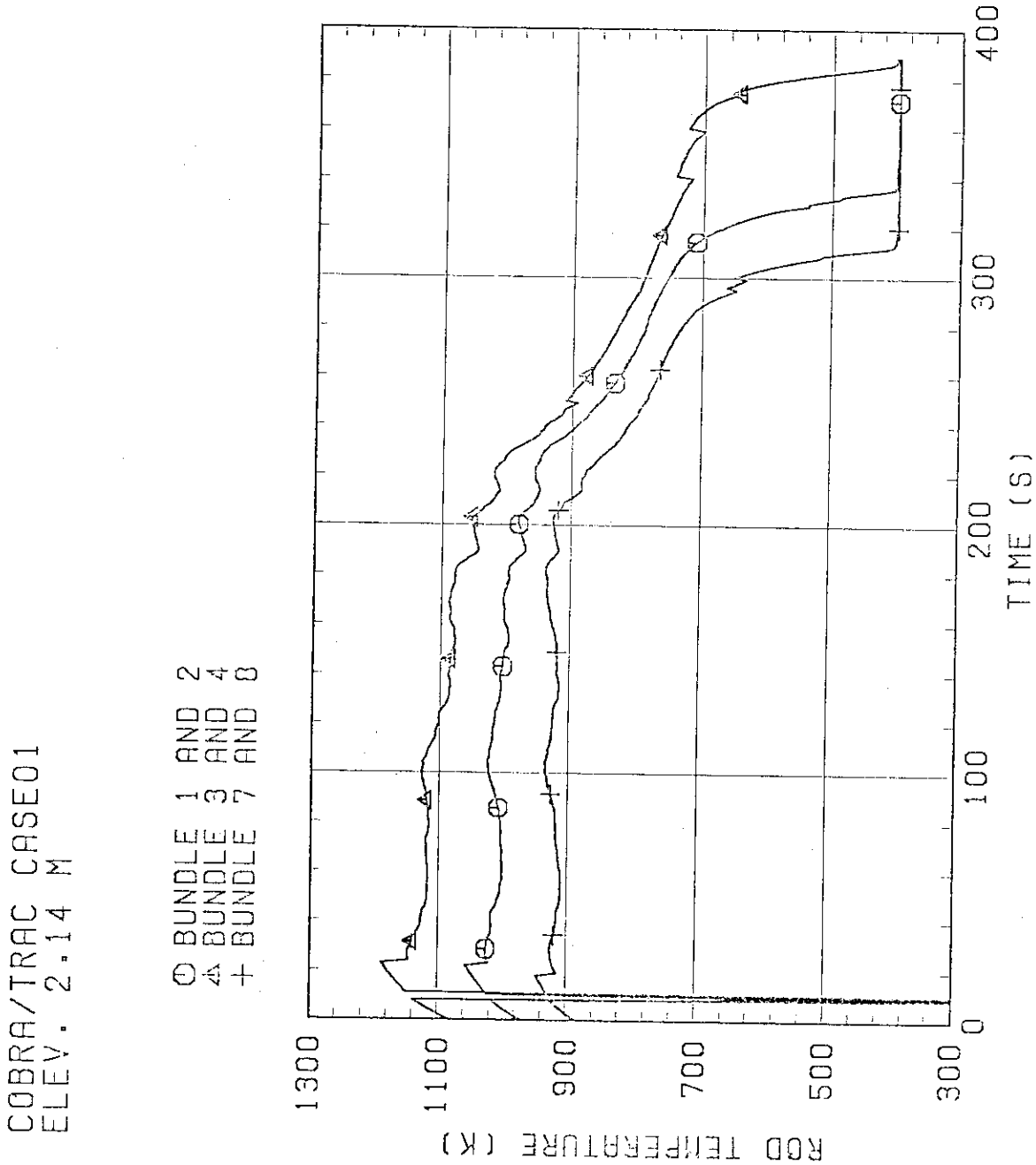

Fig. 4.15 Cladding temperatures in Case 01
(Bundles 1 & 2, 3 & 4, and 7 & 8, Elevation 2.14 m)

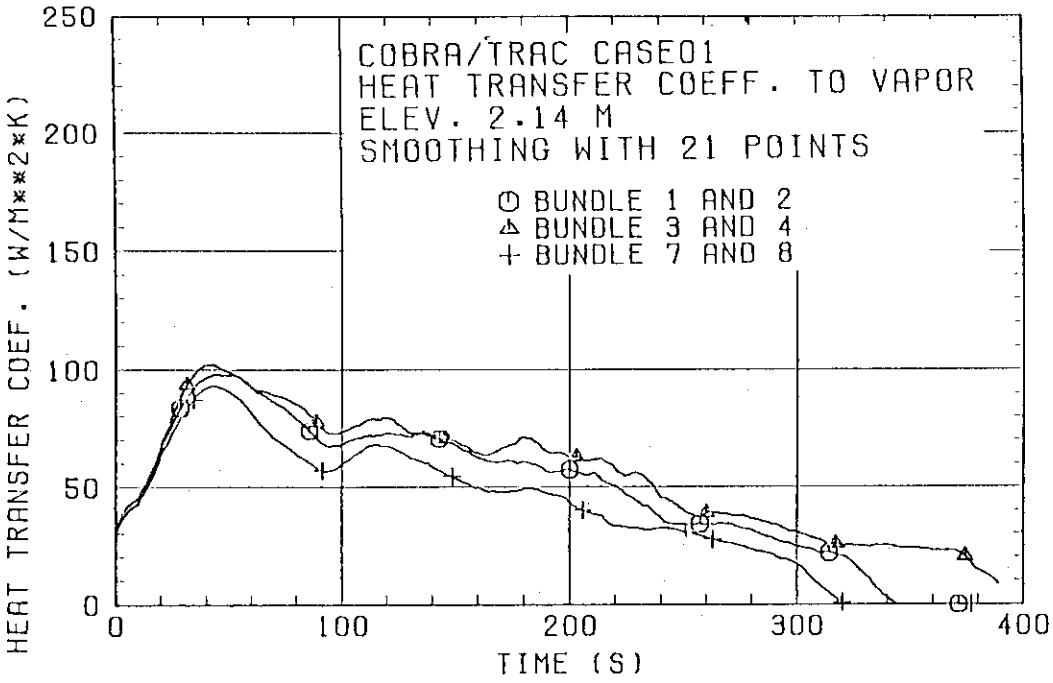

Fig. 4.16 Heat transfer coefficients to vapor in Case 01 (Bundles 1 & 2, 3 & 4, and 7 & 8, Elevation 2.14 m)

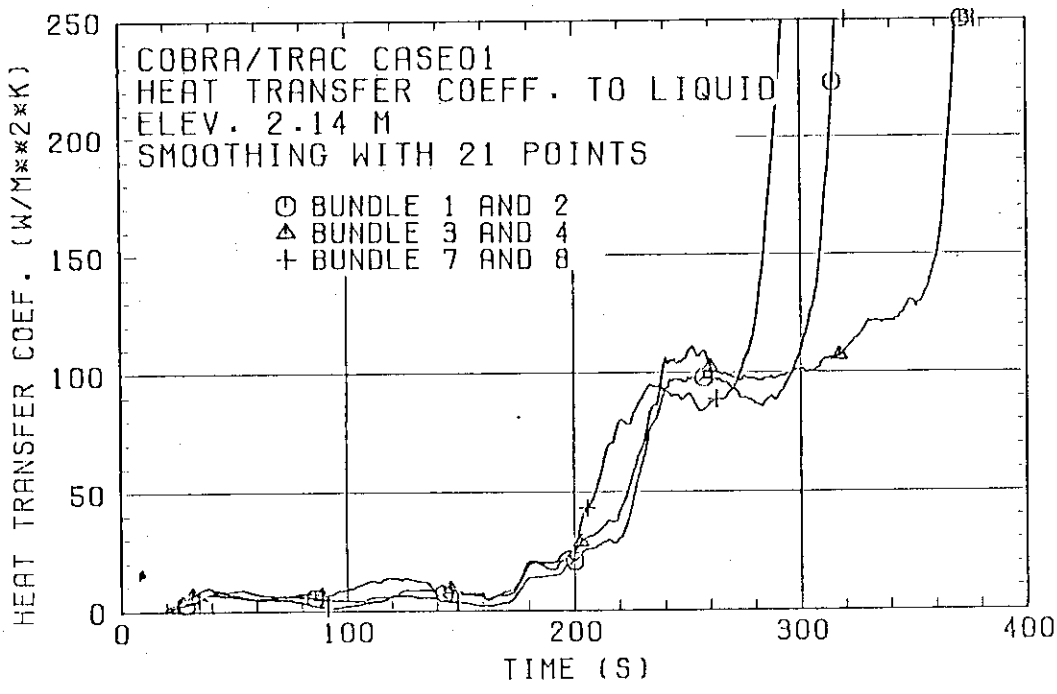

Fig. 4.17 Heat transfer coefficients to liquid in Case 01 (Bundles 1 & 2, 3 & 4, and 7 & 8, Elevation 2.14 m)

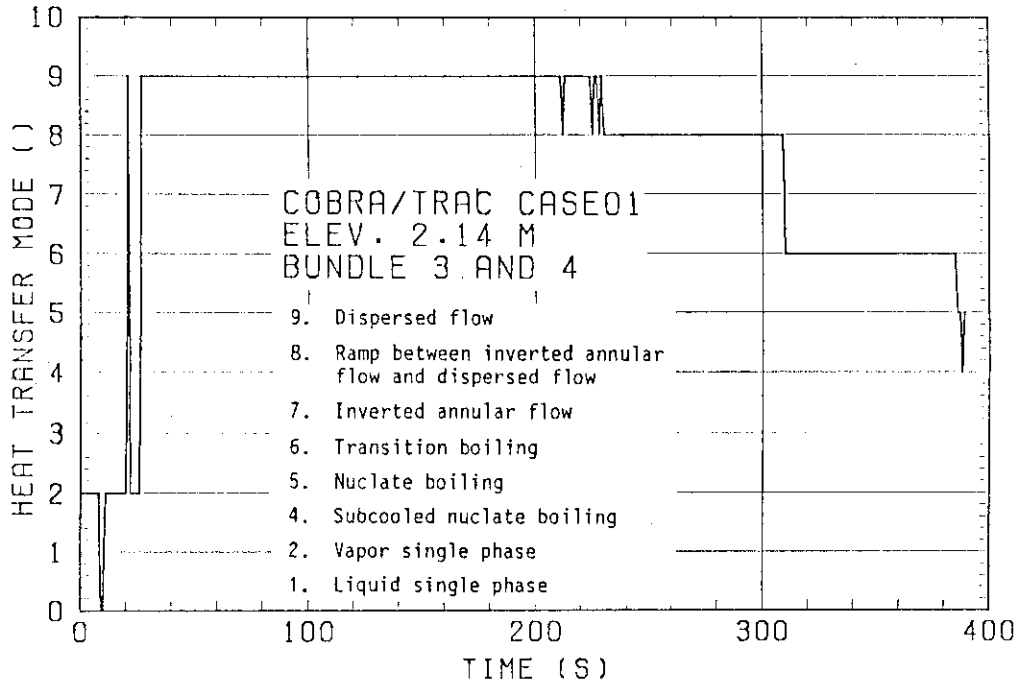

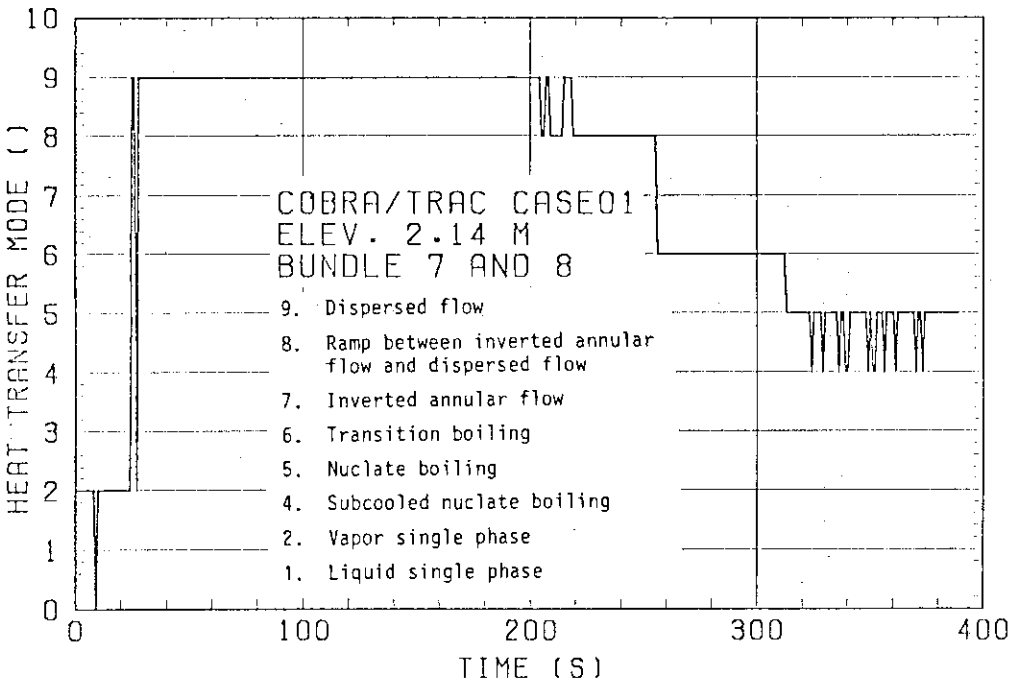

Fig. 4.18 Heat transfer modes in Case 01
(Bundles 3 & 4 and 7 & 8, Elevation 2.14 m)

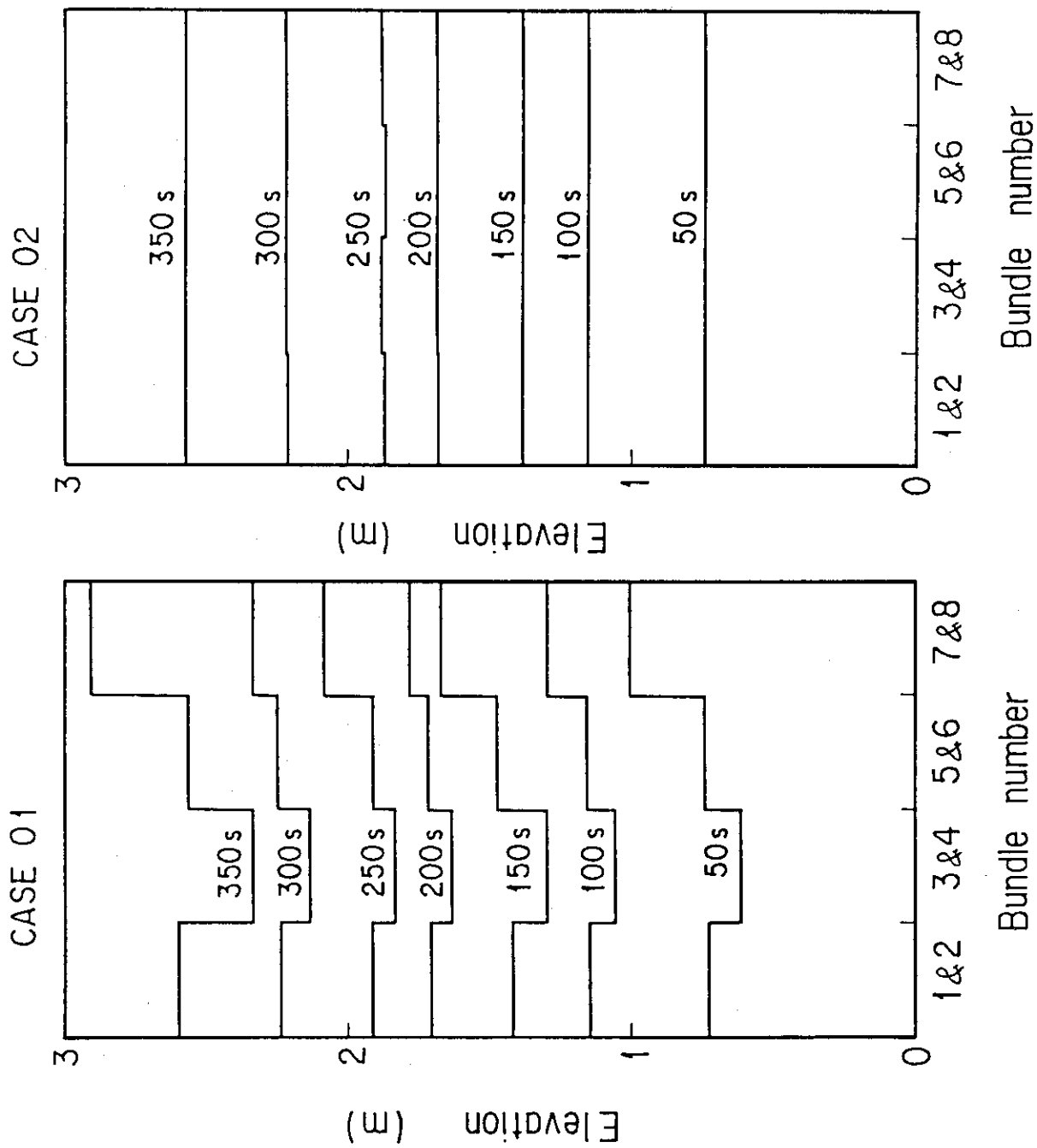

Fig. 4.19 Quench front distributions in Cases 01 and 02

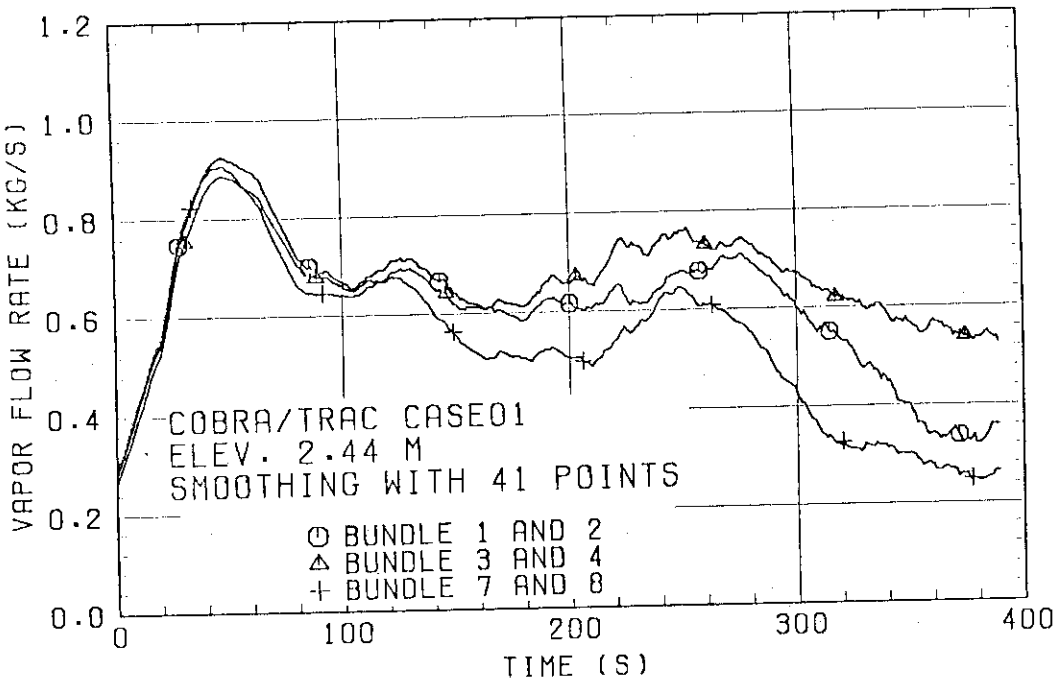

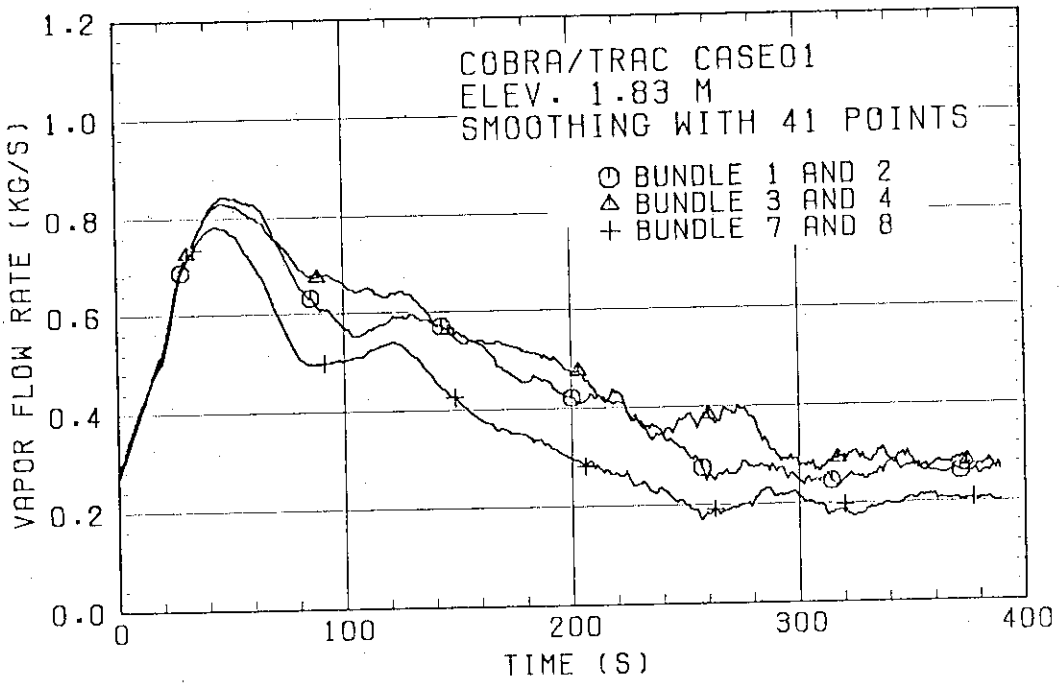

Fig. 4.20 Vapor up-flow rates in Case 01
(Bundles 1 & 2, 3 & 4 and 7 & 8, Elevations 2.44 and 1.83 m)

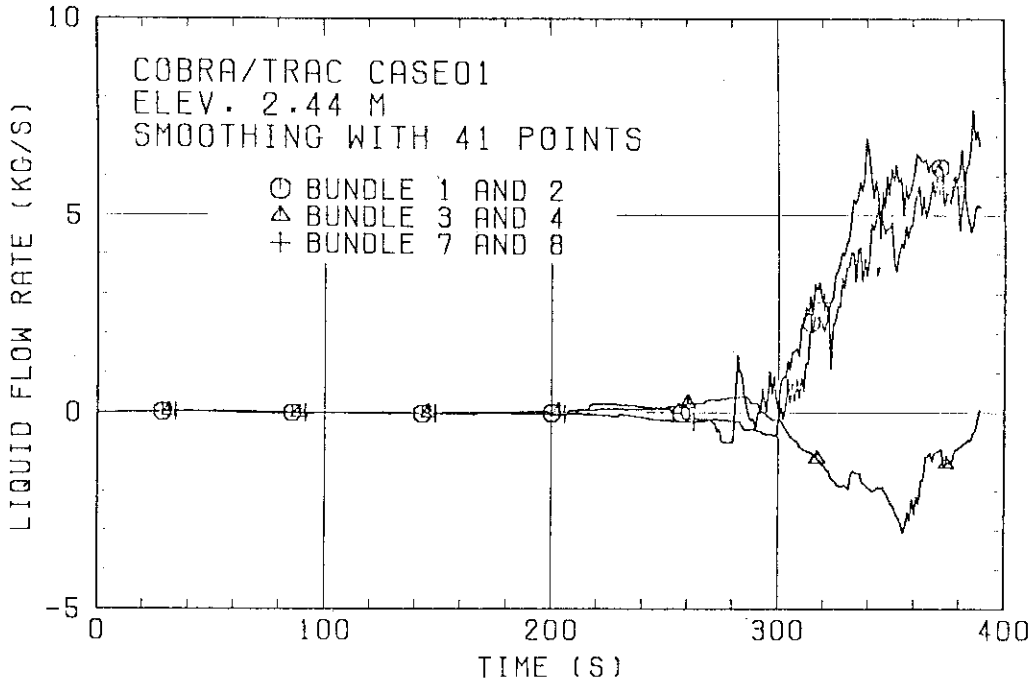

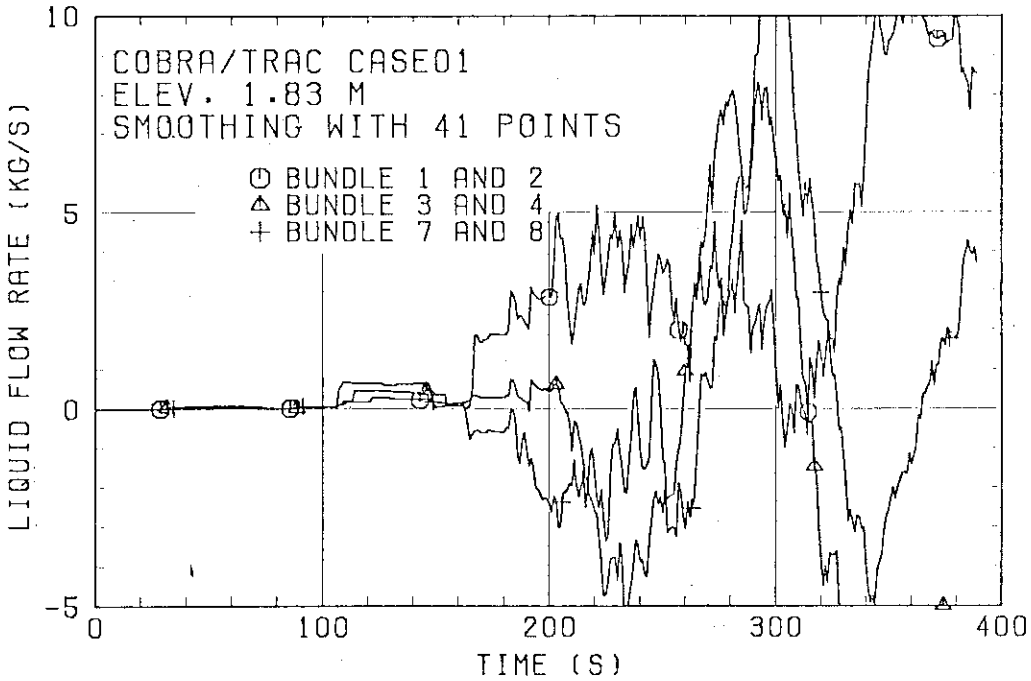

Fig. 4.21 Continuous liquid up-flow rates in Case 01 (Bundles 1 & 2, 3 & 4 and 7 & 8, Elevations 2.44 and 1.83 m)

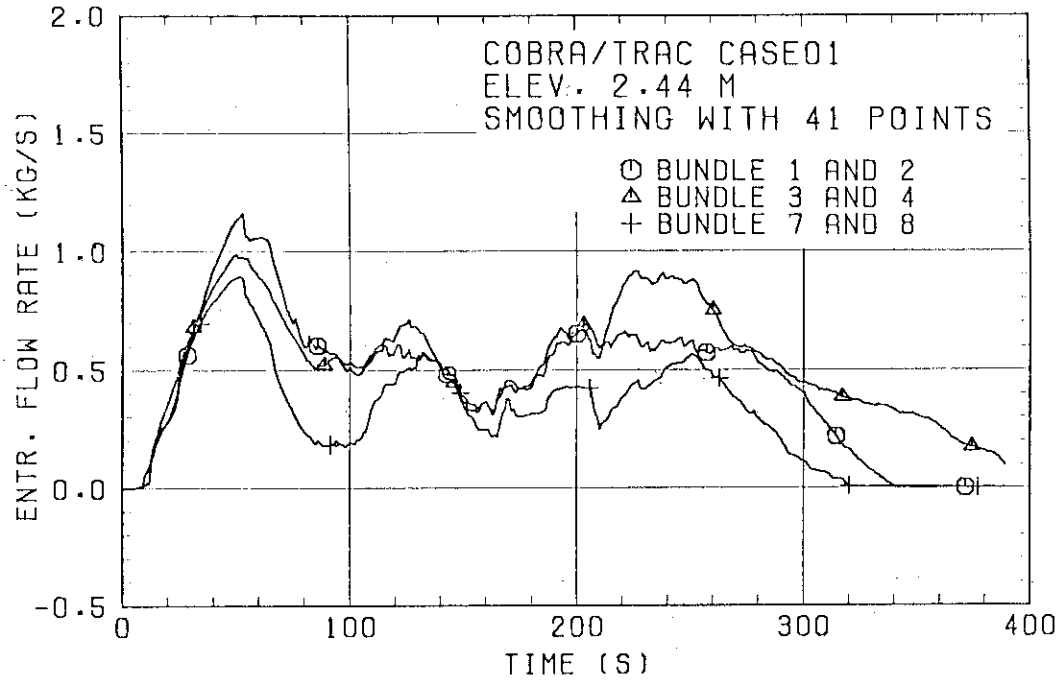

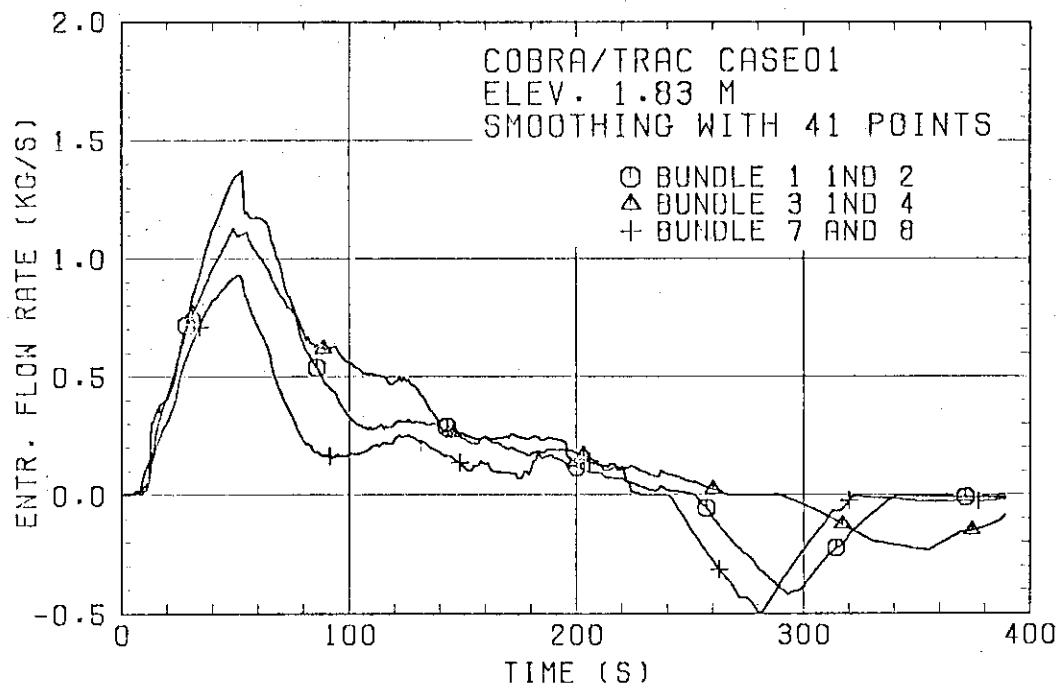

Fig. 4.22 Entrained liquid up-flow rates in Case 01 (Bundles 1 & 2, 3 & 4 and 7 & 8, Elevations 2.44 and 1.83 m)

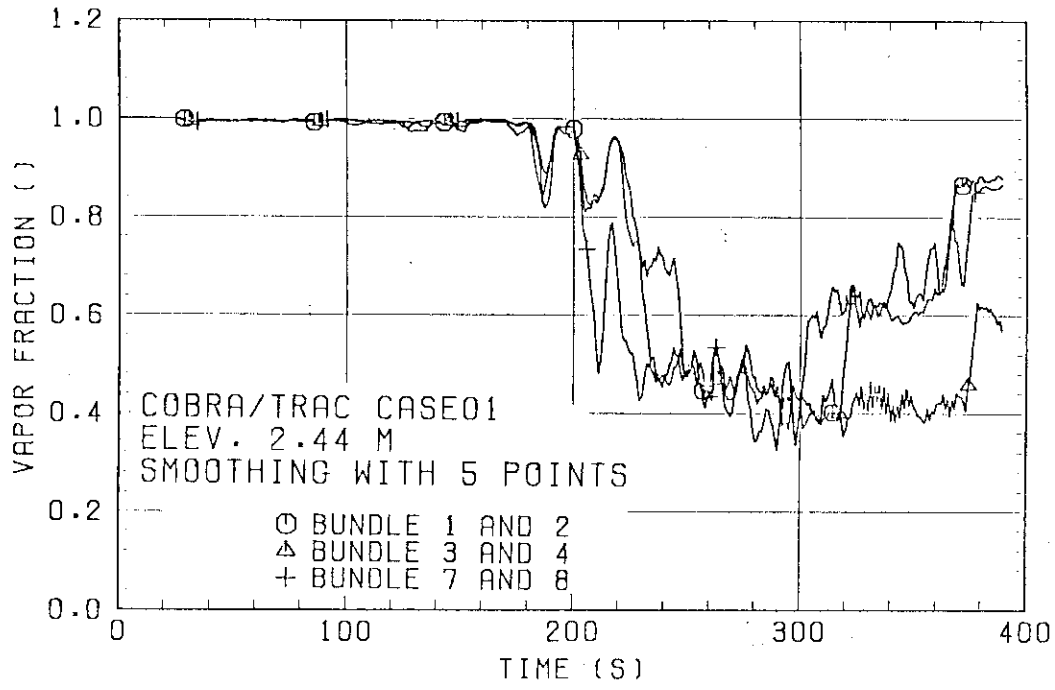

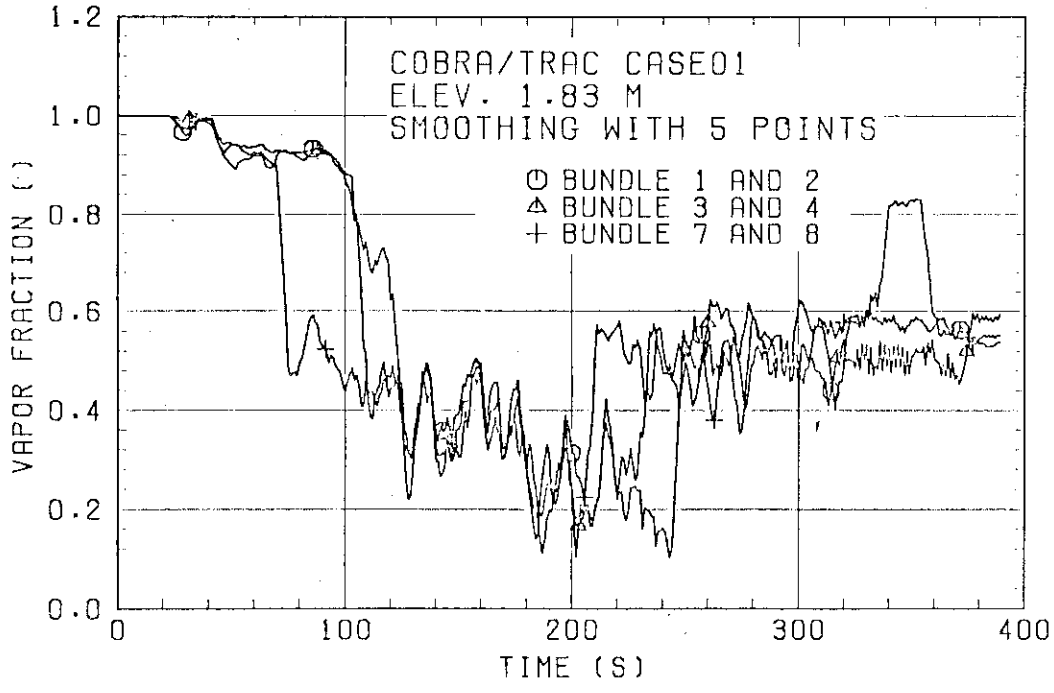

Fig. 4.23 Void fractions in Case 02
(Bundles 1 & 2, 3 & 4 and 7 & 8, Elevations 2.44 and 1.83 m)

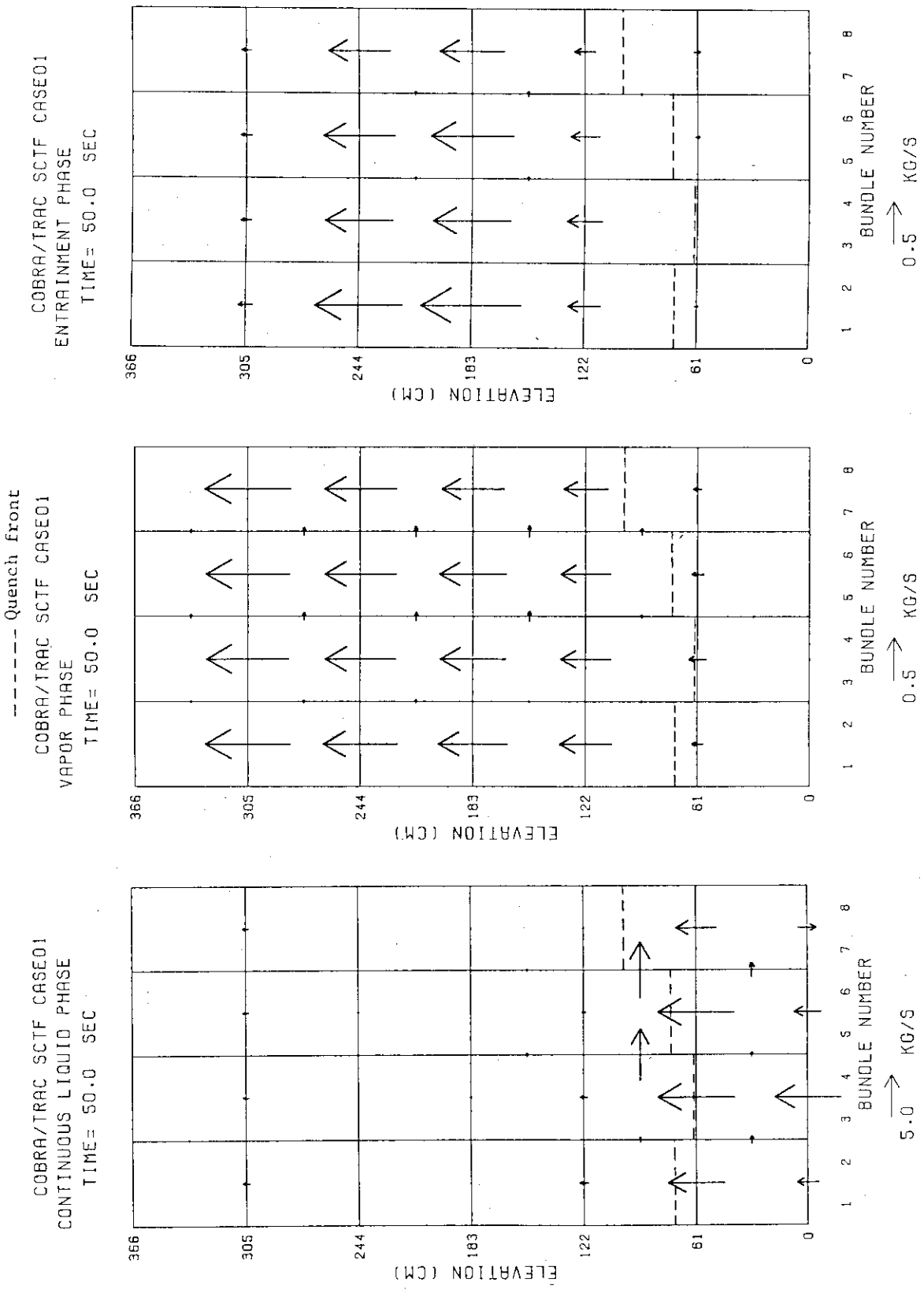

Fig. 4.24(a) Flow direction and magnitude of continuous liquid, vapor and entrained liquid phases in Case 01 (Time = 50 s)

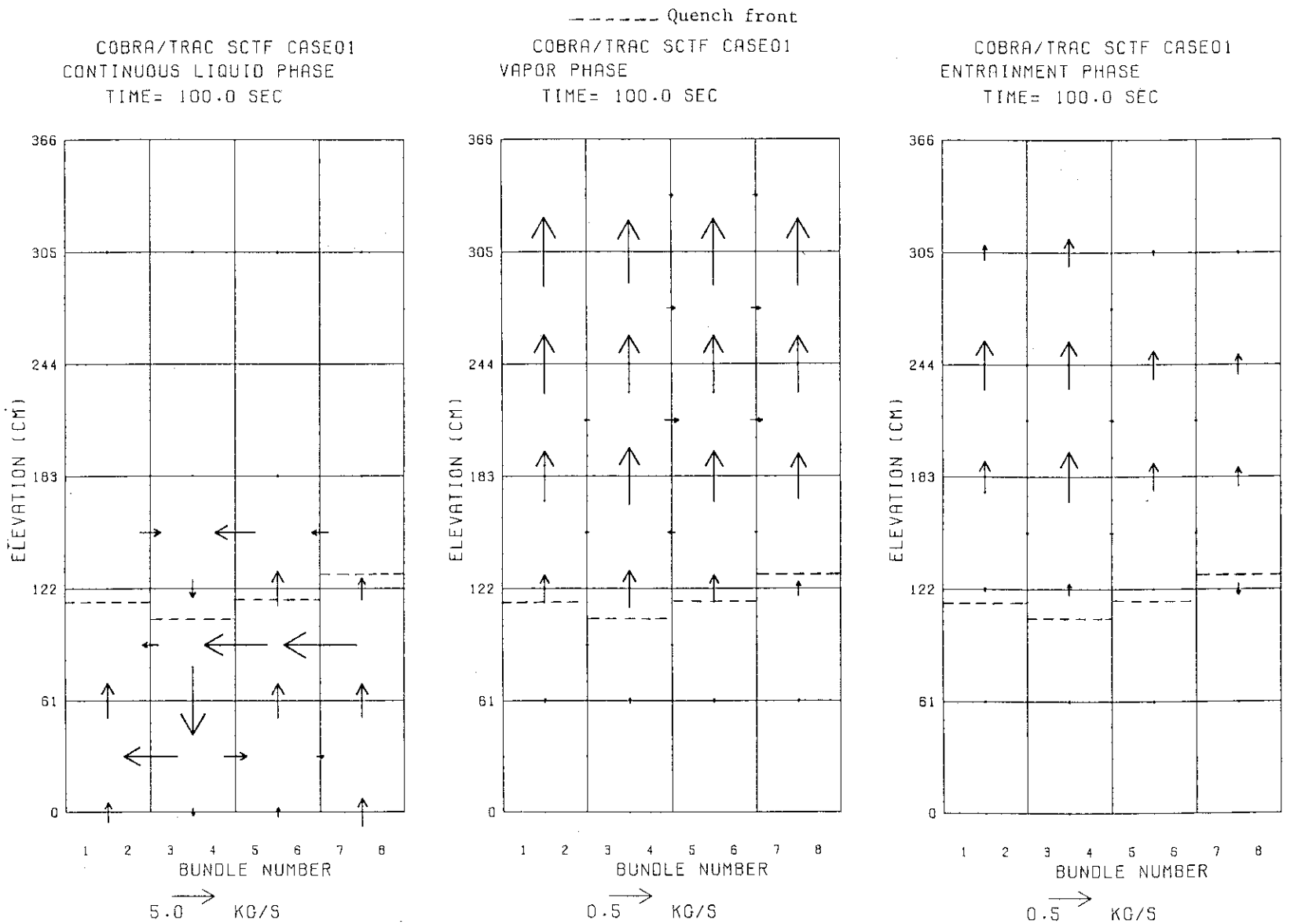

Fig. 4.24(b) Flow direction and magnitude of continuous liquid, vapor and entrained liquid phases in Case 01 (Time = 100 s)

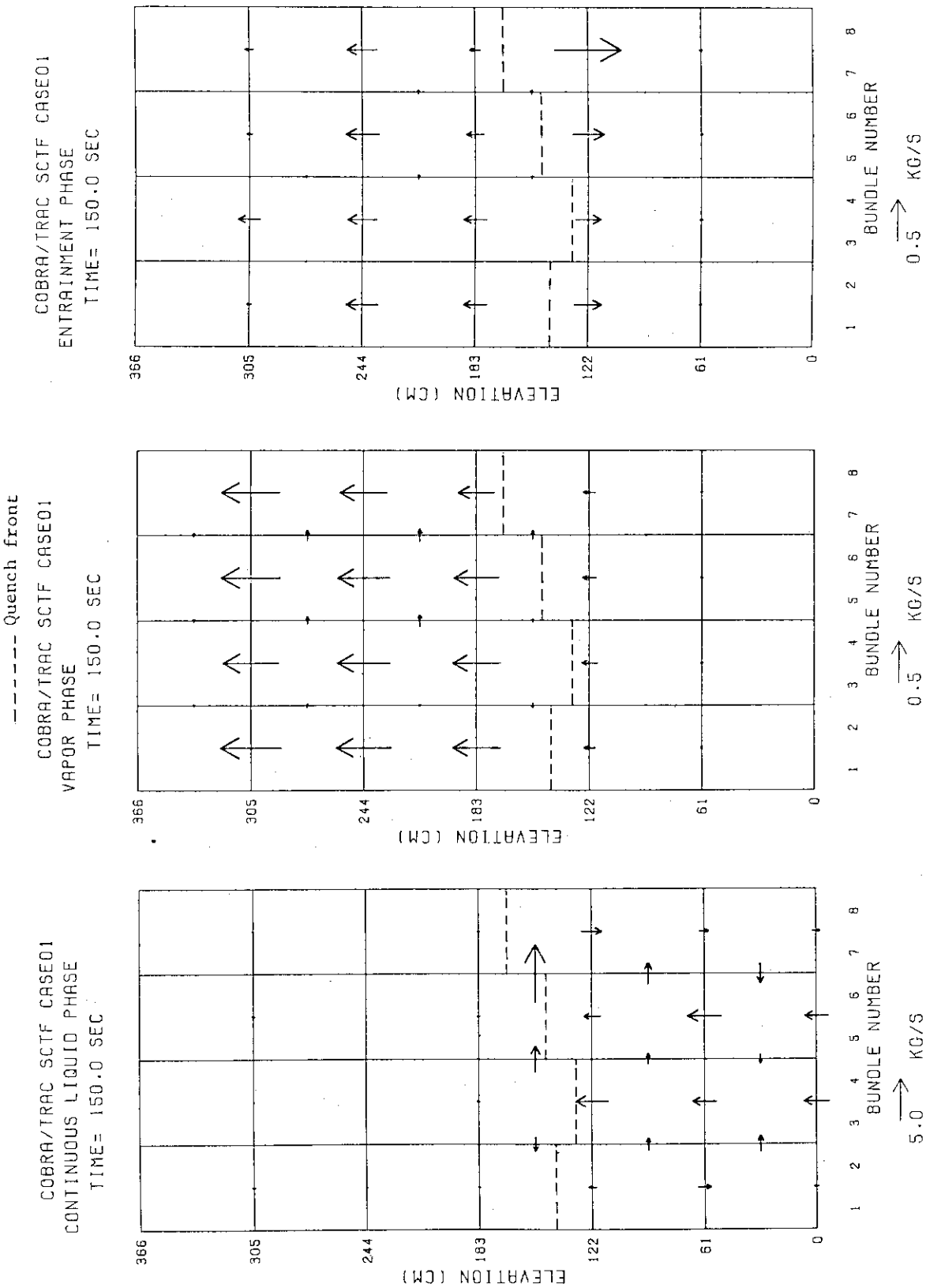

Fig. 4.24(c) Flow direction and magnitude of continuous liquid, vapor and entrained liquid phases in Case 01 (Time = 150 s)

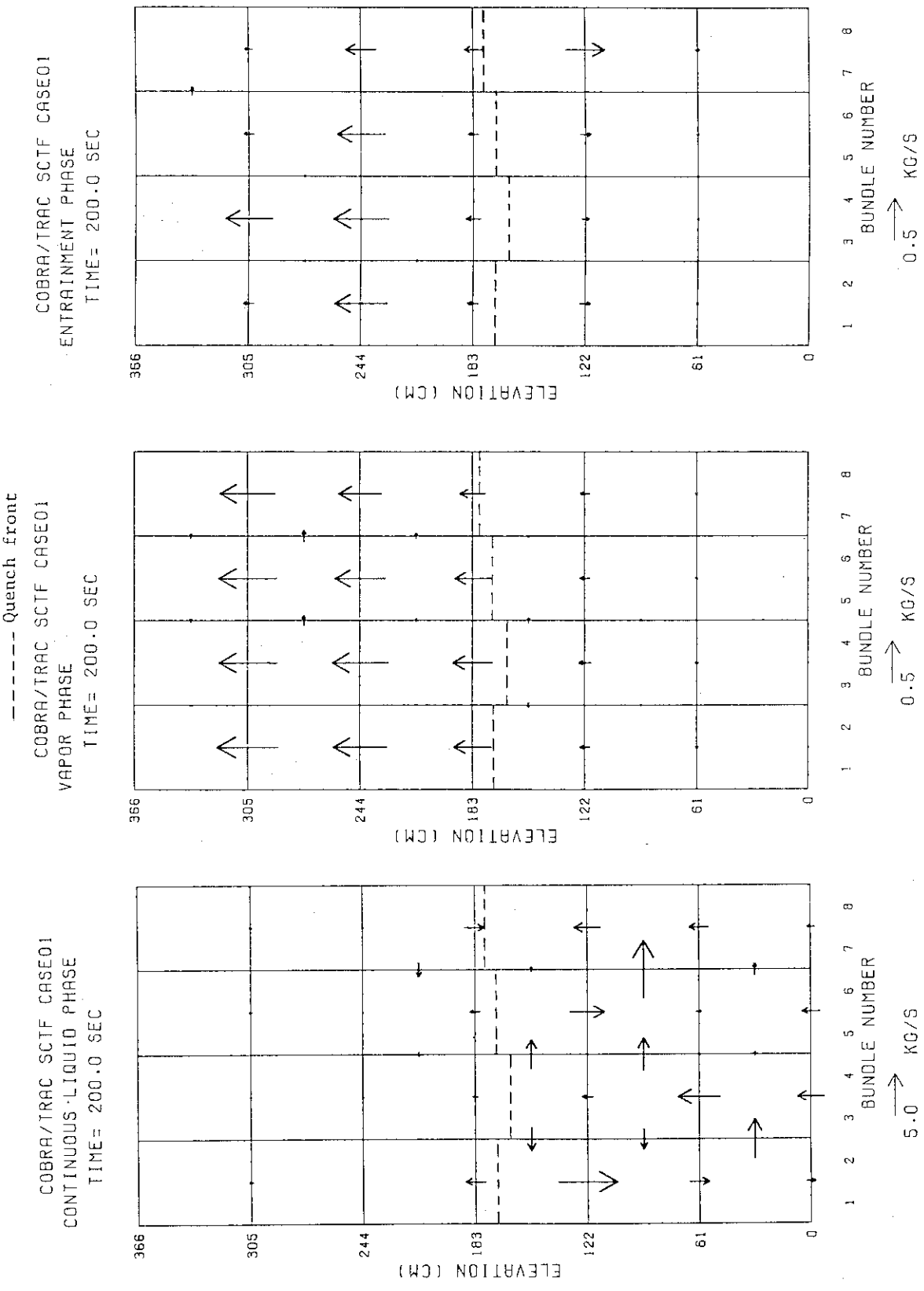

Fig. 4.24(d) Flow direction and magnitude of continuous liquid, vapor and entrained liquid phases in Case 01 (Time = 200 s)

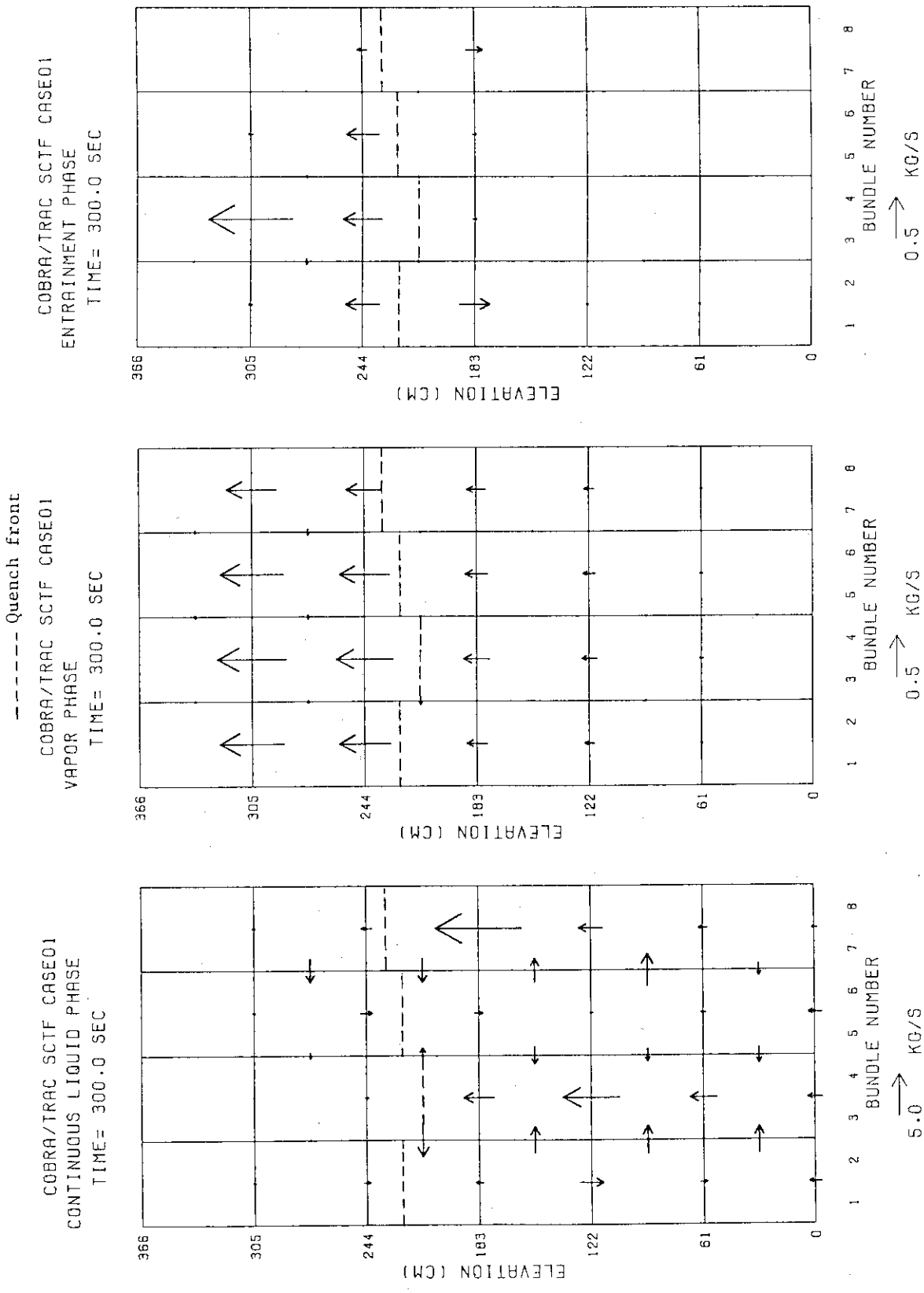

Fig. 4.24(e) Flow direction and magnitude of continuous liquid, vapor and entrained liquid phases in Case 01 (Time = 300 s)

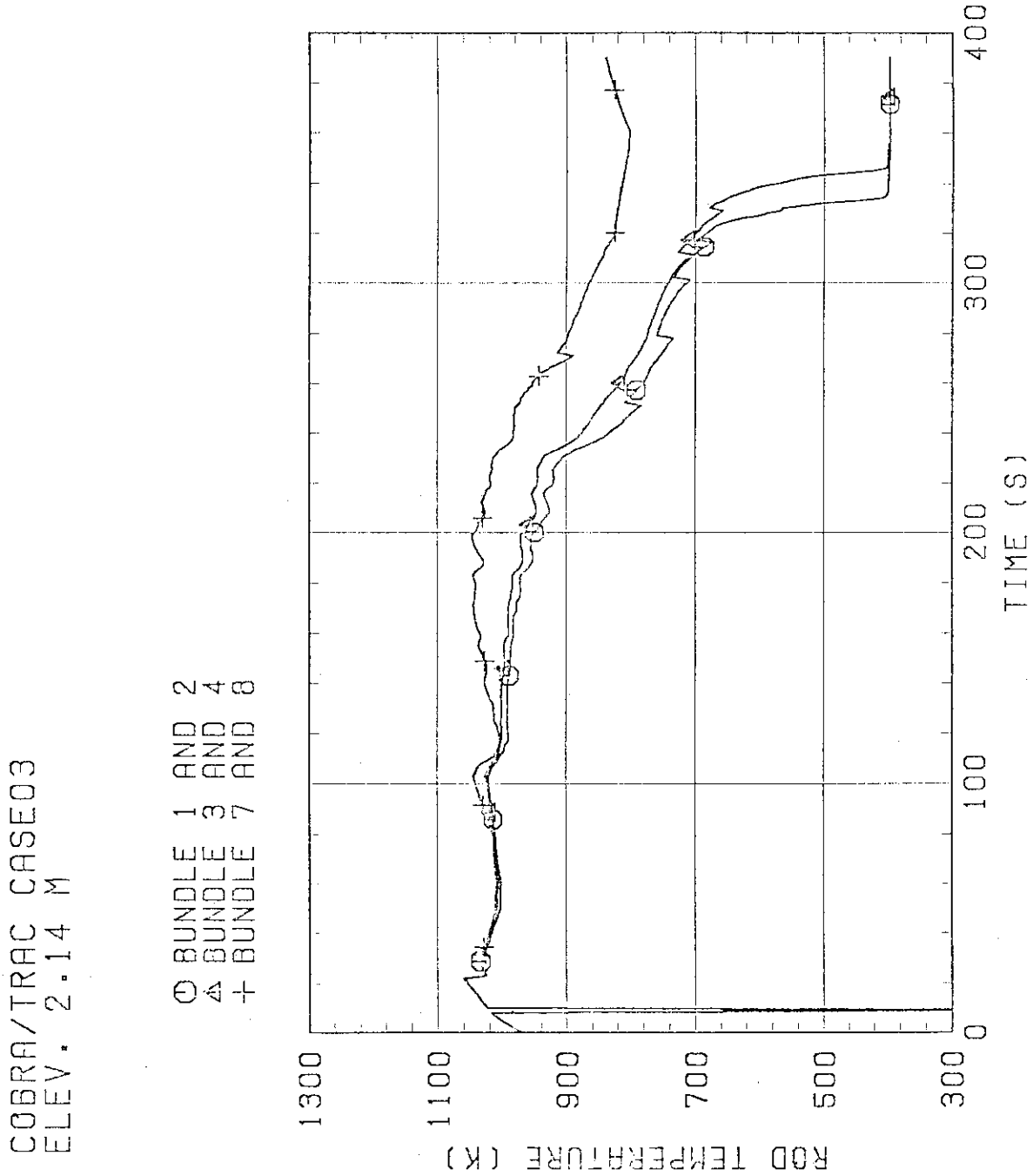

Fig. 4.25 Cladding temperatures in Case 03
(Bundles 1 & 2, 3 & 4, and 7 & 8, Elevation 2.14 m)

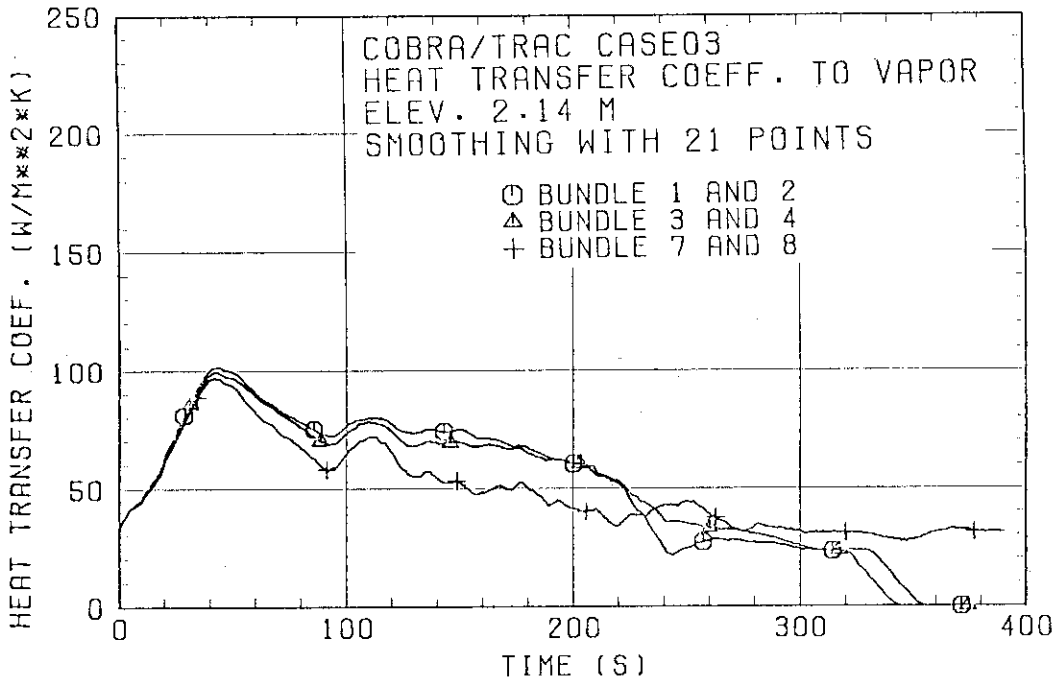

Fig. 4.26 Heat transfer coefficients to vapor in Case 03 (Bundles 1 & 2, 3 & 4, and 7 & 8, Elevation 2.14 m)

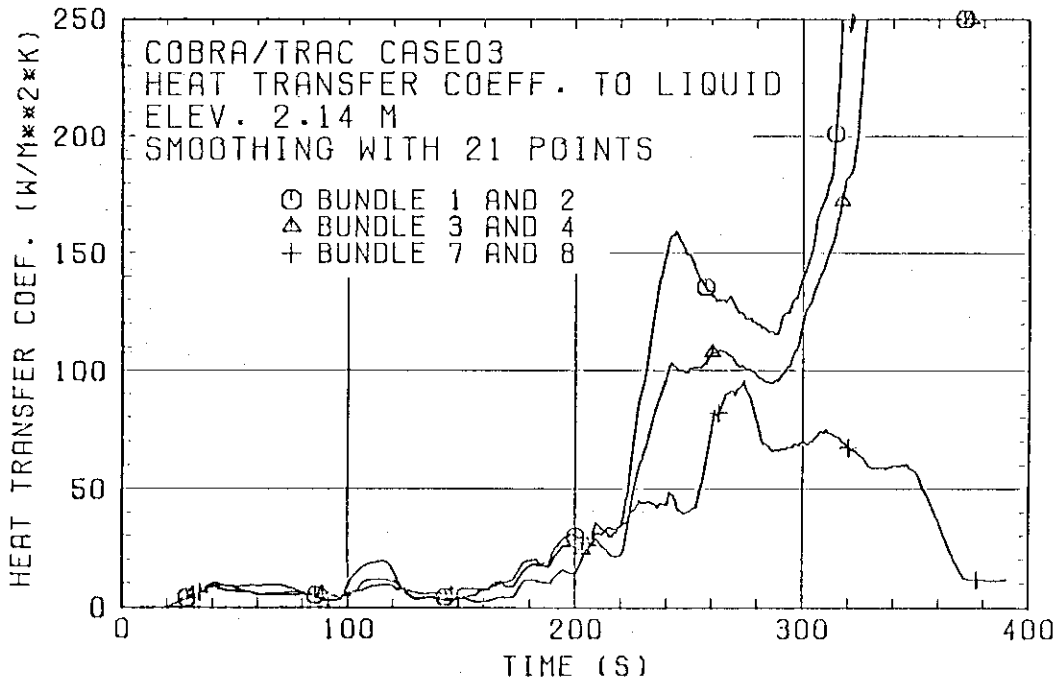

Fig. 4.27 Heat transfer coefficients to liquid in Case 03 (Bundles 1 & 2, 3 & 4, and 7 & 8, Elevation 2.14 m)

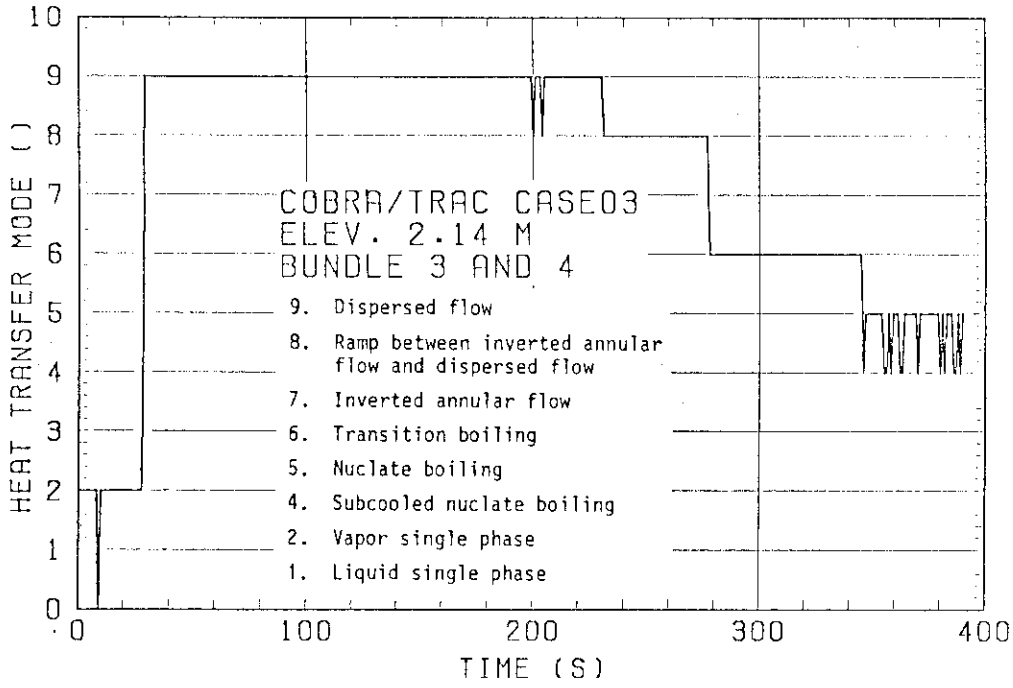

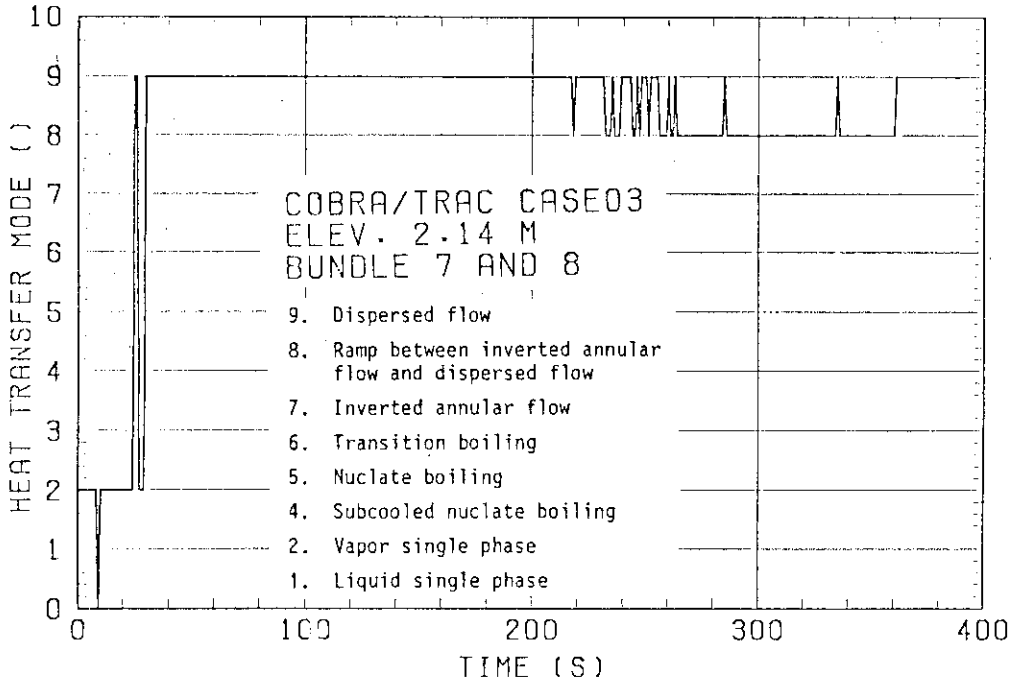

Fig. 4.28 Heat transfer modes in Case 03
(Bundles 1 & 2, 3 & 4, and 7 & 8, Elevation 2.14 m)

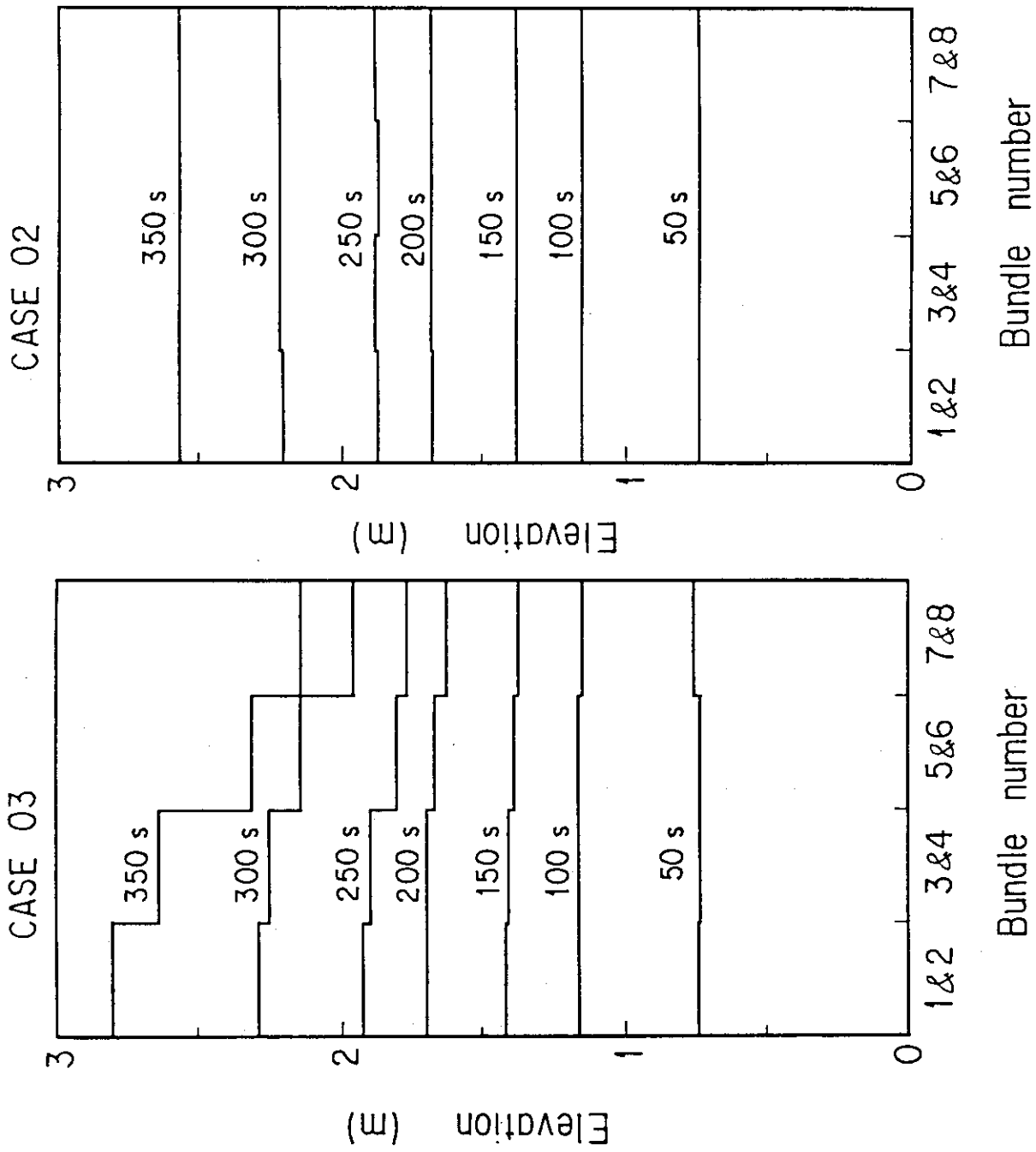

Fig. 4.29 Quench front distributions in Cases 03 and 02

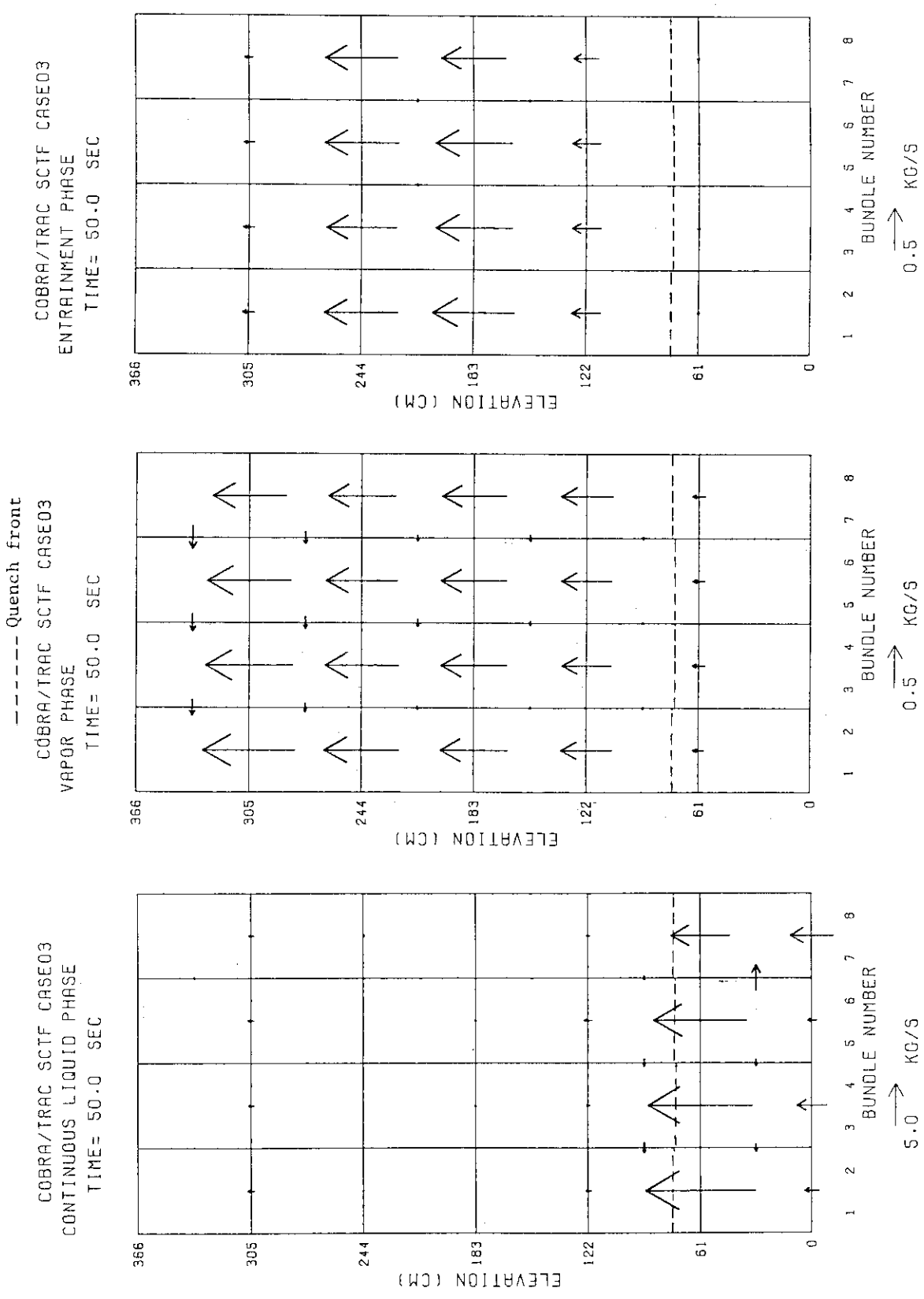

Fig. 4.30(a) Flow direction and magnitude of continuous liquid, vapor and entrained liquid phases in Case 03 (Time = 50 s)

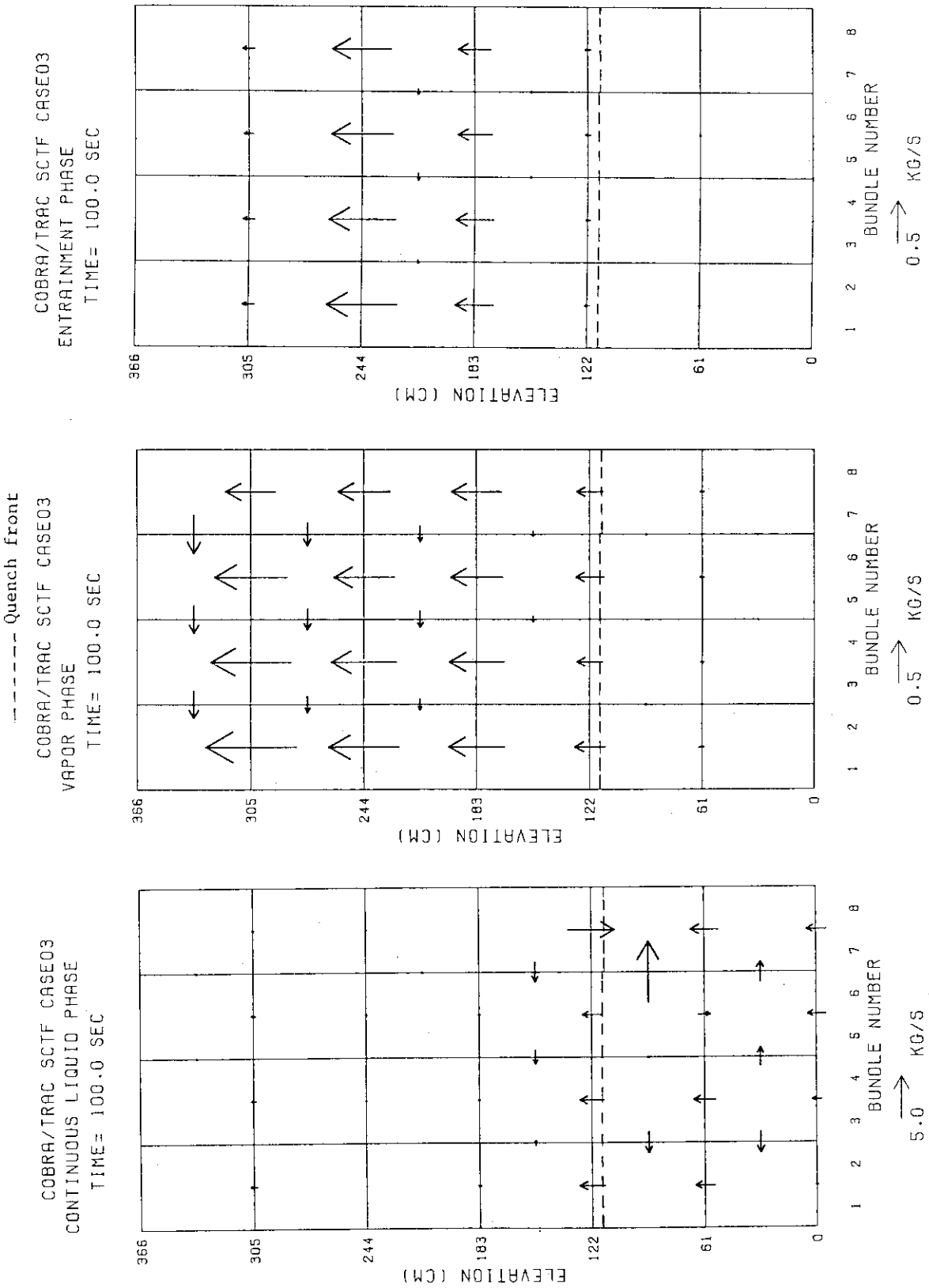

Fig. 4.30(b) Flow direction and magnitude of continuous liquid, vapor and entrained liquid phases in Case 03 (Time = 100 s)

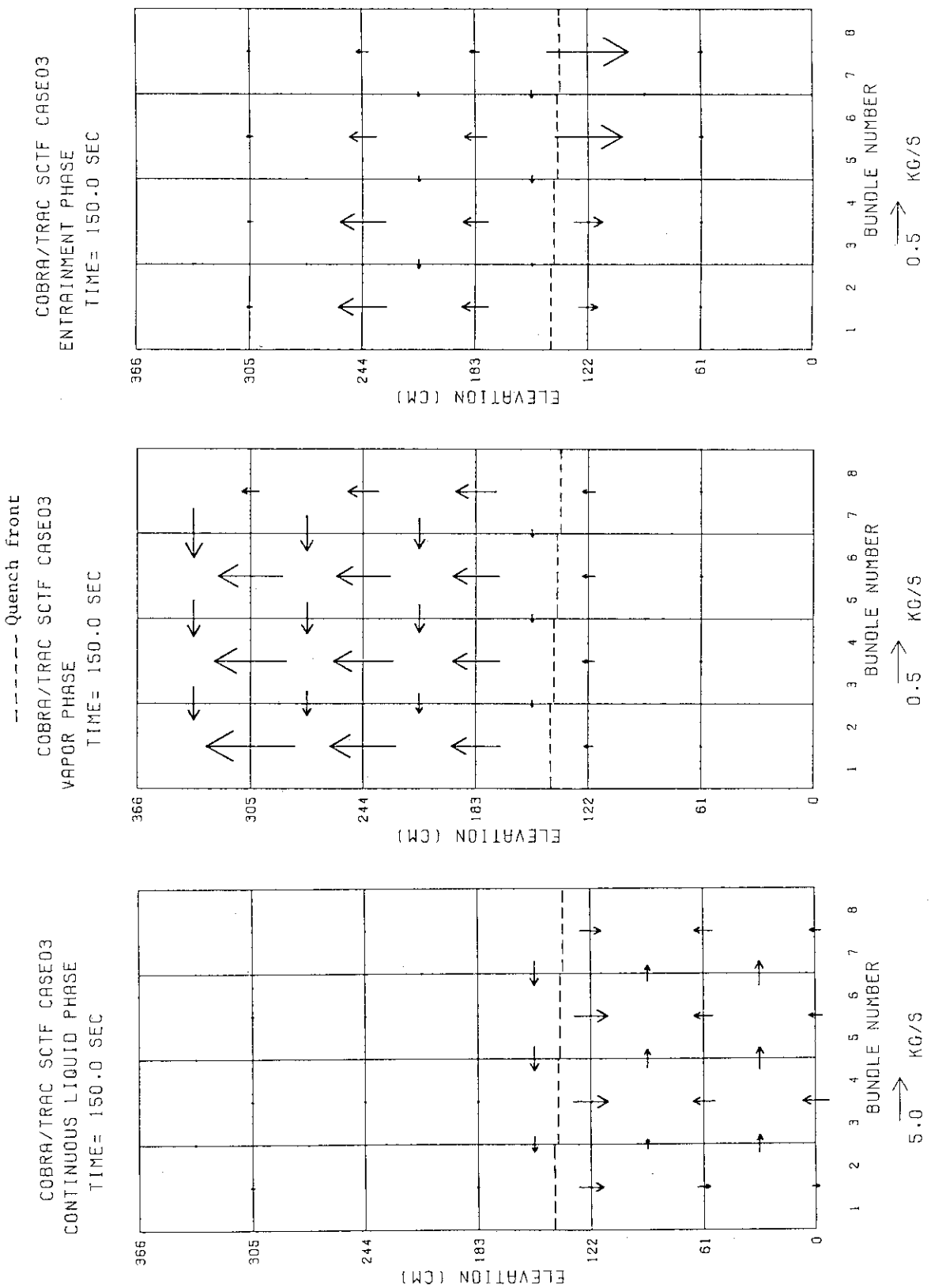

Fig. 4.30(c) Flow direction and magnitude of continuous liquid, vapor and entrained liquid phases in Case 03 (Time = 150 s)

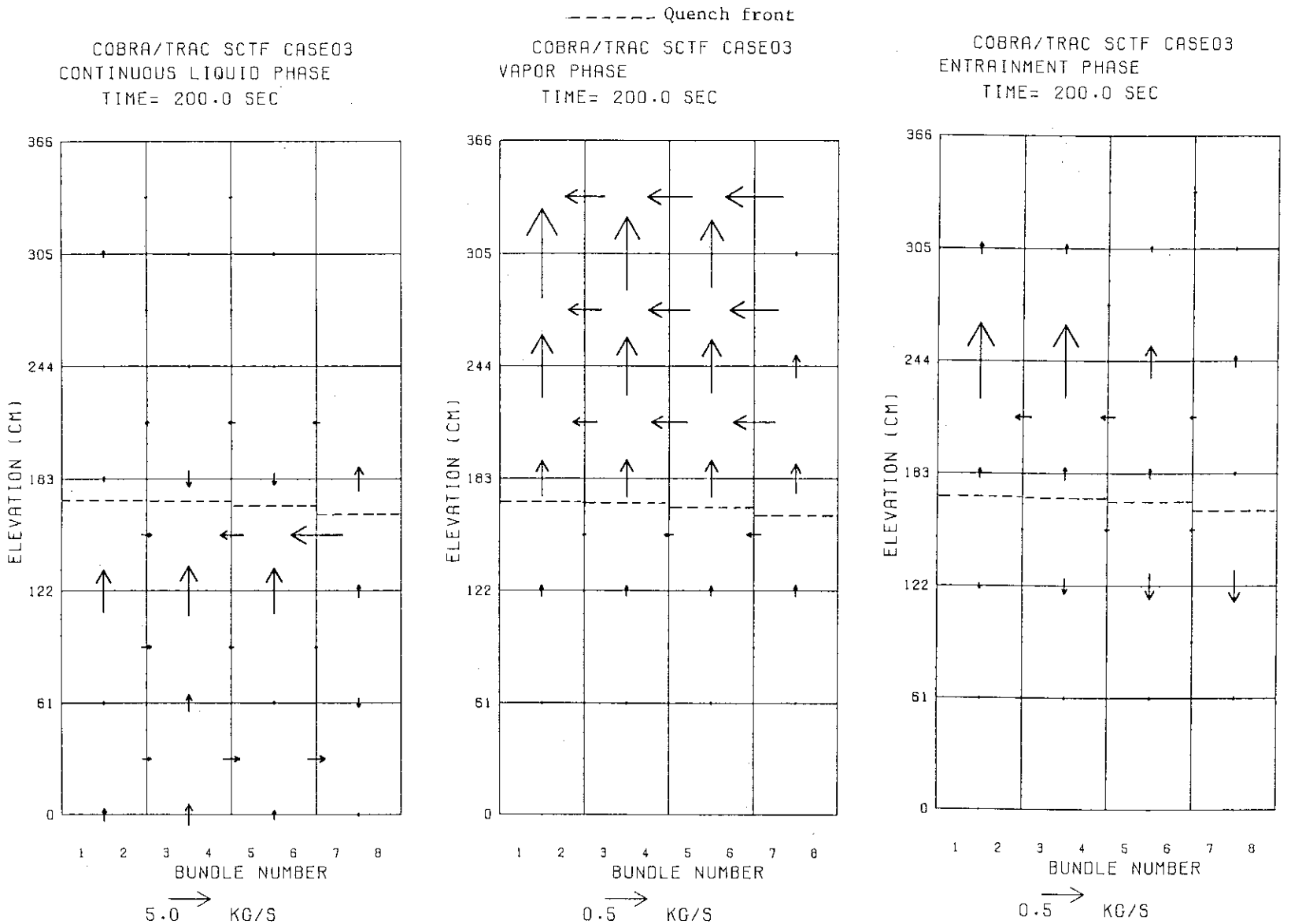

Fig. 4.30(d) Flow direction and magnitude of continuous liquid, vapor and entrained liquid phases in Case 03 (Time = 200 s)

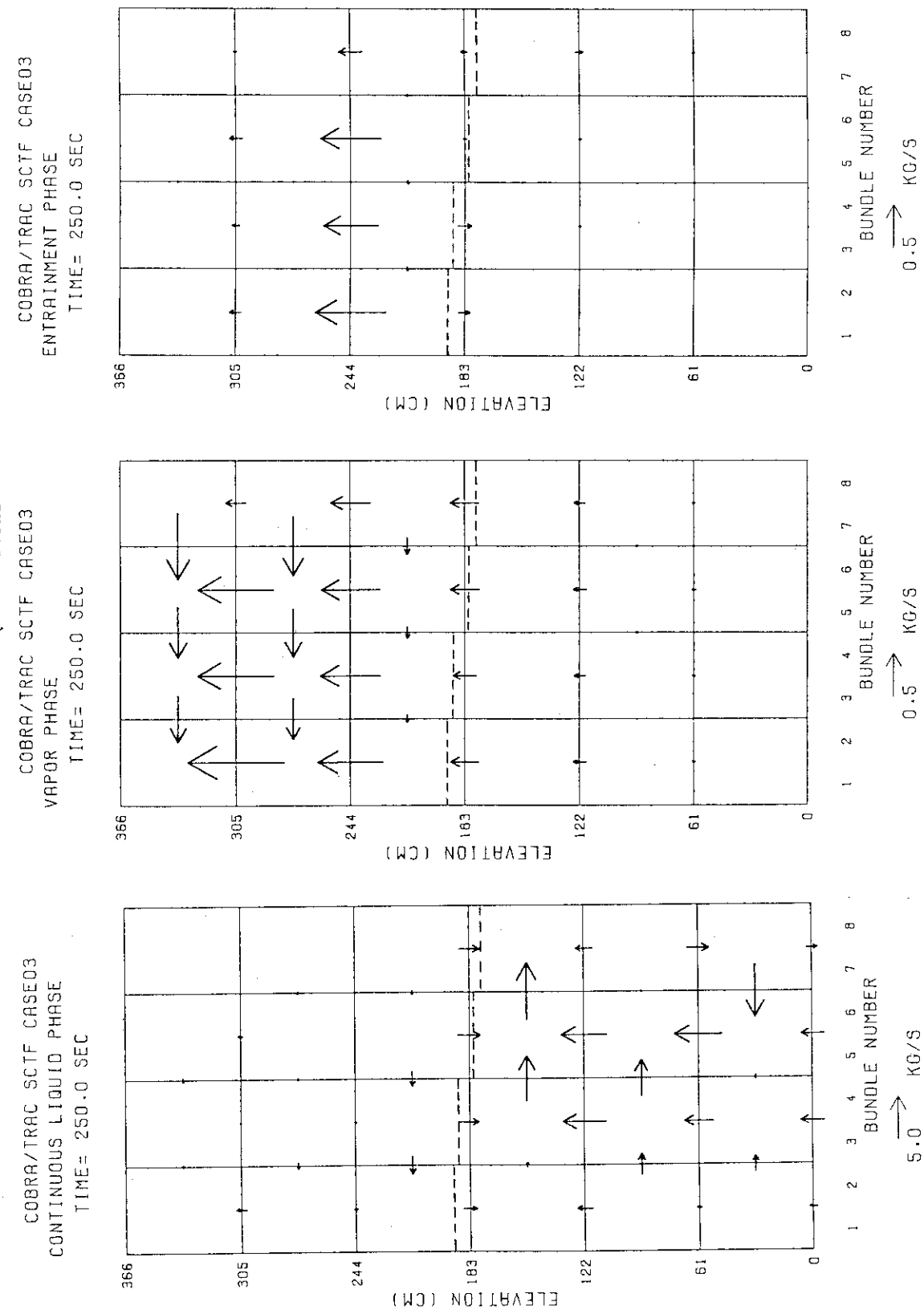

Fig. 4.30(e) Flow direction and magnitude of continuous liquid, vapor and entrained liquid phases in Case 03 (Time = 250 s)

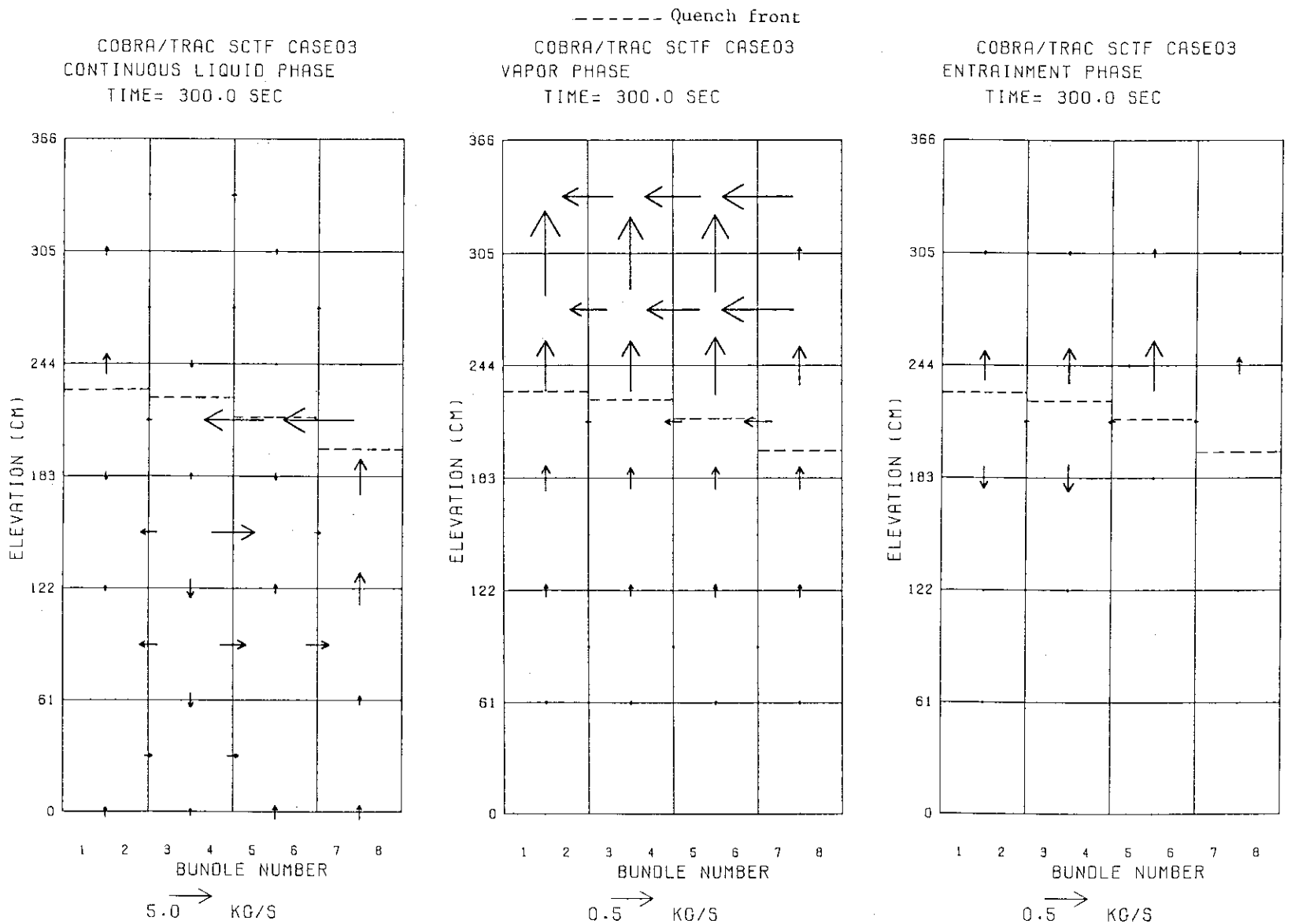

Fig. 4.30(f) Flow direction and magnitude of continuous liquid, vapor and entrained liquid phases in Case 03 (Time = 300 s)

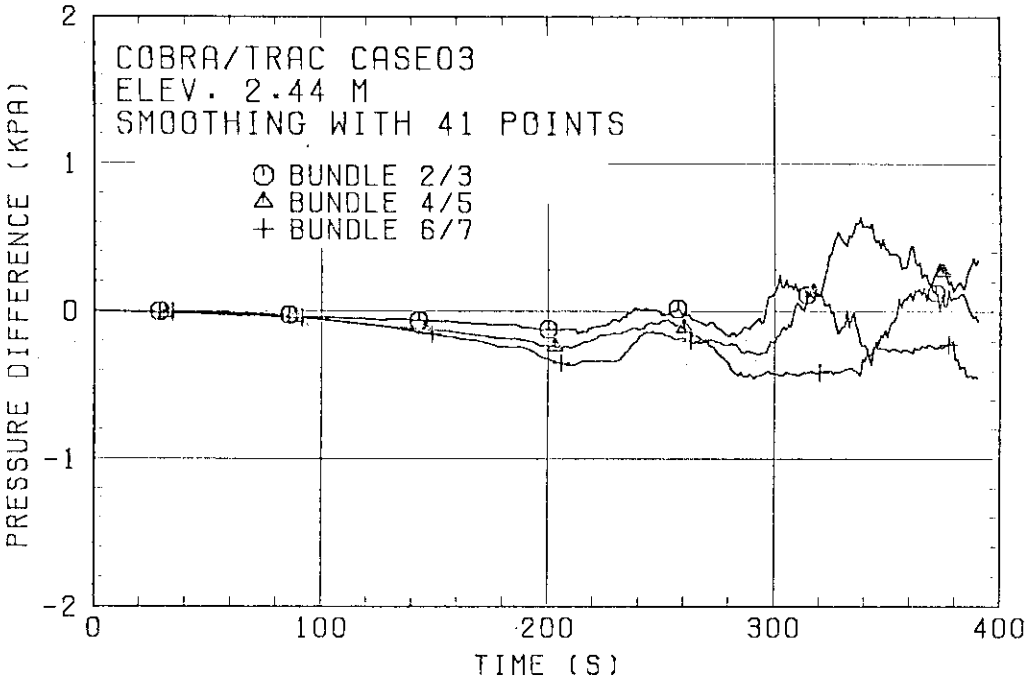

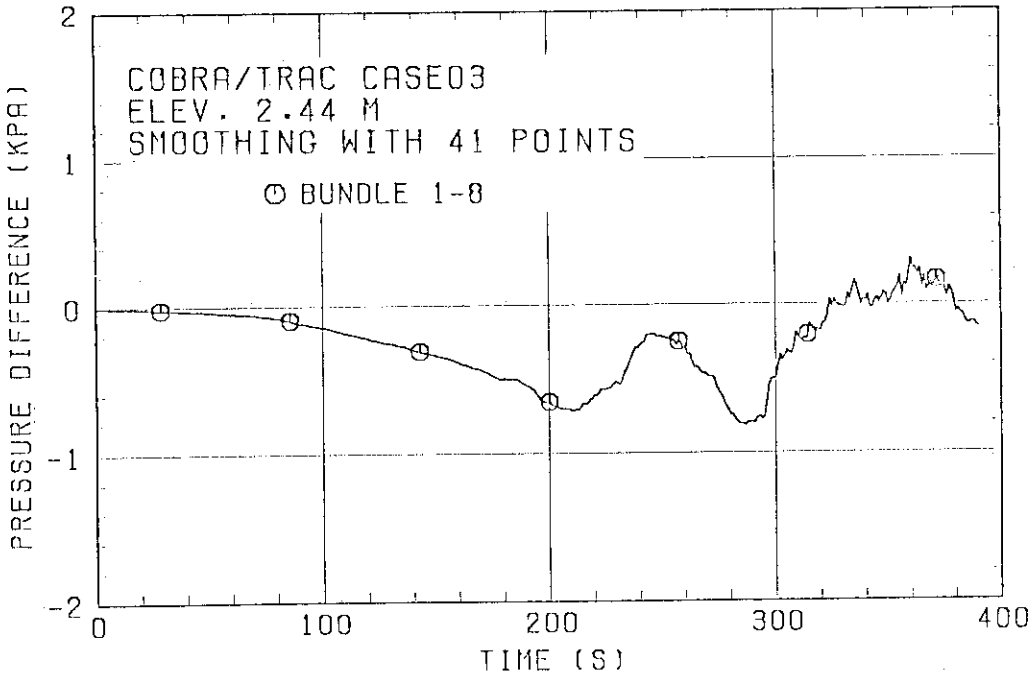

Fig. 4.31 Horizontal differential pressure between Bundles 1 and 8 in Case 03

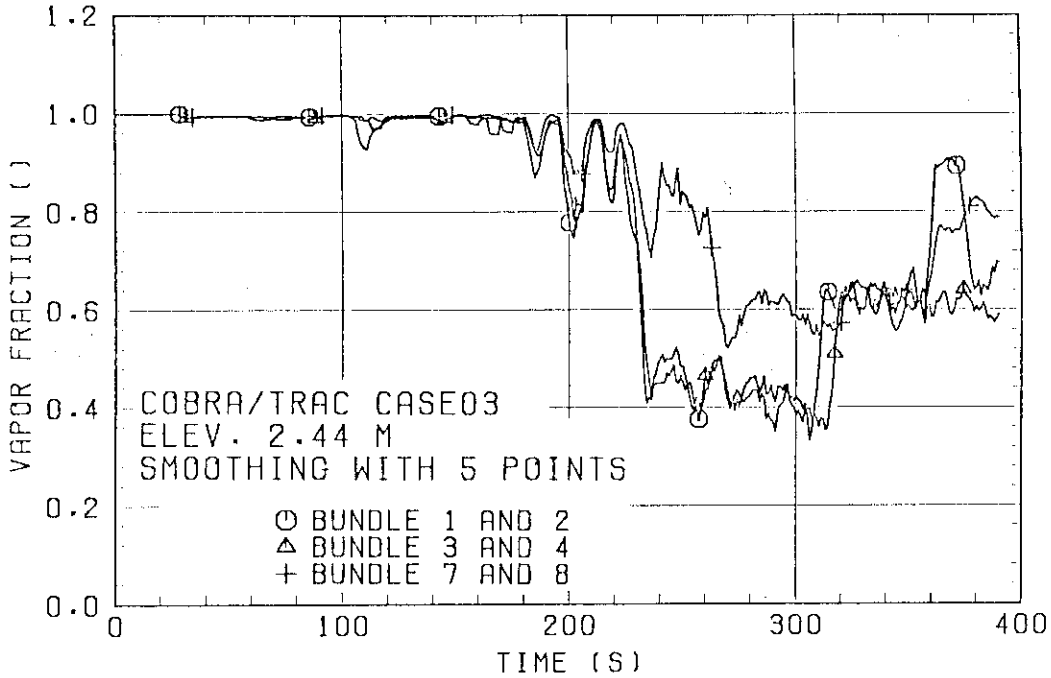

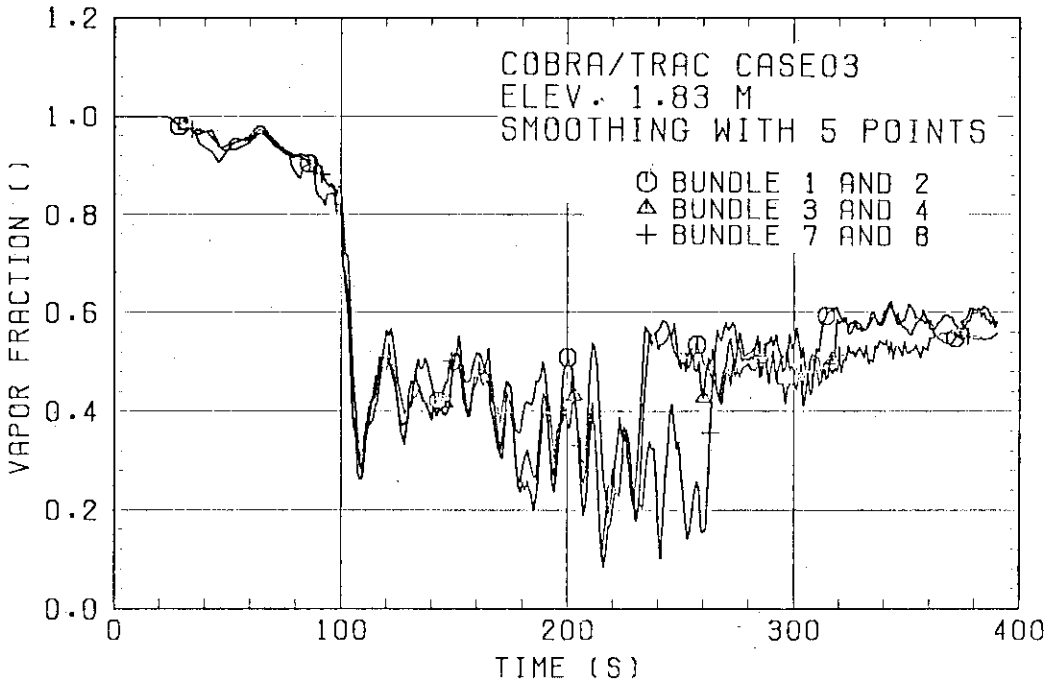

Fig. 4.32 Void fractions in Case 03
(Bundles 1 & 2, 3 & 4 and 7 & 8, Elev. 2.44 and 1.83 m)

5. CONCLUSIONS

1) The overall thermal-hydraulic behavior observed in SCTF tests such as the cladding temperature and the water accumulation in the core could be qualitatively predicted by the COBRA/TRAC code. However, the local void fraction and the horizontal differential pressure were not predicted well even qualitatively by this code.

2) The COBRA/TRAC calculation results under the conditions of flat radial core power distribution and flat pressure distribution at the core outlet (Case 02) exhibited one-dimensional thermal-hydraulic behavior in the core. However, the continuous liquid cross flow behavior below the quench front was not predicted well by this code. On the other hand, the COBRA/TRAC calculation results under steep radial power distribution (Case 01) indicated that the heat transfer was enhanced in the high power bundles and degraded in the low power bundles as observed in the SCTF results.

3) The COBRA/TRAC calculation with steep radial power distribution (Case 01) indicated that the heat transfer enhancement in the high power bundles was caused by the higher heat transfer coefficient to vapor due to the higher vapor flow rate in those bundles than in the other bundles during the dispersed flow heat transfer mode. The reason of this two-dimensional effect is attributed to the fact that the higher vapor generation rate below the quench front in the high power bundles results in the higher vapor up-flow rate through the quench front in those bundles because the vapor cross flow rate was negliegibly small below the quench front.
The contribution of liquid phase to the heat transfer enhancement due to the radial power distribution was relatively small because the difference of heat transfer coefficient between bundles was most significant during the dispersed flow mode in which the heat transfer coefficient to vapor phase was much larger than that to liquid phase.

4) The COBRA/TRAC calculation with inclined pressure distribution at the core outlet (Case 03) indicated that the heat transfer degradation in the Bundle 8 side and enhancement in the Bundle 1 side were due to the lower heat transfer to vapor during the dispersed flow mode and also the lower heat transfer to liquid during the ramp mode between the inverted annular flow and the dispersed flow in the Bundle 8 side than in the Bundle 1 side. The reason of this two-dimensional effect is attributed to the fact that the vapor and entrained liquid flow rates above the quench front become lower in the Bundle 8 side than in the Bundle 1 side as the pressure at the Bundle 8 side increases. This is because the vapor tends to concentrate in the Bundle 1 side due to the cross flow induced by the horizontal pressure gradient and resultantly the generation rate of entrained liquid tends to increase in the Bundle 1 side and decrease in the Bundle 8 side.

ACKNOWLEDGMENT

The authors are much indebted to Dr. Y. Murao for the guidance and encouragement for this work.

They express their appreciation to Mr. T. Okubo and Mr. Y. Abe for their useful discussions.

REFERENCES

(1) T. Iwamura et al., Effects of Radial Core Power Profile on Core Thermo-Hydraulic Behavior during Reflood Phase in PWR-LOCA, J. Nucl. Sci. Tech., vol. 20, No. 9, pp. 743-751, (1983).

(2) T. Iwamura et al., Two-Dimensional Thermal-Hydraulic Behavior in Core in SCTF Core-II Cold Leg Injection Tests (Radial Power Profile Test Results) JAERI-M 85-106, (1985).

(3) M. J. Thurgood et al., COBRA/TRAC A Thermal-Hydraulics Code for Transient Analysis of Nuclear Reactor Vessels and Primary Coolant Systems, NUREG/CR-3046, (1983).

4) The COBRA/TRAC calculation with inclined pressure distribution at the core outlet (Case 03) indicated that the heat transfer degradation in the Bundle 8 side and enhancement in the Bundle 1 side were due to the lower heat transfer to vapor during the dispersed flow mode and also the lower heat transfer to liquid during the ramp mode between the inverted annular flow and the dispersed flow in the Bundle 8 side than in the Bundle 1 side. The reason of this two-dimensional effect is attributed to the fact that the vapor and entrained liquid flow rates above the quench front become lower in the Bundle 8 side than in the Bundle 1 side as the pressure at the Bundle 8 side increases. This is because the vapor tends to concentrate in the Bundle 1 side due to the cross flow induced by the horizontal pressure gradient and resultantly the generation rate of entrained liquid tends to increase in the Bundle 1 side and decrease in the Bundle 8 side.

ACKNOWLEDGMENT

The authors are much indebted to Dr. Y. Murao for the guidance and encouragement for this work.

They express their appreciation to Mr. T. Okubo and Mr. Y. Abe for their useful discussions.

REFERENCES

(1) T. Iwamura et al., Effects of Radial Core Power Profile on Core Thermo-Hydraulic Behavior during Reflood Phase in PWR-LOCA, J. Nucl. Sci. Tech., vol. 20, No. 9, pp. 743-751, (1983).

(2) T. Iwamura et al., Two-Dimensional Thermal-Hydraulic Behavior in Core in SCTF Core-II Cold Leg Injection Tests (Radial Power Profile Test Results) JAERI-M 85-106, (1985).

(3) M. J. Thurgood et al., COBRA/TRAC A Thermal-Hydraulics Code for Transient Analysis of Nuclear Reactor Vessels and Primary Coolant Systems, NUREG/CR-3046, (1983).

4) The COBRA/TRAC calculation with inclined pressure distribution at the core outlet (Case 03) indicated that the heat transfer degradation in the Bundle 8 side and enhancement in the Bundle 1 side were due to the lower heat transfer to vapor during the dispersed flow mode and also the lower heat transfer to liquid during the ramp mode between the inverted annular flow and the dispersed flow in the Bundle 8 side than in the Bundle 1 side. The reason of this two-dimensional effect is attributed to the fact that the vapor and entrained liquid flow rates above the quench front become lower in the Bundle 8 side than in the Bundle 1 side as the pressure at the Bundle 8 side increases. This is because the vapor tends to concentrate in the Bundle 1 side due to the cross flow induced by the horizontal pressure gradient and resultantly the generation rate of entrained liquid tends to increase in the Bundle 1 side and decrease in the Bundle 8 side.

ACKNOWLEDGMENT

The authors are much indebted to Dr. Y. Murao for the guidance and encouragement for this work.

They express their appreciation to Mr. T. Okubo and Mr. Y. Abe for their useful discussions.

REFERENCES

(1) T. Iwamura et al., Effects of Radial Core Power Profile on Core Thermo-Hydraulic Behavior during Reflood Phase in PWR-LOCA, J. Nucl. Sci. Tech., vol. 20, No. 9, pp. 743-751, (1983).

(2) T. Iwamura et al., Two-Dimensional Thermal-Hydraulic Behavior in Core in SCTF Core-II Cold Leg Injection Tests (Radial Power Profile Test Results) JAERI-M 85-106, (1985).

(3) M. J. Thurgood et al., COBRA/TRAC A Thermal-Hydraulics Code for Transient Analysis of Nuclear Reactor Vessels and Primary Coolant Systems, NUREG/CR-3046, (1983).

(4) H. Adachi et al., Design of Slab Core Test Facility (SCTF) in Large Scale Reflood Test Program, Part I: Core I, JAERI-M 83-080, (1983).

(5) M. Sobajima et al., Design of Slab Core Test Facility (SCTF) in Large Scale Reflood Test Program, Part II: Core II, JAERI-M to be published.

(6) H. Adachi et al., Development of SCTF Cold Leg Injection Test Method for Eliminating U-Tube Oscillation during the Initial Period, JAERI-M to be published.

APPENDIX Input Data Listings for COBRA/TRAC Calculations

(1) Case 0 1

```
********************************** INPUT FILE LISTING **********************************
     12345678901234567890123456789012345678901234567890123456789012345678901234567890
  1            11                  0                  0                  50
  2  *****  SLAB CORE TEST FACILITY ANALISYS USED 'COBRA/TRAC' DATA
  3            TEST CASE    ... 01 ( JUNE 1984 ) VESSEL UNIT(BTU) GAP-DETAIL
  4            CONVERGENCE CONDITION  EPS=0.01   , DELT = 0.0001
  5            FILL COMPONENT NOT INCLUDE  ( FILL ==> VESSEL BOUNDARY )
  6             COMPONENT        BREAK     .....  4
  7                              PIPE      .....  4
  8                              JUNCTION  .....  8
  9                              VESSEL    .....  1
 10                                  AXIAL SECTION      .....   3
 11                                  CHANNELS           .....   9
 12                                  GAP                .....   6
 13              0              0.0
 14              9                8                0
 15           0.01               10               40
 16              0                0
 17              6                7                8                9                2
 18              3                4                5                1
 19  BREAK                        6                6                0
 20              2                1                6                3
 21            0.1           0.0106              1.0           392.70        0.200E+6
 22            0.0         0.200E+6             50.0         0.200E+6           100.0
 23        0.200E+6           150.0         0.200E+6            200.0        0.200E+6
 24          500.0         0.200E+6E
 25  BREAK                        7                7                0
 26              4                1                6                3
 27            0.1           0.0106              1.0           392.70        0.200E+6
 28            0.0         0.200E+6             50.0         0.200E+6           100.0
 29        0.200E+6           150.0         0.200E+6            200.0        0.200E+6
 30          500.0         0.200E+6E
     12345678901234567890123456789012345678901234567890123456789012345678901234567890
 31  BREAK                        8                8                0
 32              6                1                6                3
 33            0.1           0.0106              1.0           392.70        0.200E+6
 34            0.0         0.200E+6             50.0         0.200E+6           100.0
 35        0.200E+6           150.0         0.200E+6            200.0        0.200E+6
 36          500.0         0.200E+6E
 37  BREAK                        9                9                0
 38              8                1                6                3
 39            0.1           0.0106              1.0           392.70        0.200E+6
 40            0.0         0.200E+6             50.0         0.200E+6           100.0
 41        0.200E+6           150.0         0.200E+6            200.0        0.200E+6
 42          500.0         0.200E+6E
 43  PIPE                         2                2
 44              1                0                1                2                6
 45              0                1
 46          0.184            0.001              0.0              0.0           392.70
 47         392.70
 48  F         0.1E
 49  F      0.0106E
 50  F       0.106E
 51  F         0.0E
 52  F         0.0E
 53  F       0.367E
 54  F          5E
 55  F         0.0E
 56  F         1.0E
 57  F         0.0E
 58  F      392.70E
 59  F    0.200E+6E
```

```
 60 PIPE                          3              3
    12345678901234567890123456789012345678901234567890123456789012345678901234567890
 61              1              0              3              4              6
 62              0              1
 63          0.184          0.001            0.0            0.0         392.70
 64         392.70
 65 F          0.1E
 66 F        0.0106E
 67 F         0.106E
 68 F          0.0E
 69 F          0.0E
 70 F         0.367E
 71 F             5E
 72 F          0.0E
 73 F          1.0E
 74 F          0.0E
 75 F        392.70E
 76 F      0.200E+6E
 77 PIPE                          4              4
 78              1              0              5              6              6
 79              0              1
 80          0.184          0.001            0.0            0.0         392.70
 81         392.70
 82 F          0.1E
 83 F        0.0106E
 84 F         0.106E
 85 F          0.0E
 86 F          0.0E
 87 F         0.367E
 88 F             5E
 89 F          0.0E
 90 F          1.0E
    12345678901234567890123456789012345678901234567890123456789012345678901234567890
 91 F          0.0E
 92 F        392.70E
 93 F      0.200E+6E
 94 PIPE                          5              5
 95              1              0              7              8              6
 96              0              1
 97          0.184          0.001            0.0            0.0         392.70
 98         392.70
 99 F          0.1E
100 F        0.0106E
101 F         0.106E
102 F          0.0E
103 F          0.0E
104 F         0.367E
105 F             5E
106 F          0.0E
107 F          1.0E
108 F          0.0E
109 F        392.70E
110 F      0.200E+6E
111 VESSEL                        1              1
112          1  ****  S.C.T.F.  VESSEL DATA  SECTION= 5,CHANNEL= 20,GAP= 15
113     1    3
114 163.8
115      29.01    1164.0       0.0       0.32
116     2    9    8
117     1527.22456.
118     2135.6740.2              1
119     4    1    428.98
```

```
120      3135.6730.7                2
    12345678901234567890123456789012345678901234567890123456789012345678901234567890
121      4     1     428.98     4     2     528.98
122      4135.6730.7                2
123      4     2     528.98     4     3     628.98
124      5135.6740.2                1
125      4     3     628.98
126      6135.6740.2                1
127      4     4     028.98
128      7135.6730.7                2
129      4     4     028.98     4     5     028.98
130      8135.6730.7                2
131      4     5     028.98     4     6     028.98
132      9135.6740.2                1
133      4     6     028.98
134      2     1     2                          1
135      3     3     4                          2
136      4     5     6                          3
137      5     7     8                          4
138      6     1     2                          5
139      7     3     4                          6
140      8     5     6                          7
141      9     7     8                          8
142      3     6
143      1     2     3  3.218.11 16.     1.     0     4     1.    -1     2     0     0     0     0
144     17   1.0
145      2     3     4  3.218.11 16.     1.     0     5     1.     1     3     0     0     0     0
146     17   1.0
147      3     4     5  3.218.11 16.     1.     0     6     1.     2    -1     0     0     0     0
148     17   1.0
149      4     6     7  3.218.11 16.     1.     1     0     1.    -1     5     0     0     0     0
150     17   1.0
    12345678901234567890123456789012345678901234567890123456789012345678901234567890
151      5     7     8  3.218.11 16.     1.     2     0     1.     4     6     0     0     0     0
152     17   1.0
153      6     8     9  3.218.11 16.     1.     3     0     1.     5    -1     0     0     0     0
154     17   1.0
155      0
156      4     3     1     1
157      1     1     1     19.685
158      1     2     3     4     5                1
159      2     4     3      24.02
160      2     6                                  1
161      3     7                                  1
162      4     8                                  1
163      5     9                                  1
164      3     4     3      24.02
165      6     6                                  2
166      7     7                                  3
167      8     8                                  4
168      9     9                                  5
169      4
170     25
171      7     3
172   1.82     1     2     3     4     5     6     7     8     9
173   1.82     2     2     3     4     5     6     7     8     9
174   1.82     3     2     3     4     5     6     7     8     9
175      8     8     8     2     8
176      1     1     1     1   0.07874       234.      1.000     50000.
177      2     1     1     1   0.07874       234.      1.000     50000.
178      3     1     1     1   0.07874       234.      1.200     50000.
179      4     1     1     1   0.07874       234.      1.200     50000.
```

```
180      5     1     1     1   0.07874       234.      1.000     50000.
    12345678901234567890123456789012345678901234567890123456789012345678901234567890
181      6     1     1     1   0.07874       234.      1.000     50000.
182      7     1     1     1   0.07874       234.      0.800     50000.
183      8     1     1     1   0.07874       234.      0.800     50000.
184      1     2      1.707         .0        44.
185      2     2      1.707         .0        44.
186      3     2      1.707         .0        44.
187      4     2      1.707         .0        44.
188      5     2      1.707         .0        44.
189      6     2      1.707         .0        44.
190      7     2      1.707         .0        44.
191      8     2      1.707         .0        44.
192      1     2     0   12
193      1     2
194     19.685       485.       43.7       921.       43.8       921.       67.7      1229.
195       67.8      1229.       91.9      1331.       92.0      1331.      115.9      1241.
196      116.0      1241.      139.9       946.      140.0       946.      164.0       512.
197      2     2     0   12
198      3     4
199     19.685       512.       43.7      1043.       43.8      1043.       67.7      1385.
200       67.8      1385.       91.9      1547.       92.0      1547.      115.9      1430.
201      116.0      1430.      139.9      1088.      140.0      1088.      164.0       575.
202      3     2     0   12
203      5     6
204     19.685       485.       43.7       917.       43.8       917.       67.7      1259.
205       67.8      1259.       91.9      1391.       92.0      1391.      115.9      1259.
206      116.0      1259.      139.9       946.      140.0       946.      164.0       512.
207      4     2     0   12
208      7     8
209     19.685       485.       43.7       800.       43.8       800.       67.7      1038.
210       67.8      1038.       91.9      1178.       92.0      1178.      115.9      1092.
    12345678901234567890123456789012345678901234567890123456789012345678901234567890
211      116.0      1092.      139.9       827.      140.0       827.      164.0       467.
212      5     0     2   12
213      1     5
214     19.685       527.       43.7       509.       43.8       509.       67.7       493.
215       67.8       493.       91.9       440.       92.0       440.      115.9       365.
216      116.0       365.      139.9       318.      140.0       318.      164.0       277.
217      6     0     2   12
218      2     6
219     19.685       538.       43.7       559.       43.8       559.       67.7       566.
220       67.8       566.       91.9       494.       92.0       494.      115.9       394.
221      116.0       394.      139.9       356.      140.0       356.      164.0       282.
222      7     0     2   12
223      3     7
224     19.685       449.       43.7       473.       43.8       473.       67.7       476.
225       67.8       476.       91.9       412.       92.0       412.      115.9       345.
226      116.0       345.      139.9       307.      140.0       307.      164.0       268.
227      8     0     2   12
228      4     8
229     19.685       395.       43.7       415.       43.8       415.       67.7       421.
230       67.8       421.       91.9       381.       92.0       381.      115.9       329.
231      116.0       329.      139.9       293.      140.0       293.      164.0       250.
232      9     2
233      1 HROD      .422         .0     4     2
234      1    10.102    0.     1    30.022    1.     4    10.049    0.     2    20.038    0.
235      2 HROD     .5434         .0     2     2
236      2    10.189    0.     1    2.0827    0.
237     10     3
238      1    11     156.07
239       212.      0.253     0.3434      302.       0.261     0.3434
```

```
240        482.      0.273     0.3434      662.       0.281     0.3434
    12345678901234567890123456789012345678901234567890123456789012345678901234567890
241        842.      0.287     0.3434     1022.       0.292     0.3434
242       1202.      0.296     0.3434     1382.       0.300     0.3434
243       1562.      0.303     0.3434     1742.       0.306     0.3434
244       1922.      0.309     0.3434
245      2   11     526.07
246        212.     0.1050     8.4590      302.      0.1066     9.5600
247        482.     0.1202     11.150      662.      0.1264     12.340
248        842.     0.1312     13.300     1022.      0.1350     14.130
249       1202.     0.1390     14.860     1382.      0.1420     15.510
250       1562.     0.1440     16.110     1742.      0.1470     16.660
251       1922.     0.1490     17.170
252      3    1     525.02
253        200.      0.104      6.529     2000.       0.104      6.259
254     11    1     8
255      1   19
256     19.685       .379       24.0       .379       31.7      .5786       40.0       .771
257       48.0        .95       56.7       1.10       65.4      1.229       74.1      1.321
258       82.8     1.3786       91.7        1.4      100.6     1.3786      109.3      1.321
259      118.0      1.229      126.6       1.10      135.2       0.95      143.6      0.771
260      151.7     0.5786      159.8      0.379      164.0      0.379
261        0.0        1.0       34.0        1.0       57.0       .922      107.0       .837
262      157.0       .795      257.0       .702      357.0       .646      400.0       .626
263     13    1     0    2     0
264      6    9
265     .0        1.0  4.0        1.0  7.0      0.426 52.0      0.426 76.5  0.185    .6186
266 400.0      0.185                                                                   .5766
267     .0        1.0 46.0        1.0 57.0      0.958105.0      0.890157.0  0.857    .6186
268 208.0      0.890250.0      0.933315.0      0.975400.0      0.992                  .5766
269      1    1     2    1     2      59.52      216.6
270     14    5                          0     2
    12345678901234567890123456789012345678901234567890123456789012345678901234567890
                                                                        END GROUP14
271                                                                     END GROUP14
272
273      4
274      6    4    -1    1
275      7    4    -1    3
276      8    4    -1    5
277      9    4    -1    7
278      0
279      9    0     450.0
280      1    2    3    4    5    6    7    8    9
281           .0001              .1            350.            1.0          7190.
282            50.0             1.0            50.          1000.0
283
284
285
286
287
```

(2) Case 0 2

```
********************************** INPUT FILE LISTING **********************************
    12345678901234567890123456789012345678901234567890123456789012345678901234567890
  1            11                0                0                50
  2  *****  SLAB CORE TEST FACILITY ANALISYS USED 'COBRA/TRAC' DATA
  3            TEST CASE   ... 01 ( JUNE 1984 ) VESSEL UNIT(BTU) GAP-DETAIL
  4            CONVERGENCE CONDITION  EPS=0.01  , DELT = 0.0001
  5            FILL COMPONENT NOT INCLUDE  ( FILL ==> VESSEL BOUNDARY )
  6             COMPONENT       BREAK     .....  4
  7                             PIPE      .....  4
  8                             JUNCTION .....  8
  9                             VESSEL    .....  1
 10                                AXIAL SECTION      .....   3
 11                                CHANNELS           .....   9
 12                                GAP                .....   6
 13             0            0.0
 14             9              8              0
 15          0.01             10             40
 16             0              0
 17             6              7              8              9              2
 18             3              4              5              1
 19 BREAK                      6              6              0
 20             2              1              3              3
 21           0.1         0.0106            1.0         392.70       0.200E+6
 22           0.0       0.200E+6            7.0       0.200E+6          407.0
 23       0.200E+6
 24 BREAK                      7              7              0
 25             4              1              3              3
 26           0.1         0.0106            1.0         392.70       0.200E+6
 27           0.0       0.200E+6            7.0       0.200E+6          407.0
 28       0.200E+6
 29 BREAK                      8              8              0
 30             6              1              3              3
    12345678901234567890123456789012345678901234567890123456789012345678901234567890
 31           0.1         0.0106            1.0         392.70       0.200E+6
 32           0.0       0.200E+6            7.0       0.200E+6          407.0
 33       0.200E+6
 34 BREAK                      9              9              0
 35             8              1              3              3
 36           0.1         0.0106            1.0         392.70       0.200E+6
 37           0.0       0.200E+6            7.0       0.200E+6          407.0
 38       0.200E+6
 39 PIPE                       2              2
 40             1              0              1              2              6
 41             0              1
 42         0.184          0.001            0.0            0.0         392.70
 43        392.70
 44 F         0.1E
 45 F      0.0106E
 46 F       0.106E
 47 F         0.0E
 48 F         0.0E
 49 F       0.367E
 50 F           5E
 51 F         0.0E
 52 F         1.0E
 53 F         0.0E
 54 F      392.70E
 55 F    0.200E+6E
 56 PIPE                       3              3
 57             1              0              3              4              6
 58             0              1
 59         0.184          0.001            0.0            0.0         392.70
```

```
 60          392.70
    12345678901234567890123456789012345678901234567890123456789012345678901234567890
 61 F           0.1E
 62 F        0.0106E
 63 F         0.106E
 64 F           0.0E
 65 F           0.0E
 66 F         0.367E
 67 F             5E
 68 F           0.0E
 69 F           1.0E
 70 F           0.0E
 71 F        392.70E
 72 F      0.200E+6E
 73 PIPE                          4              4
 74                1              0              5              6              6
 75                0              1
 76            0.184          0.001            0.0            0.0         392.70
 77          392.70
 78 F           0.1E
 79 F        0.0106E
 80 F         0.106E
 81 F           0.0E
 82 F           0.0E
 83 F         0.367E
 84 F             5E
 85 F           0.0E
 86 F           1.0E
 87 F           0.0E
 88 F        392.70E
 89 F      0.200E+6E
 90 PIPE                          5              5
    12345678901234567890123456789012345678901234567890123456789012345678901234567890
 91                1              0              7              8              6
 92                0              1
 93            0.184          0.001            0.0            0.0         392.70
 94          392.70
 95 F           0.1E
 96 F        0.0106E
 97 F         0.106E
 98 F           0.0E
 99 F           0.0E
100 F         0.367E
101 F             5E
102 F           0.0E
103 F           1.0E
104 F           0.0E
105 F        392.70E
106 F      0.200E+6E
107 VESSEL                        1              1
108            1  ****  S.C.T.F.  VESSEL DATA  SECTION= 5,CHANNEL= 20,GAP= 15
109      1     3
110 163.8
111       29.01     1164.0        0.0       0.32
112      2     9     8
113      1527.22456.
114      2135.6740.2                1
115      4     1     428.98
116      3135.6730.7                2
117      4     1     428.98     4     2     528.98
118      4135.6730.7                2
119      4     2     528.98     4     3     628.98
```

```
120     5135.6740.2                 1
    12345678901234567890123456789012345678901234567890123456789012345678901234567890
121     4    3    628.98
122     6135.6740.2                 1
123     4    4    028.98
124     7135.6730.7                 2
125     4    4    028.98    4    5    028.98
126     8135.6730.7                 2
127     4    5    028.98    4    6    028.98
128     9135.6740.2                 1
129     4    6    028.98
130     2    1    2                         1
131     3    3    4                         2
132     4    5    6                         3
133     5    7    8                         4
134     6    1    2                         5
135     7    3    4                         6
136     8    5    6                         7
137     9    7    8                         8
138     3    6
139     1    2    3  3.218.11 16.    1.    0    4    1.   -1    2    0    0    0    0
140    17  1.0
141     2    3    4  3.218.11 16.    1.    0    5    1.    1    3    0    0    0    0
142    17  1.0
143     3    4    5  3.218.11 16.    1.    0    6    1.    2   -1    0    0    0    0
144    17  1.0
145     4    6    7  3.218.11 16.    1.    1    0    1.   -1    5    0    0    0    0
146    17  1.0
147     5    7    8  3.218.11 16.    1.    2    0    1.    4    6    0    0    0    0
148    17  1.0
149     6    8    9  3.218.11 16.    1.    3    0    1.    5   -1    0    0    0    0
150    17  1.0
    12345678901234567890123456789012345678901234567890123456789012345678901234567890
151     0
152     4    3    1    1
153     1    1    1    19.685
154     1    2    3    4    5                1
155     2    4    3     24.02
156     2    6                              1
157     3    7                              1
158     4    8                              1
159     5    9                              1
160     3    4    3     24.02
161     6    6                              2
162     7    7                              3
163     8    8                              4
164     9    9                              5
165     4
166    25
167     7    3
168  1.82    1    2    3    4    5    6    7    8    9
169  1.82    2    2    3    4    5    6    7    8    9
170  1.82    3    2    3    4    5    6    7    8    9
171     8    8    8    2    8
172     1    1    1    1   0.07874      234.     1.000    50000.
173     2    1    1    1   0.07874      234.     1.000    50000.
174     3    1    1    1   0.07874      234.     1.000    50000.
175     4    1    1    1   0.07874      234.     1.000    50000.
176     5    1    1    1   0.07874      234.     1.000    50000.
177     6    1    1    1   0.07874      234.     1.000    50000.
178     7    1    1    1   0.07874      234.     1.000    50000.
179     8    1    1    1   0.07874      234.     1.000    50000.
```

```
180      1     2      1.707         .0        44.
    12345678901234567890123456789012345678901234567890123456789012345678901234567890
181      2     2      1.707         .0        44.
182      3     2      1.707         .0        44.
183      4     2      1.707         .0        44.
184      5     2      1.707         .0        44.
185      6     2      1.707         .0        44.
186      7     2      1.707         .0        44.
187      8     2      1.707         .0        44.
188      1     2     0   12
189      1     2
190     19.685       485.       43.7       921.       43.8       921.       67.7      1229.
191       67.8      1229.       91.9      1331.       92.0      1331.      115.9      1241.
192      116.0      1241.      139.9       946.      140.0       946.      164.0       512.
193      2     2     0   12
194      3     4
195     19.685       485.       43.7       921.       43.8       921.       67.7      1229.
196       67.8      1229.       91.9      1331.       92.0      1331.      115.9      1241.
197      116.0      1241.      139.9       946.      140.0       946.      164.0       512.
198      3     2     0   12
199      5     6
200     19.685       485.       43.7       921.       43.8       921.       67.7      1229.
201       67.8      1229.       91.9      1331.       92.0      1331.      115.9      1241.
202      116.0      1241.      139.9       946.      140.0       946.      164.0       512.
203      4     2     0   12
204      7     8
205     19.685       485.       43.7       921.       43.8       921.       67.7      1229.
206       67.8      1229.       91.9      1331.       92.0      1331.      115.9      1241.
207      116.0      1241.      139.9       946.      140.0       946.      164.0       512.
208      5     0     2   12
209      1     5
210     19.685       527.       43.7       509.       43.8       509.       67.7       493.
    12345678901234567890123456789012345678901234567890123456789012345678901234567890
211       67.8       493.       91.9       440.       92.0       440.      115.9       365.
212      116.0       365.      139.9       318.      140.0       318.      164.0       277.
213      6     0     2   12
214      2     6
215     19.685       527.       43.7       509.       43.8       509.       67.7       493.
216       67.8       493.       91.9       440.       92.0       440.      115.9       365.
217      116.0       365.      139.9       318.      140.0       318.      164.0       277.
218      7     0     2   12
219      3     7
220     19.685       527.       43.7       509.       43.8       509.       67.7       493.
221       67.8       493.       91.9       440.       92.0       440.      115.9       365.
222      116.0       365.      139.9       318.      140.0       318.      164.0       277.
223      8     0     2   12
224      4     8
225     19.685       527.       43.7       509.       43.8       509.       67.7       493.
226       67.8       493.       91.9       440.       92.0       440.      115.9       365.
227      116.0       365.      139.9       318.      140.0       318.      164.0       277.
228      9     2
229      1 HROD       .422         .0     4     2
230      1     10.102    0.     1     30.022    1.     4     10.049    0.     2     20.038    0.
231      2 HROD      .5434         .0     2     2
232      2     10.189    0.     1     2.0827    0.
233     10     3
234      1    11     156.07
235       212.      0.253     0.3434      302.      0.261     0.3434
236       482.      0.273     0.3434      662.      0.281     0.3434
237       842.      0.287     0.3434     1022.      0.292     0.3434
238      1202.      0.296     0.3434     1382.      0.300     0.3434
239      1562.      0.303     0.3434     1742.      0.306     0.3434
```

```
240       1922.      0.309     0.3434
    12345678901234567890123456789012345678901234567890123456789012345678901234567890
241      2   11     526.07
242        212.     0.1050    8.4590      302.      0.1066    9.5600
243        482.     0.1202    11.150      662.      0.1264    12.340
244        842.     0.1312    13.300     1022.      0.1350    14.130
245       1202.     0.1390    14.860     1382.      0.1420    15.510
246       1562.     0.1440    16.110     1742.      0.1470    16.660
247       1922.     0.1490    17.170
248      3    1     525.02
249        200.      0.104     6.529     2000.       0.104     6.259
250     11    1     8
251      1   19
252      19.685       .379      24.0       .379      31.7      .5786      40.0       .771
253        48.0        .95      56.7      1.10      65.4      1.229      74.1      1.321
254        82.8     1.3786      91.7       1.4     100.6     1.3786     109.3      1.321
255       118.0      1.229     126.6      1.10     135.2       0.95     143.6      0.771
256       151.7     0.5786     159.8     0.379     164.0      0.379
257         0.0        1.0      34.0       1.0      57.0       .922     107.0       .837
258       157.0       .795     257.0      .702     357.0       .646     400.0       .626
259     13    1     0    2     0
260      6    9
261     .0        1.0  4.0        1.0  7.0      0.426 52.0      0.426 76.5  0.185
262 400.0      0.185
263     .0        1.0 46.0        1.0 57.0      0.958105.0      0.890157.0  0.857
264 208.0      0.890250.0      0.933315.0      0.975400.0      0.992
265      1    1     2    1     2      59.52      216.6
266     14    5                          0    2
267                                                                END GROUP14
268                                                                END GROUP14
269      4
270      6    4    -1    1
    12345678901234567890123456789012345678901234567890123456789012345678901234567890
271      7    4    -1    3
272      8    4    -1    5
273      9    4    -1    7
274      0
275      9    0      450.0
276      1    2    3    4    5    6    7    8    9
277           .0001            .1           390.           1.0          7190.
278            50.0           1.0           50.0        1000.0
279
280
281
282
283
```

(3) Case 0 3

```
********************************** INPUT FILE LISTING **********************************
    12345678901234567890123456789012345678901234567890123456789012345678901234567890
  1             11             0             0            50
  2  *****  SLAB CORE TEST FACILITY ANALISYS USED 'COBRA/TRAC' DATA
  3            TEST CASE   ... 01 ( JUNE 1984 ) VESSEL UNIT(BTU) GAP-DETAIL
  4            CONVERGENCE CONDITION  EPS=0.01  , DELT = 0.0001
  5            FILL COMPONENT NOT INCLUDE  ( FILL ==> VESSEL BOUNDARY )
  6             COMPONENT      BREAK    .....  4
  7                            PIPE     .....  4
  8                            JUNCTION .....  8
  9                            VESSEL   .....  1
 10                                AXIAL SECTION     .....   3
 11                                CHANNELS          .....   9
 12                                GAP               .....   6
 13             0           0.0
 14             9             8             0
 15          0.01            10            40
 16             0             0
 17             6             7             8             9             2
 18             3             4             5             1
 19 BREAK                     6             6             0
 20             2             1             3             3
 21           0.1        0.0106           1.0        392.70      0.200E+6
 22           0.0      0.200E+6           7.0      0.200E+6         407.0
 23       0.200E+6
 24 BREAK                     7             7             0
 25             4             1             3             3
 26           0.1        0.0106           1.0        392.70      0.200E+6
 27           0.0      0.200E+6           7.0      0.200E+6         407.0
 28      0.2005E+6
 29 BREAK                     8             8             0
 30             6             1             3             3
    12345678901234567890123456789012345678901234567890123456789012345678901234567890
 31           0.1        0.0106           1.0        392.70      0.200E+6
 32           0.0      0.200E+6           7.0      0.200E+6         407.0
 33       0.201E+6
 34 BREAK                     9             9             0
 35             8             1             3             3
 36           0.1        0.0106           1.0        392.70      0.200E+6
 37           0.0      0.200E+6           7.0      0.200E+6         407.0
 38       0.202E+6
 39 PIPE                      2             2
 40             1             0             1             2             6
 41             0             1
 42         0.184         0.001           0.0           0.0        392.70
 43        392.70
 44 F         0.1E
 45 F      0.0106E
 46 F       0.106E
 47 F         0.0E
 48 F         0.0E
 49 F       0.367E
 50 F           5E
 51 F         0.0E
 52 F         1.0E
 53 F         0.0E
 54 F      392.70E
 55 F    0.200E+6E
 56 PIPE                      3             3
 57             1             0             3             4             6
 58             0             1
 59         0.184         0.001           0.0           0.0        392.70
```

```
60          392.70
   12345678901234567890123456789012345678901234567890123456789012345678901234567890
61 F           0.1E
62 F        0.0106E
63 F         0.106E
64 F           0.0E
65 F           0.0E
66 F         0.367E
67 F             5E
68 F           0.0E
69 F           1.0E
70 F           0.0E
71 F        392.70E
72 F      0.200E+6E
73 PIPE                          4              4
74                1              0              5              6              6
75                0              1
76           0.184          0.001            0.0            0.0         392.70
77          392.70
78 F           0.1E
79 F        0.0106E
80 F         0.106E
81 F           0.0E
82 F           0.0E
83 F         0.367E
84 F             5E
85 F           0.0E
86 F           1.0E
87 F           0.0E
88 F        392.70E
89 F      0.200E+6E
90 PIPE                          5              5
   12345678901234567890123456789012345678901234567890123456789012345678901234567890
91                1              0              7              8              6
92                0              1
93           0.184          0.001            0.0            0.0         392.70
94          392.70
95 F           0.1E
96 F        0.0106E
97 F         0.106E
98 F           0.0E
99 F           0.0E
100 F        0.367E
101 F            5E
102 F          0.0E
103 F          1.0E
104 F          0.0E
105 F       392.70E
106 F     0.200E+6E
107 VESSEL                       1              1
108           1  ****  S.C.T.F.  VESSEL DATA  SECTION= 5,CHANNEL= 20,GAP= 15
109      1    3
110 163.8
111       29.01    1164.0       0.0      0.32
112      2    9    8
113      1527.22456.
114      2135.6740.2              1
115      4    1    428.98
116      3135.6730.7              2
117      4    1    428.98    4    2    528.98
118      4135.6730.7              2
119      4    2    528.98    4    3    628.98
```

```
120     5135.6740.2                1
    12345678901234567890123456789012345678901234567890123456789012345678901234567890
121     4    3    628.98
122     6135.6740.2                1
123     4    4    028.98
124     7135.6730.7                2
125     4    4    028.98    4    5    028.98
126     8135.6730.7                2
127     4    5    028.98    4    6    028.98
128     9135.6740.2                1
129     4    6    028.98
130     2    1    2                         1
131     3    3    4                         2
132     4    5    6                         3
133     5    7    8                         4
134     6    1    2                         5
135     7    3    4                         6
136     8    5    6                         7
137     9    7    8                         8
138     3    6
139     1    2    3  3.218.11 16.    1.    0    4   1.   -1    2    0    0    0    0
140    17  1.0
141     2    3    4  3.218.11 16.    1.    0    5   1.    1    3    0    0    0    0
142    17  1.0
143     3    4    5  3.218.11 16.    1.    0    6   1.    2   -1    0    0    0    0
144    17  1.0
145     4    6    7  3.218.11 16.    1.    1    0   1.   -1    5    0    0    0    0
146    17  1.0
147     5    7    8  3.218.11 16.    1.    2    0   1.    4    6    0    0    0    0
148    17  1.0
149     6    8    9  3.218.11 16.    1.    3    0   1.    5   -1    0    0    0    0
150    17  1.0
    12345678901234567890123456789012345678901234567890123456789012345678901234567890
151     0
152     4    3    1    1
153     1    1    1    19.685
154     1    2    3    4    5                1
155     2    4    3     24.02
156     2    6                              1
157     3    7                              1
158     4    8                              1
159     5    9                              1
160     3    4    3     24.02
161     6    6                              2
162     7    7                              3
163     8    8                              4
164     9    9                              5
165     4
166    25
167     7    3
168  1.82    1    2    3    4    5    6    7    8    9
169  1.82    2    2    3    4    5    6    7    8    9
170  1.82    3    2    3    4    5    6    7    8    9
171     8    8    8    2    8
172     1    1    1    1   0.07874      234.     1.000    50000.
173     2    1    1    1   0.07874      234.     1.000    50000.
174     3    1    1    1   0.07874      234.     1.000    50000.
175     4    1    1    1   0.07874      234.     1.000    50000.
176     5    1    1    1   0.07874      234.     1.000    50000.
177     6    1    1    1   0.07874      234.     1.000    50000.
178     7    1    1    1   0.07874      234.     1.000    50000.
179     8    1    1    1   0.07874      234.     1.000    50000.
```

```
180      1     2      1.707          .0        44.
    12345678901234567890123456789012345678901234567890123456789012345678901234567890
181      2     2      1.707          .0        44.
182      3     2      1.707          .0        44.
183      4     2      1.707          .0        44.
184      5     2      1.707          .0        44.
185      6     2      1.707          .0        44.
186      7     2      1.707          .0        44.
187      8     2      1.707          .0        44.
188      1     2     0   12
189      1     2
190     19.685       485.       43.7       921.       43.8       921.       67.7      1229.
191       67.8      1229.       91.9      1331.       92.0      1331.      115.9      1241.
192      116.0      1241.      139.9       946.      140.0       946.      164.0       512.
193      2     2     0   12
194      3     4
195     19.685       485.       43.7       921.       43.8       921.       67.7      1229.
196       67.8      1229.       91.9      1331.       92.0      1331.      115.9      1241.
197      116.0      1241.      139.9       946.      140.0       946.      164.0       512.
198      3     2     0   12
199      5     6
200     19.685       485.       43.7       921.       43.8       921.       67.7      1229.
201       67.8      1229.       91.9      1331.       92.0      1331.      115.9      1241.
202      116.0      1241.      139.9       946.      140.0       946.      164.0       512.
203      4     2     0   12
204      7     8
205     19.685       485.       43.7       921.       43.8       921.       67.7      1229.
206       67.8      1229.       91.9      1331.       92.0      1331.      115.9      1241.
207      116.0      1241.      139.9       946.      140.0       946.      164.0       512.
208      5     0     2   12
209      1     5
210     19.685       527.       43.7       509.       43.8       509.       67.7       493.
    12345678901234567890123456789012345678901234567890123456789012345678901234567890
211       67.8       493.       91.9       440.       92.0       440.      115.9       365.
212      116.0       365.      139.9       318.      140.0       318.      164.0       277.
213      6     0     2   12
214      2     6
215     19.685       527.       43.7       509.       43.8       509.       67.7       493.
216       67.8       493.       91.9       440.       92.0       440.      115.9       365.
217      116.0       365.      139.9       318.      140.0       318.      164.0       277.
218      7     0     2   12
219      3     7
220     19.685       527.       43.7       509.       43.8       509.       67.7       493.
221       67.8       493.       91.9       440.       92.0       440.      115.9       365.
222      116.0       365.      139.9       318.      140.0       318.      164.0       277.
223      8     0     2   12
224      4     8
225     19.685       527.       43.7       509.       43.8       509.       67.7       493.
226       67.8       493.       91.9       440.       92.0       440.      115.9       365.
227      116.0       365.      139.9       318.      140.0       318.      164.0       277.
228      9     2
229      1 HROD      .422          .0    4    2
230      1    10.102   0.    1    30.022   1.    4    10.049   0.    2    20.038   0.
231      2 HROD     .5434          .0    2    2
232      2    10.189   0.    1    2.0827   0.
233     10     3
234      1    11     156.07
235       212.      0.253    0.3434      302.      0.261    0.3434
236       482.      0.273    0.3434      662.      0.281    0.3434
237       842.      0.287    0.3434     1022.      0.292    0.3434
238      1202.      0.296    0.3434     1382.      0.300    0.3434
239      1562.      0.303    0.3434     1742.      0.306    0.3434
```

```
240      1922.      0.309    0.3434
    12345678901234567890123456789012345678901234567890123456789012345678901234567890
241     2   11     526.07
242       212.     0.1050    8.4590      302.      0.1066    9.5600
243       482.     0.1202    11.150      662.      0.1264    12.340
244       842.     0.1312    13.300     1022.      0.1350    14.130
245      1202.     0.1390    14.860     1382.      0.1420    15.510
246      1562.     0.1440    16.110     1742.      0.1470    16.660
247      1922.     0.1490    17.170
248     3    1     525.02
249       200.      0.104     6.529     2000.       0.104     6.259
250    11    1     8
251     1   19
252     19.685       .379      24.0       .379       31.7     .5786       40.0       .771
253       48.0        .95      56.7       1.10       65.4     1.229       74.1      1.321
254       82.8     1.3786      91.7        1.4      100.6    1.3786      109.3      1.321
255      118.0      1.229     126.6       1.10      135.2      0.95      143.6      0.771
256      151.7     0.5786     159.8      0.379      164.0     0.379
257        0.0        1.0      34.0        1.0       57.0      .922      107.0       .837
258      157.0       .795     257.0       .702      357.0      .646      400.0       .626
259    13    1    0    2    0
260     6    9
261    .0        1.0  4.0        1.0  7.0      0.426 52.0      0.426 76.5  0.185
262 400.0      0.185
263    .0        1.0 46.0        1.0 57.0      0.958105.0      0.890157.0  0.857
264 208.0      0.890250.0      0.933315.0      0.975400.0      0.992
265     1    1    2    1    2      59.52      216.6
266    14    5                         0    2
267                                                                  END GROUP14
268                                                                  END GROUP14
269     4
270     6    4   -1    1
    12345678901234567890123456789012345678901234567890123456789012345678901234567890
271     7    4   -1    3
272     8    4   -1    5
273     9    4   -1    7
274     0
275     9    0     450.0
276     1    2    3    4    5    6    7    8    9
277          .0001            .1          350.          1.0          7100.
278           25.0           1.0          50.0        1000.0
279
280
281
282
283
```